A&A 601, A19 (2017)
DOI: 10.1051/0004-6361/201730552

Astronomy & Astrophysics

Special issue

Gaia Data Release 1

Gaia Data Release 1

Open cluster astrometry: performance, limitations, and future prospects★

Gaia Collaboration, F. van Leeuwen[1], A. Vallenari[2], C. Jordi[3], L. Lindegren[4], U. Bastian[5], T. Prusti[6], J. H. J. de Bruijne[6], A. G. A. Brown[7], C. Babusiaux[8], C. A. L. Bailer-Jones[9], M. Biermann[5], D. W. Evans[1], L. Eyer[10], F. Jansen[11], S. A. Klioner[12], U. Lammers[13], X. Luri[3], F. Mignard[14], C. Panem[15], D. Pourbaix[16,17], S. Randich[18], P. Sartoretti[8], H. I. Siddiqui[19], C. Soubiran[20], V. Valette[15], N. A. Walton[1], C. Aerts[21,22], F. Arenou[8], M. Cropper[23], R. Drimmel[24], E. Høg[25], D. Katz[8], M. G. Lattanzi[24], W. O'Mullane[13], E. K. Grebel[5], A. D. Holland[26], C. Huc[15], X. Passot[15], M. Perryman[6], L. Bramante[27], C. Cacciari[28], J. Castañeda[3], L. Chaoul[15], N. Cheek[29], F. De Angeli[1], C. Fabricius[3], R. Guerra[13], J. Hernández[13], A. Jean-Antoine-Piccolo[15], E. Masana[3], R. Messineo[27], N. Mowlavi[10], K. Nienartowicz[30], D. Ordóñez-Blanco[30], P. Panuzzo[8], J. Portell[3], P. J. Richards[31], M. Riello[1], G. M. Seabroke[23], P. Tanga[14], F. Thévenin[14], J. Torra[3], S. G. Els[32,5], G. Gracia-Abril[32,3], G. Comoretto[19], M. Garcia-Reinaldos[13], T. Lock[13], E. Mercier[32,5], M. Altmann[5,33], R. Andrae[9], T. L. Astraatmadja[9], I. Bellas-Velidis[34], K. Benson[23], J. Berthier[35], R. Blomme[36], G. Busso[1], B. Carry[14,35], A. Cellino[24], G. Clementini[28], S. Cowell[1], O. Creevey[14,37], J. Cuypers[36], M. Davidson[38], J. De Ridder[21], A. de Torres[39], L. Delchambre[40], A. Dell'Oro[18], C. Ducourant[20], Y. Frémat[36], M. García-Torres[41], E. Gosset[40,17], J.-L. Halbwachs[42], N. C. Hambly[38], D. L. Harrison[1,43], M. Hauser[5], D. Hestroffer[35], S. T. Hodgkin[1], H. E. Huckle[23], A. Hutton[44], G. Jasniewicz[45], S. Jordan[5], M. Kontizas[46], A. J. Korn[47], A. C. Lanzafame[48,49], M. Manteiga[50], A. Moitinho[51], K. Muinonen[52,53], J. Osinde[54], E. Pancino[18,55], T. Pauwels[36], J.-M. Petit[56], A. Recio-Blanco[14], A. C. Robin[56], L. M. Sarro[57], C. Siopis[16], M. Smith[23], K. W. Smith[9], A. Sozzetti[24], W. Thuillot[35], W. van Reeven[44], Y. Viala[8], U. Abbas[24], A. Abreu Aramburu[58], S. Accart[59], J. J. Aguado[57], P. M. Allan[31], W. Allasia[60], G. Altavilla[28], M. A. Álvarez[50], J. Alves[61], R. I. Anderson[62,10], A. H. Andrei[63,64,33], E. Anglada Varela[54,29], E. Antiche[3], T. Antoja[6], S. Antón[65,66], B. Arcay[50], N. Bach[44], S. G. Baker[23], L. Balaguer-Núñez[3], C. Barache[33], C. Barata[51], A. Barbier[59], F. Barblan[10], D. Barrado y Navascués[67], M. Barros[51], M. A. Barstow[68], U. Becciani[49], M. Bellazzini[28], A. Bello García[69], V. Belokurov[1], P. Bendjoya[14], A. Berihuete[70], L. Bianchi[60], O. Bienaymé[42], F. Billebaud[20], N. Blagorodnova[1], S. Blanco-Cuaresma[10,20], T. Boch[42], A. Bombrun[39], R. Borrachero[3], S. Bouquillon[33], G. Bourda[20], H. Bouy[67], A. Bragaglia[28], M. A. Breddels[71], N. Brouillet[20], T. Brüsemeister[5], B. Bucciarelli[24], P. Burgess[1], R. Burgon[26], A. Burlacu[15], D. Busonero[24], R. Buzzi[24], E. Caffau[8], J. Cambras[72], H. Campbell[1], R. Cancelliere[73], T. Cantat-Gaudin[2], T. Carlucci[33], J. M. Carrasco[3], M. Castellani[74], P. Charlot[20], J. Charnas[30], A. Chiavassa[14], M. Clotet[3], G. Cocozza[28], R. S. Collins[38], G. Costigan[7], F. Crifo[8], N. J. G. Cross[38], M. Crosta[24], C. Crowley[39], C. Dafonte[50], Y. Damerdji[40,75], A. Dapergolas[34], P. David[35], M. David[76], P. De Cat[36], F. de Felice[77], P. de Laverny[14], F. De Luise[78], R. De March[27], D. de Martino[79], R. de Souza[80], J. Debosscher[21], E. del Pozo[44], M. Delbo[14], A. Delgado[1], H. E. Delgado[57], P. Di Matteo[8], S. Diakite[56], E. Distefano[49], C. Dolding[23], S. Dos Anjos[80], P. Drazinos[46], J. Durán[54], Y. Dzigan[81,82], B. Edvardsson[47], H. Enke[83], N. W. Evans[1], G. Eynard Bontemps[59], C. Fabre[84], M. Fabrizio[55,78], S. Faigler[85], A. J. Falcão[86], M. Farràs Casas[3], L. Federici[28], G. Fedorets[52], J. Fernández-Hernández[29], P. Fernique[42], A. Fienga[87], F. Figueras[3], F. Filippi[27], K. Findeisen[8], A. Fonti[27], M. Fouesneau[9], E. Fraile[88], M. Fraser[1], J. Fuchs[89], M. Gai[24], S. Galleti[28], L. Galluccio[14], D. Garabato[50], F. García-Sedano[57], A. Garofalo[28], N. Garralda[3], P. Gavras[8,34,46], J. Gerssen[83], R. Geyer[12], G. Gilmore[1], S. Girona[90], G. Giuffrida[55], M. Gomes[51], A. González-Marcos[91], J. González-Núñez[29,92], J. J. González-Vidal[3], M. Granvik[52], A. Guerrier[59], P. Guillout[42], J. Guiraud[15], A. Gúrpide[3], R. Gutiérrez-Sánchez[19], L. P. Guy[30], R. Haigron[8], D. Hatzidimitriou[46,34], M. Haywood[8], U. Heiter[47], A. Helmi[71], D. Hobbs[4], W. Hofmann[5], B. Holl[10], G. Holland[1], J. A. S. Hunt[23], A. Hypki[7], V. Icardi[27], M. Irwin[1], G. Jevardat de Fombelle[30], P. Jofré[1,20], P. G. Jonker[93,22], A. Jorissen[16], F. Julbe[3], A. Karampelas[46,34], A. Kochoska[94], R. Kohley[13], K. Kolenberg[95,21,96], E. Kontizas[34], S. E. Koposov[1], G. Kordopatis[83,14], P. Koubsky[89], A. Krone-Martins[51], M. Kudryashova[35], I. Kull[85], R. K. Bachchan[4], F. Lacoste-Seris[59], A. F. Lanza[49], J.-B. Lavigne[59], C. Le Poncin-Lafitte[33], Y. Lebreton[8,97], T. Lebzelter[61], S. Leccia[79], N. Leclerc[8], I. Lecoeur-Taibi[30], V. Lemaitre[59], H. Lenhardt[5], F. Leroux[59], S. Liao[24,98], E. Licata[60], H. E. P. Lindstrøm[25,99], T. A. Lister[100], E. Livanou[46], A. Lobel[36], W. Löffler[5], M. López[67], D. Lorenz[61], I. MacDonald[38], T. Magalhães Fernandes[86], S. Managau[59], R. G. Mann[38], G. Mantelet[5], O. Marchal[8], J. M. Marchant[101], M. Marconi[79], S. Marinoni[74,55], P. M. Marrese[74,55], G. Marschalkó[102,103], D. J. Marshall[104], J. M. Martín-Fleitas[44], M. Martino[27], N. Mary[59], G. Matijevič[83], T. Mazeh[85], P. J. McMillan[4], S. Messina[49],

D. Michalik[4], N. R. Millar[1], B. M. H. Miranda[51], D. Molina[3], R. Molinaro[79], M. Molinaro[105], L. Molnár[102], M. Moniez[106], P. Montegriffo[28], R. Mor[3], A. Mora[44], R. Morbidelli[24], T. Morel[40], S. Morgenthaler[107], D. Morris[38], A. F. Mulone[27], T. Muraveva[28], I. Musella[79], J. Narbonne[59], G. Nelemans[22,21], L. Nicastro[108], L. Noval[59], C. Ordénovic[14], J. Ordieres-Meré[109], P. Osborne[1], C. Pagani[68], I. Pagano[49], F. Pailler[15], H. Palacin[59], L. Palaversa[10], P. Parsons[19], M. Pecoraro[60], R. Pedrosa[110], H. Pentikäinen[52], B. Pichon[14], A. M. Piersimoni[78], F.-X. Pineau[42], E. Plachy[102], G. Plum[8], E. Poujoulet[111], A. Prša[112], L. Pulone[74], S. Ragaini[28], S. Rago[24], N. Rambaux[35], M. Ramos-Lerate[113], P. Ranalli[4], G. Rauw[40], A. Read[68], S. Regibo[21], C. Reylé[56], R. A. Ribeiro[86], L. Rimoldini[30], V. Ripepi[79], A. Riva[24], G. Rixon[1], M. Roelens[10], M. Romero-Gómez[3], N. Rowell[38], F. Royer[8], L. Ruiz-Dern[8], G. Sadowski[16], T. Sagristà Sellés[5], J. Sahlmann[13], J. Salgado[54], E. Salguero[54], M. Sarasso[24], H. Savietto[114], M. Schultheis[14], E. Sciacca[49], M. Segol[115], J. C. Segovia[29], D. Segransan[10], I.-C. Shih[8], R. Smareglia[105], R. L. Smart[24], E. Solano[67,116], F. Solitro[27], R. Sordo[2], S. Soria Nieto[3], J. Souchay[33], A. Spagna[24], F. Spoto[14], U. Stampa[5], I. A. Steele[101], H. Steidelmüller[12], C. A. Stephenson[19], H. Stoev[117], F. F. Suess[1], M. Süveges[30], J. Surdej[40], L. Szabados[102], E. Szegedi-Elek[102], D. Tapiador[118,119], F. Taris[33], G. Tauran[59], M. B. Taylor[120], R. Teixeira[80], D. Terrett[31], B. Tingley[121], S. C. Trager[71], C. Turon[8], A. Ulla[122], E. Utrilla[44], G. Valentini[78], A. van Elteren[7], E. Van Hemelryck[36], M. van Leeuwen[1], M. Varadi[10,102], A. Vecchiato[24], J. Veljanoski[71], T. Via[72], D. Vicente[90], S. Vogt[123], H. Voss[3], V. Votruba[89], S. Voutsinas[38], G. Walmsley[15], M. Weiler[3], K. Weingrill[83], T. Wevers[22], Ł. Wyrzykowski[1,124], A. Yoldas[1], M. Žerjal[94], S. Zucker[81], C. Zurbach[45], T. Zwitter[94], A. Alecu[1], M. Allen[6], C. Allende Prieto[23,125,126], A. Amorim[51], G. Anglada-Escudé[3], V. Arsenijevic[51], S. Azaz[6], P. Balm[19], M. Beck[30], H.-H. Bernstein[†5], L. Bigot[14], A. Bijaoui[14], C. Blasco[127], M. Bonfigli[78], G. Bono[74], S. Boudreault[23,128], A. Bressan[129], S. Brown[1], P.-M. Brunet[15], P. Bunclark[†1], R. Buonanno[74], A. G. Butkevich[12], C. Carret[110], C. Carrion[57], L. Chemin[20,130], F. Chéreau[8], L. Corcione[24], E. Darmigny[15], K. S. de Boer[131], P. de Teodoro[29], P. T. de Zeeuw[7,132], C. Delle Luche[8,59], C. D. Domingues[133], P. Dubath[30], F. Fodor[15], B. Frézouls[15], A. Fries[3], D. Fustes[50], D. Fyfe[68], E. Gallardo[3], J. Gallegos[29], D. Gardiol[24], M. Gebran[3,134], A. Gomboc[94,135], A. Gómez[8], E. Grux[56], A. Gueguen[8,136], A. Heyrovsky[38], J. Hoar[13], G. Iannicola[74], Y. Isasi Parache[3], A.-M. Janotto[15], E. Joliet[39,137], A. Jonckheere[36], R. Keil[138,139], D.-W. Kim[9], P. Klagyivik[102], J. Klar[83], J. Knude[25], O. Kochukhov[47], I. Kolka[140], J. Kos[94,141], A. Kutka[89,142], V. Lainey[35], D. LeBouquin[59], C. Liu[9,143], D. Loreggia[24], V. V. Makarov[144], M. G. Marseille[59], C. Martayan[36,145], O. Martinez-Rubi[3], B. Massart[14,59,146], F. Meynadier[8,33], S. Mignot[8], U. Munari[2], A.-T. Nguyen[15], T. Nordlander[47], K. S. O'Flaherty[147], P. Ocvirk[83,42], A. Olias Sanz[148], P. Ortiz[68], J. Osorio[65], D. Oszkiewicz[52,149], A. Ouzounis[38], M. Palmer[3], P. Park[10], E. Pasquato[16], C. Peltzer[1], J. Peralta[3], F. Péturaud[8], T. Pieniluoma[52], E. Pigozzi[27], J. Poels[†40], G. Prat[150], T. Prod'homme[7,151], F. Raison[152,136], J. M. Rebordao[133], D. Risquez[7], B. Rocca-Volmerange[153], S. Rosen[23,68], M. I. Ruiz-Fuertes[30], F. Russo[24], S. Sembay[68], I. Serraller Vizcaino[154], A. Short[6], A. Siebert[42,83], H. Silva[86], D. Sinachopoulos[34], E. Slezak[14], M. Soffel[12], D. Sosnowska[10], V. Straižys[155], M. ter Linden[39,156], D. Terrell[157], S. Theil[158], C. Tiede[9,159], L. Troisi[55,160], P. Tsalmantza[9], D. Tur[72], M. Vaccari[161,162], F. Vachier[35], P. Valles[3], W. Van Hamme[163], L. Veltz[83,37], J. Virtanen[52,53], J.-M. Wallut[15], R. Wichmann[164], M. I. Wilkinson[1,68], H. Ziaeepour[56], and S. Zschocke[12]

(Affiliations can be found after the references)

Received 3 February 2017 / Accepted 25 February 2017

ABSTRACT

Context. The first *Gaia* Data Release contains the *Tycho-Gaia* Astrometric Solution (TGAS). This is a subset of about 2 million stars for which, besides the position and photometry, the proper motion and parallax are calculated using HIPPARCOS and *Tycho-2* positions in 1991.25 as prior information.

Aims. We investigate the scientific potential and limitations of the TGAS component by means of the astrometric data for open clusters.

Methods. Mean cluster parallax and proper motion values are derived taking into account the error correlations within the astrometric solutions for individual stars, an estimate of the internal velocity dispersion in the cluster, and, where relevant, the effects of the depth of the cluster along the line of sight. Internal consistency of the TGAS data is assessed.

Results. Values given for standard uncertainties are still inaccurate and may lead to unrealistic unit-weight standard deviations of least squares solutions for cluster parameters. Reconstructed mean cluster parallax and proper motion values are generally in very good agreement with earlier HIPPARCOS-based determination, although the *Gaia* mean parallax for the Pleiades is a significant exception. We have no current explanation for that discrepancy. Most clusters are observed to extend to nearly 15 pc from the cluster centre, and it will be up to future *Gaia* releases to establish whether those potential cluster-member stars are still dynamically bound to the clusters.

Conclusions. The *Gaia* DR1 provides the means to examine open clusters far beyond their more easily visible cores, and can provide membership assessments based on proper motions and parallaxes. A combined HR diagram shows the same features as observed before using the HIPPARCOS data, with clearly increased luminosities for older A and F dwarfs.

Key words. astrometry – open clusters and associations: general

⋆ Tables D.1 to D.19 are also available at the CDS via anonymous ftp to cdsarc.u-strasbg.fr (130.79.128.5) or via http://cdsarc.u-strasbg.fr/viz-bin/qcat?J/A+A/601/A19

† Deceased.

1. Introduction

The homogeneity in age and composition of stars in open clusters makes them unique and very valuable potential tracers of stellar evolution and galactic structure. However, to reach this potential it is essential that cluster membership and absolute distances are determined fully independent of assumptions on luminosities. Photometric and spectroscopic data should be obtained on a single accurate and full-sky-coverage system. To determine distances for open clusters, a sizeable fraction of the members need to be covered, and for the nearby clusters the variations along the line of sight, and direction on the sky, in parallax and proper motion need to be fully accounted for. This is the kind of task that is only possible to achieve with a dedicated satellite mission, and was first done using the HIPPARCOS astrometric data in conjunction with the Geneva photometric surveys (van Leeuwen 2009, fvl09 from hereon).

The TGAS catalogue in the first *Gaia* data release (Gaia Collaboration 2016b; DR1 from hereon) provides an order of magnitude more data than the HIPPARCOS catalogue did, but at the same time, because of the limitations in its construction, it is more problematic and complicated in its use and interpretation (Lindegren et al. 2016; Gaia Collaboration 2016a; Arenou et al. 2017). The combination with the first epoch from the new reduction of the HIPPARCOS data (ESA 1997; van Leeuwen 2007) and *Tycho-2* (Høg et al. 2000) data, as well as the still very limited scan coverage of the *Gaia* data in this first data release, creates locally strong and systematic correlations between the astrometric parameters as determined for individual stars. Error-correlation coefficients between the five astrometric parameters still frequently exceed values as high as 0.8, and need to be taken into account when determining both mean parallax and mean proper motion data for a cluster. Many details on this can be found in Lindegren et al. (2016).

The way the data had to be processed also plays an important role. In particular simplifications in the attitude reconstruction (because of low numbers of reference stars) meant that the effects of clanks[1] and minor hits[2] were smoothed over, leading to locally correlated errors on the epoch astrometric data, a problem that should be largely resolved in future releases. This first release on the *Gaia* star cluster data is therefore a taste of things to come, and provides some ideas on how to handle the *Gaia* astrometric data for a star cluster. The data derived for the clusters can still be affected by local systematics in the TGAS catalogue, claimed to be at a level of 0.3 mas (Gaia Collaboration 2016a), and, as we will show, comparisons with the HIPPARCOS astrometric data for clusters are consistent with a slightly lower level of systematics, at 0.25 mas.

The homogeneity of the astrometric data for members of an open cluster offers possibilities to study some aspects of the proper motions and parallaxes as presented in the TGAS section of the *Gaia* DR1. In particular the reliability of the standard uncertainties (*su* from hereon) as quoted in DR1 can be checked, and localized correlated errors may show up. Different roles are there for the nearest cluster (Hyades), eight medium distance clusters (within 300 pc: Coma Berenices, Pleiades, IC 2391, IC 2602, α Per cluster, Praesepe, Blanco 1, NGC 2451A) and ten more distant clusters (between 300 and 500 pc: NGC 6475, NGC 7092, NGC 2516, NGC 2232, IC 4665, NGC 6633, Coll 140, NGC 2422, NGC 3532 and NGC 2547).

[1] Discrete adjustments of the satellite structure, and thus telescope pointing, to temperature changes.
[2] Impacts of external particles, causing discrete rate changes.

Table 1. Open cluster names and identifiers.

Name	Lynga	Melotte
Hyades	C0423+157	25
Coma Ber	C1222+263	111
Praesepe	C0837+201	88
Pleiades	C0344+239	22
α Per	C0318+484	20
IC 2391	C0838−528	
IC 2602	C1041−641	
Blanco 1	C0001−302	
NGC 2451A	C0743−378	
NGC 6475	C1750−348	
NGC 7092	C2130+482	
NGC 2516	C0757−607	
NGC 2232	C0624−047	
IC 4665	C1743+057	179
NGC 6633	C1825+065	
Coll 140	C0722−321	
NGC 2422	C0734−143	
NGC 3532	C1104−584	
NGC 2547	C0809−491	

Table 1 provides further identifiers of the clusters presented in this paper. The Hyades permits a consistency comparison between proper motions and parallaxes over an area up to 36 degrees in diameter on the sky. The second group is used to assess consistency of the *su* on the astrometric parameters of individual stars. The third group, for which the density on the sky of potential cluster members is higher, can be used to assess the effects of error correlations between neighbouring stars. Most of these tests are ultimately limited by the uncertainty in the estimate of the internal velocity dispersion in the clusters, and in particular its dependence on the 3D position within the cluster. For the more distant clusters there is the additional limitation of ascertaining membership of a cluster.

Comparisons of the astrometric data are generally kept limited to fvl09, based on the re-reduction of the HIPPARCOS data (van Leeuwen 2007), and which superseded the earlier analysis of the HIPPARCOS astrometry for open clusters in van Leeuwen (1999) and Robichon et al. (1999). The paper fvl09 provides more extensive references to earlier studies of the clusters selected for the current study. Table 2 summarizes, where available, external data on the clusters.

In order to appreciate the possibilities as well as the limitations inherent to the TGAS component of the *Gaia* DR1, and in particular where these affect our analysis of cluster data, we provide some background information on the data in Sect. 2. This includes a discussion of the not-published epoch astrometry data in order to assess the potential level of error correlations between neighbouring stars.

A summary of the methods used to derive cluster astrometry is presented in Sect. 3, with more details provided in Appendix A. This is followed by the analysis of the Hyades (Sect. 4) and the nearby clusters (Sect. 5). The distant clusters (Sect. 6) pose their own specific problems, and are only briefly discussed here. A summary of the results is presented in Sect. 7.

Gaia source identifiers are based on the HEALPix pixelization (Nested, level 12) of the sky (Górski et al. 2005), and all-sky maps shown in the current paper use this pixelization, usually at level 5 or 6, where level 6 has pixel-size of just under one square degree. An integer division of the source identifier by 2^{35} gives the level 12 HEALPix pixel for the source location

Table 2. Supplementary data.

Name	Fe/H	$E(B-V)$	log(age)
Hyades	0.15 ± 0.004	0.00	8.90
Coma Ber	0.00 ± 0.08	0.00	8.75
Praesepe	0.16 ± 0.004	0.01	8.90
Pleiades	−0.01 ± 0.05	0.04	8.08
α Per	0.14 ± 0.11	0.09	7.55
IC 2391	−0.01 ± 0.03	0.05	7.55
IC 2606	−0.02 ± 0.02	0.03	7.88
Blanco 1	0.03 ± 0.07	0.01	8.32
NGC 2451A	-0.08	0.00	7.76
NGC 6475	0.02 ± 0.02	0.21	8.22
NGC 7092	0.00	0.01	8.57
NGC 2516	+0.05 ± 0.11	0.07	8.08
NGC 2232	0.11	0.03	7.49
IC 4665	−0.03 ± 0.04	0.17	7.63
NGC 6633	−0.08 ± 0.12	0.17	8.76
Coll 140	0.01 ± 0.04	0.05	7.57
NGC 2422	0.09 ± 0.03	0.10	8.12
NGC 3532	0.00 ± 0.07	0.04	8.45
NGC 2547	−0.14 ± 0.10	0.04	7.70

Notes. Metallicities for Hyades and Praesepe are from Cummings et al. (2017). For the other clusters are from Netopil et al. (2016). E_{B-V} are from Kharchenko et al. (2016).

on the sky. Source identifiers may change in future releases. The positions, magnitudes and HD numbers are therefore the more relevant source identifiers.

The additional photometric data used here comes primarily from the Geneva photometric catalogue (Rufener 1989), which provides multi-colour intermediate bandwidth photometry for a wide range of open clusters. Where possible the photometric data as presented is for cluster members confirmed by *Gaia* or HIPPARCOS astrometric data only.

2. The input data

The *Gaia* data is obtained from an array of CCDs in the focal plane, operating in Time-Delayed Integration (TDI) mode. The CCD charges are following the images as these move across the CCDs, taking about 4.5 s to cross a single CCD. In order to extend the brightness range for sources to be observed, gates are applied to shorten the integration time for the brighter stars. For more details see Gaia Collaboration (2016a,b).

The TGAS astrometric data, forming part of the *Gaia* DR1 (Gaia Collaboration 2016a,b), are based on first-epoch positions from the new reduction of the HIPPARCOS catalogue (van Leeuwen 2007) and the *Tycho-2* (Høg et al. 2000) catalogue (when a star was not included in the HIPPARCOS catalogue) and overall 14 months of *Gaia* data, though locally the coverage will often be significantly less than 14 months. The *Gaia* survey nominally covers the sky in at least two scan directions every six months. Having been collected at the start of the mission, this is not the best data *Gaia* will obtain. There have been a range of issues that affected the data and the data processing, most of it leading to some form of (temporary) data loss and still poorly defined *su* values on extracted parameters. In particular the transit time *su* estimates were still inaccurate due to early limitations on the modelling of the point-spread functions, leading to large χ^2 values for astrometric solutions (see Fig. 1). When the normalized χ^2 values are as large as observed

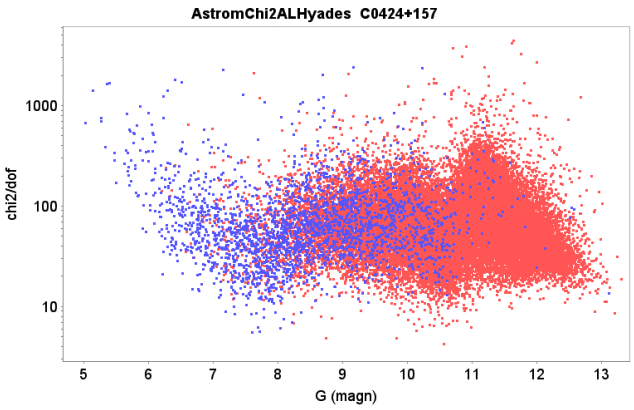

Fig. 1. Logarithm of the square root of the normalized χ^2 values for the astrometric solutions as a function of the G-band magnitude. The data come from an 18 degrees radius field, centred on the Hyades cluster. The blue dots used first epoch from the HIPPARCOS catalogue, the red dots from the *Tycho-2* catalogue.

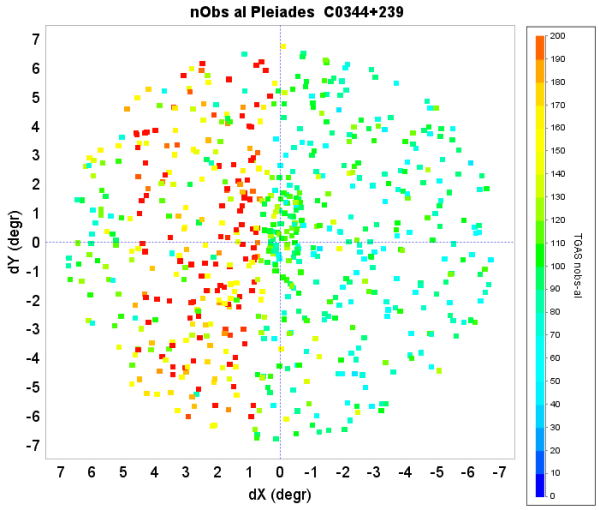

Fig. 2. Number of observations (CCD transits) per source in the TGAS catalogue for the Pleiades field. At this early stage there are still large local variations in the coverage. Positions are relative to the assumed centre of the Pleiades cluster. Each point represents a cluster or field star in the area.

here it means that there are quite significant modelling errors still present. Naturally, the worst affected are the brightest stars (brighter than $G \approx 6$), of which, as a result, a large fraction is not included in the *Gaia* DR1. Modelling errors tend to be non-Gaussian, and can hide a range of systematic errors in the data.

Quite large variations in the number of transits per star across the field of a cluster do often occur. This is an early-mission feature and is due to the scanning law and data gaps when it concerns large-scale features, such as shown in Fig. 2 for the Pleiades field. For small-scale, local variations this is probably due to a variety of source-identification problems which, at this early stage, still appears to cause a significant loss of data. The approximate level of data loss can be derived from the epoch astrometric data (see below), which shows typically a coincidence of scans between stars at relatively short separations on the sky (much shorter than the size of the field of view) to be around 55 to 70 per cent (an example is shown in Fig. 3), when values close to 100 per cent would be expected, as has been observed for the

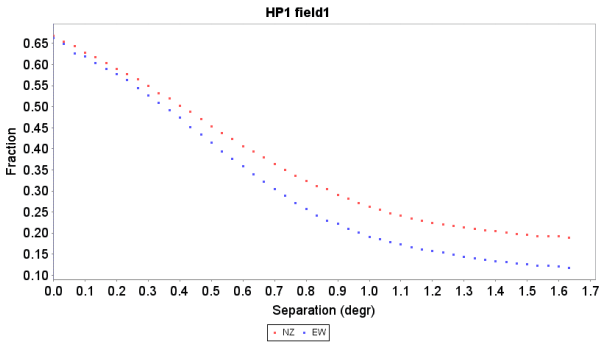

Fig. 3. An example of the scan-coincidence fraction as a function of separation on the sky. The coincidence level should be approaching 1 at separations much smaller than the size of the field of view (as it is for the HIPPARCOS data), but is found to be between 0.55 and 0.7 in the TGAS data. The red dots represent correlations (in ecliptic coordinates) in the north and south quadrants (between ±45° from the north or south directions), the blue dots in the east and west quadrants (between ±45° from the east or west directions). The scan coverage is significantly different between north-south and east-west directions. The data are for all stars in HEALPix (level 2), pixel 1, an area of about 833 square degrees (equatorial coordinates).

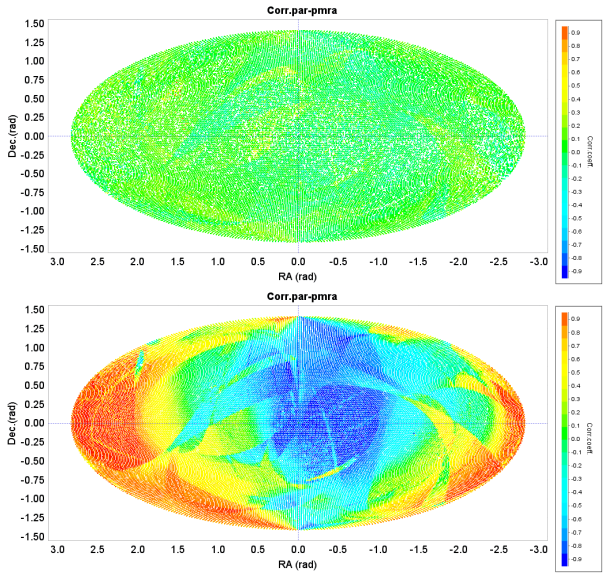

Fig. 4. Correlation coefficients between the proper motion in Right Ascension and the parallax, averaged over HEALPix level 5 pixels. *Top*: for stars with first-epoch HIPPARCOS positions; *bottom*: for stars with first-epoch *Tycho-2* positions. Correlations in the bottom graph are clearly systematic over the sky (linked to scan coverage) and can reach values over ±0.9. Similar correlations, but differently distributed, are observed between all the astrometric parameters for data with first epoch *Tycho-2* positions.

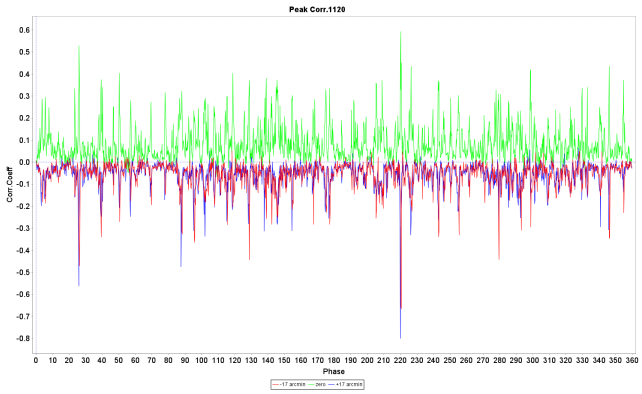

Fig. 5. An extract from the along-scan error correlations averaged over 20 satellite revolutions, against the rotation phase of the satellite. The green line shows the positive error correlations for sources separated by no more than 1 arcmin in transit phase (1 s in transit time). The red and blue lines show the error correlations for sources separated by ±17 arcmin respectively. All of the larger peaks can be related to clanks, and can be observed as such in a reconstruction of the satellite spin rate.

HIPPARCOS data (see van Leeuwen 2007, Fig. 9). Assuming that neighbouring stars are affected by the same percentage of data loss, then a 60 per cent coincidence of scans would indicate that this loss amounts to 22.5 per cent. These differences in coverage may explain the large local variations observed in the covariance matrices for the individual stellar astrometric solutions, which have to be taken properly into account. This is shown to affect stars with first-epoch *Tycho-2* data much more severely than those with first-epoch HIPPARCOS data. An example of the correlation coefficients, and the variations thereof, between the derived astrometric parameters is shown in Fig. 4.

The modulation of the basic angle, though corrected for with great care, adds uncertainty about the local parallax zero point, which is reflected in the assumed additional noise on the parallax determinations. The orientation of the payload as a function of time, which is referred to as the satellite attitude, is controlled by micro-propulsion thrusters, and affected by numerous clanks and hits (Lindegren et al. 2016; Risquez et al. 2013). The on-ground reconstruction of the attitude provides an estimate of the orientation of the telescope reference frame as a function of time, and as such is the reference against which the observed transit times are converted to positions, creating the so-called one-dimensional epoch astrometric data. These are the measurements used in the astrometric solutions. Inaccuracies in the modelling of the reconstructed attitude will reflect in the epoch astrometric data as correlated errors for neighbouring stars. Simplifications in the attitude reconstruction model as used in GDR1 concern:

1. use of gated observations in the attitude reconstructions;
2. smoothing over clanks and hits.

A gated observation is one for which the integration was done over a fraction of the CCD to avoid saturation for very bright stars. The effects on the attitude reconstruction are described in Risquez et al. (2013). In simple terms, the different integration times affect the way clanks are "seen" by transits.

Against this background, one has to be careful in deriving conclusions on, for example, open cluster astrometric data, which relies on combining data as obtained for individual member stars contained within a small area on the sky, within which the data may be affected by correlated errors.

For the current study we had access to the TGAS epoch astrometric data to study the error correlation levels, and to see if these effects are significant and sufficiently predictable to be compensated for. Systematics and correlation levels for residuals were, as expected, found to be strongly correlated with the occurrence of clanks. Most of the clanks are linked to the rotation phase of the satellite over period of days to weeks, where the rotation phase is defined with respect to the direction of the Sun as seen from the satellite. This created significant error-correlation patterns as a function of the rotation phase of the satellite (Fig. 5).

An error correlation pattern such as this is very complicated and cannot reasonably be corrected for in the data reductions.

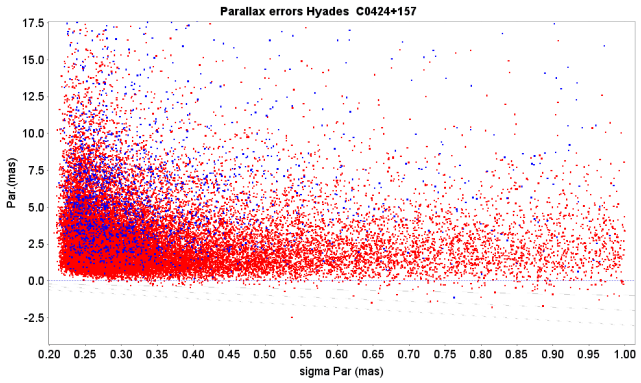

Fig. 6. Distribution of parallaxes as a function of *su* for stars in a field of 18 degrees radius centred on the Hyades cluster. The red and blue points as in Fig. 1. The three grey lines show the 1–3σ *su* levels.

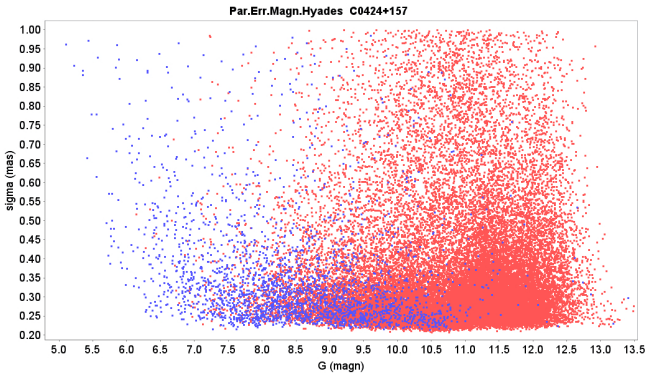

Fig. 7. Standard uncertainties for parallax measurements in TGAS, as a function of the *G* magnitude, for stars in a field of 18 degrees radius centred on the Hyades cluster. The red and blue points as in Fig. 1.

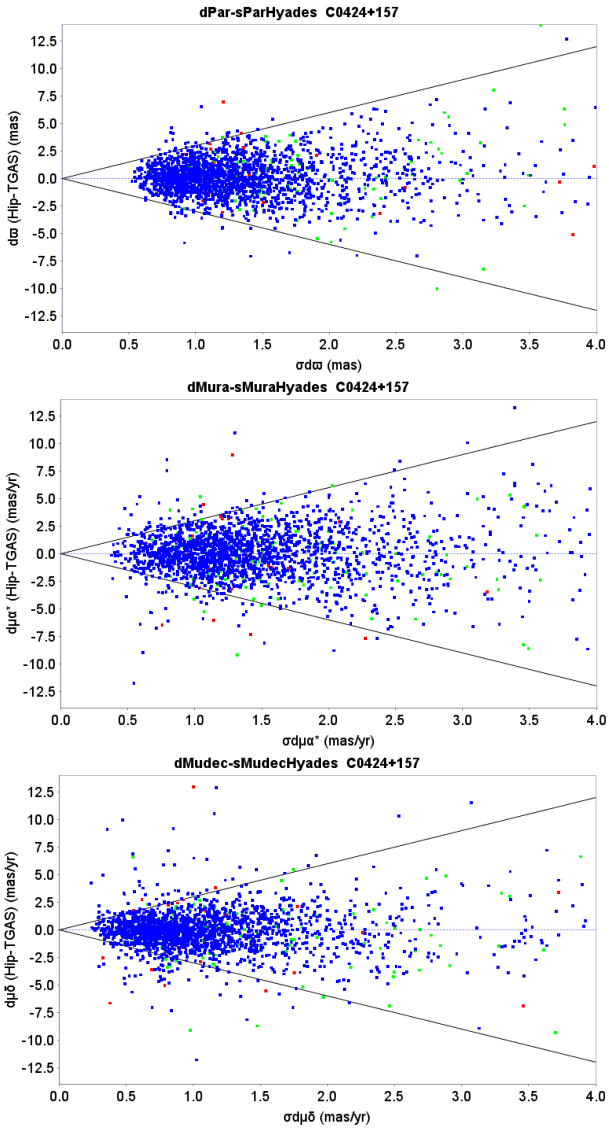

Fig. 8. Differences in astrometric parameters as a function of the *su* of the differences between the HIPPARCOS and TGAS solutions for stars, as measured in a field of 18° radius centred on the Hyades cluster. The blue dots represent clean 5-parameter solutions in the HIPPARCOS data. The red dots represent primarily accelerated solutions (so-called 7 and 9 parameter solutions). The green dots were solved as double stars in the HIPPARCOS solution. The two black lines show the ±3σ *su* levels. *From top to bottom*: parallaxes, proper motions in right ascension, proper motion in declination.

It must be left to the next *Gaia* data release, where the clanks are planned to be incorporated in the attitude model, to derive astrometric solutions from data much less seriously affected by this type disturbances. In the current TGAS data these events have to be accepted as unresolved and contributing to the overall astrometric noise.

The distribution of σ_ϖ (*su*) for the TGAS parallax measurements is furthermore affected by post-processing adjustments and filtering. The effect of the applied filter cutoff at 1 mas can be seen in Figs. 6 and 7. The majority of values for σ_ϖ is found in the range 0.22 to 0.35 mas.

Differences with the HIPPARCOS parallaxes and their *su* values show generally small systematics and underestimates of the combined *su* values of the parallax differences. For the an area of 18° radius field centred on the Hyades the differences for 2059 stars in common with the HIPPARCOS catalogue showed a difference of 0.14 ± 0.03 mas and a unit weight standard deviation of 1.25 (see also Fig. 8). The situation for the differences in proper motions is different. Because of the much longer epoch span for the TGAS data compared to the HIPPARCOS data, these differences will start to show the presence of long-period orbital effects on the HIPPARCOS proper motions of some stars, leading to more outliers than observed for the parallax differences.

There is at least one further aspect in which the data differ depending on the origin of the first epoch positions, and that is the addition of excess noise. Here the stars with first-epoch HIPPARCOS data are much more affected than those using *Tycho-2* data (Fig. 9). In addition, the application of excess noise, which effectively compensates the astrometric solution for imperfections in the data model, is predominantly found there where the number of observations is highest. These imperfections may be caused by the unresolved issues in the along-scan attitude reconstruction, such as clanks and hits, in which case the astrometric parameters can partly absorb these effects when relatively few observations are available. But it may also be caused by a very small mis-alignment between the HIPPARCOS first-epoch positions and the TGAS proper motion reference frame. Stars with first epoch *Tycho-2* positions are much less affected, as those positions had assigned significantly larger *su* values than the HIPPARCOS positions. In both cases, it would affect the astrometric solutions more severely when more *Gaia* data is available and relatively more weight in the astrometric solution comes from the *Gaia* data, as appears to be the case.

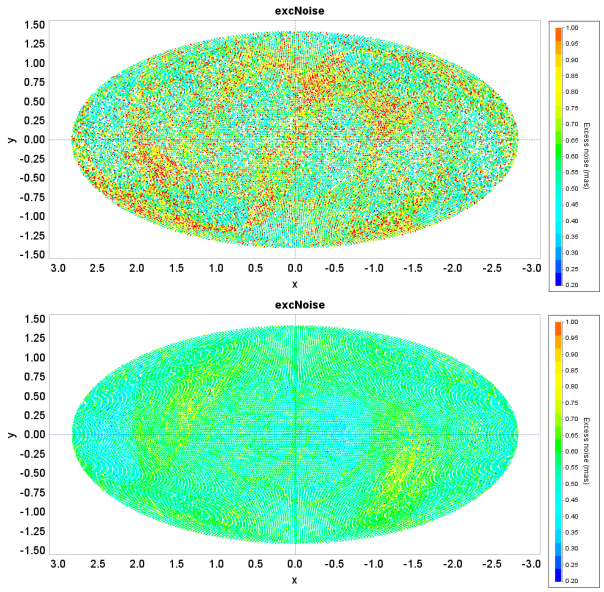

Fig. 9. Excess noise levels as applied to astrometric solutions. *Top*: for stars with HIPPARCOS first epoch positions; *bottom*: for stars with *Tycho-2* first epoch positions.

For the field of each cluster that we analyzed, the weighted mean differences, with *su* and unit-weight standard deviation, between the HIPPARCOS and TGAS data are provided in Table 8 for the parallaxes and proper motions. The unit-weight standard deviation is obtained by normalizing the error on each observation by its estimated *su*. In these comparisons only those stars are used which have simple 5-parameter astrometric solutions in the HIPPARCOS catalogue, while initial selection of stars in the field of a cluster was done independent of solution type.

3. General approach to the cluster data analysis

3.1. Cluster membership selection

Different approaches to cluster membership were used for the selection of cluster members, depending on the distance of the cluster. For the nearest clusters, the Hyades and initially also Coma Ber, the cluster membership has been determined based on first of all the coincidence in space within a volume around the assumed 3D position $\boldsymbol{R}_c$ of the cluster centre

$$\boldsymbol{R}_c = R_c \cdot \begin{bmatrix} \cos\alpha\cos\delta_c \\ \sin\alpha_c\cos\delta_c \\ \sin\delta_c \end{bmatrix}, \quad (1)$$

where $R_c = 1/\varpi_c$ is the assumed distance of the cluster, and (α_c, δ_c) are the equatorial coordinates of the projected cluster centre. It is further based on the assumed space motion $\dot{\boldsymbol{R}}_c$, and an assumed outer radius r of the cluster. The position in space of a potential cluster member is derived from its position and parallax, where the main uncertainty comes from the measured parallax. The observed proper motion and its standard errors are compared with the projection of the space motion of the cluster at the coordinates of the star. Determining the 3D positions of individual stars limits this method for the TGAS data to the nearest clusters. Details on the calculations and associated accuracies are presented in Appendix C, where it is shown that the uncertainties in the estimates of the 3D positions of individual stars increases with the square of the distance of the cluster. Thus, in future releases, with potentially a ten-fold improvement in parallax and proper motion accuracies, we may expect this method to be applicable up to about 100 to 150 pc distance.

For the more distant clusters, which in the case of the TGAS is any cluster more distant than about 50 to 75 pc, an iteration between membership selection and mean parallax and proper motion is performed. As first approximation for the parallax and proper motion (or space velocity) the astrometric data for open clusters from the HIPPARCOS data presented in fvl09 are used. Margins around these initial values are set generously to avoid introducing a bias on the *Gaia* solution.

3.2. Radial velocity projection

The radial velocity values used in these solutions play only a minor role through projection on the sky away from the cluster centre. Only in the analysis of the Hyades data this is an important quantity. The projection of the radial velocity V_{rad} onto the proper motion at a distance ρ from the projected cluster centre for a cluster with a mean parallax ϖ_c is given by:

$$\Delta\mu = \varpi_c \sin\rho V_{rad}/\kappa, \quad (2)$$

where the parallax and proper motion are expressed in mas and mas yr^{-1} respectively, and the radial velocity in km s^{-1}. The constant $\kappa = 4.74047$ provides the scaling factor between the proper motions and radial velocities. For example, the Pleiades cluster has a radial velocity of 8.6 km s^{-1} and most members are found within about 4.5 degrees on the sky from the cluster centre. At a parallax of about 8 mas this gives a maximum projection of the radial velocity of 1 mas yr^{-1}. This is at the same level as the internal velocity dispersion in the cluster (Vasilevskis et al. 1979). For the Hyades the radial velocity is, at 39 km s^{-1}, much higher. The spread over the sky and the parallax are three times larger. This leads to projection effects as large as 41 mas yr^{-1}. The projection effects for the tangential component of the space motion on the proper motions are still smaller, being proportional to $\cos\rho$. This amounts to 3 to 4 per cent for the Hyades (about 5 mas yr^{-1}) and less than 0.5 per cent for the Pleiades (less than 0.2 mas yr^{-1}). The observed proper motions are also affected by a systematic scaling of the cluster proper motion, depending on the offset along the line-of-sight for an individual cluster member, relative to the cluster centre. It can be observed as an increased dispersion in the proper motions of the cluster members along the direction of the cluster proper motion, an effect also known as the relative secular parallax. In the analysis of the cluster data this can be treated as an individual correction per star, based on the observed proper motion and parallax and their standard errors, and using the latest estimate of the cluster parallax and space velocity vector. Within the constraints of the current data set this is still only possible for the Hyades cluster.

4. The Hyades

The HIPPARCOS data for the Hyades cluster have been covered extensively by Perryman et al. (1998), Madsen (1999), de Bruijne et al. (2001) for the 1997 reduction, and in fvl09 for the new reduction. The HIPPARCOS input catalogue (Perryman et al. 1989) contained a selection of around 150 stars considered from earlier studies to be members of the Hyades cluster. Many of these are relatively bright and are not included in the TGAS catalogue. Because of the pre-selection done for the HIPPARCOS catalogue, there is only a small number of members found among the additional *Tycho-2* stars, and the total number

of members, with HIPPARCOS first epoch data, available for the current study is just over half the number that was available for the HIPPARCOS studies.

Starting with the cluster centre and parallax as derived in fvl09, 285 stars are found within the *Gaia* DR1 TGAS catalogue for which the position is likely to be within 16 pc from the assumed cluster centre in space, taking into account the *su* on the parallaxes of the individual stars and their positions as projected on the sky, relative to the projected cluster centre. The data selection has to be limited to relative errors on the parallaxes of at most 20 per cent, else distances to the individual stars become effectively undetermined. In Appendix C further details are presented on deriving the relative distance and its *su* for a star from the assumed cluster centre.

The next selection step calculates predicted proper motions from the space velocity of the cluster as projected perpendicular to the line of sight, and scaled according to the observed parallax. The details for the projection calculations are given in Appendix A.2. These predicted proper motions only account for the projection of the space motion of the entire cluster at the position on the sky and the observed parallax of the star. When comparing these predicted proper motions with the observed values there are three types of error contributions that need to be considered:

1. the *su* on the observed proper motions;
2. the *su* of the predicted proper motions, mainly resulting from the errors on the observed parallaxes;
3. the internal velocity dispersion and possible systematic motions in the cluster, estimated to be at a level of about 0.6 km s^{-1}.

In the *Gaia* DR1 TGAS data the first item is by far the smallest contribution, while the second and third items give comparable error contributions, at a level of 1 to 2 mas yr^{-1}. Added in quadrature, these three contributions provide the estimated uncertainty on the differences between predicted and observed proper motions. Applying this to the initial selection of 285 stars within the space of the Hyades cluster leaves 112 stars for which the observed proper motions are in both coordinates within 3 sigma from the predicted proper motions. Of the original 150 Hyades members found in the HIPPARCOS data only 85 are included here, primarily because of the problems still experienced with the calibrations for bright stars and filters applied to the TGAS data. A further 27 possible members with first epoch *Tycho-2* data are included. Figure 10 shows the observed differences in proper motions, and the membership selection based on this. It is clear that there is a generally very good agreement with the cluster distance and space motion as derived in fvl09.

A new value for the space motion $\dot{\boldsymbol{R}}_c$ of the cluster can be derived from applying Eq. (A.13) in a least squares solution with the observed proper motions and parallaxes for the cluster members, indicated with index i:

$$\begin{bmatrix} -\sin\alpha_i & \cos\alpha_i & 0 \\ -\cos\alpha_i \sin\delta_i & -\sin\alpha_i \sin\delta_i & \cos\delta_i \end{bmatrix} \cdot \dot{\boldsymbol{R}}_c = \begin{bmatrix} \kappa\mu_{\alpha\cdot,i}/\varpi_i \\ \kappa\mu_{\delta,i}/\varpi_i \end{bmatrix} \tag{3}$$

The standard errors on the observations are derived from the errors on the proper motions and parallaxes and a contribution from the internal velocity dispersion. The value for the latter was determined at 0.58 km s^{-1}, which should be interpreted as the weighted-average velocity dispersion over the whole cluster, where most of the weight comes from the projected centre of the cluster. Two solutions were obtained, the first solution is based on the proper motions only, and in the second solution an additional observation of the radial velocity of the cluster was added. For this second solution a value of $V_{\rm rad} = 39.1 \pm 0.2$ km s^{-1} was used, as derived by Detweiler et al. (1984) based on radial velocity measurements for 17 non-variable cluster members. The two solutions gave the following results (first without, second with radial velocity constraint):

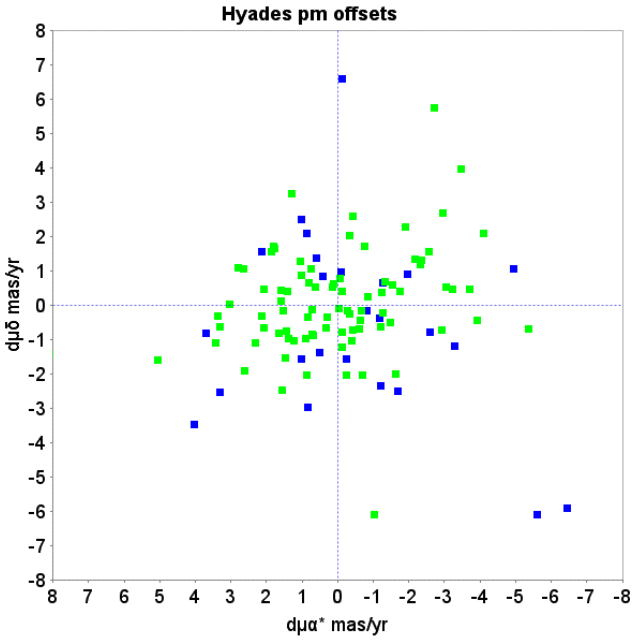

Fig. 10. Differences between predicted and observed proper motions for stars within the space volume of the Hyades cluster, showing the results for 112 possible members. Green dots: First epoch HIPPARCOS; blue dots: first epoch *Tycho-2*.

$$\dot{\boldsymbol{R}} = \begin{bmatrix} -6.03 \pm 0.08 & -6.14 \pm 0.03 \\ 45.56 \pm 0.18 & 45.28 \pm 0.02 \\ 5.57 \pm 0.06 & 5.48 \pm 0.02 \end{bmatrix} \text{km s}^{-1}. \tag{4}$$

A standard deviation of 1.00 was obtained by adjusting the internal velocity dispersion to the value of 0.58 km s^{-1} given above. Of the 112 possible members entering the solution, initially 6, and later (in the fitting of the kinematically improved parallaxes, see Appendix A.3) still 3 more were rejected in the iterations, leaving 103 probable members, for which identifiers are presented in Table D.1, and a map is shown in Fig. D.2.

The following data apply to the second solution in Eq. (4), i.e. including the mean radial velocity measurement for the cluster as an observation. The position of the convergent point is

$$\begin{aligned} \alpha_{\rm conv} &= 97\overset{\circ}{.}73 \pm 0\overset{\circ}{.}04 \;\; = 6^{\rm h}30.92^{\rm m}, \\ \delta_{\rm conv} &= \;\; 6\overset{\circ}{.}83 \pm 0\overset{\circ}{.}03 = 6^{\circ}49.8'. \end{aligned} \tag{5}$$

The result in Eq. (4) can be transformed back to a radial velocity and proper motion for the cluster centre:

$$\begin{aligned} v_{\rm rad,c} &= \;\; 39.10 \pm 0.02 \;\; \text{km s}^{-1}, \\ \mu_{\alpha*,c} &= 104.92 \pm 0.12 \;\; \text{mas yr}^{-1}, \\ \mu_{\delta,c} &= -28.00 \pm 0.09 \;\; \text{mas yr}^{-1}. \end{aligned} \tag{6}$$

From the first solution, using only proper motion data, the radial velocity of the cluster is recovered at a value of 39.38 ± 0.16 km s^{-1}, not significantly different from the spectroscopic

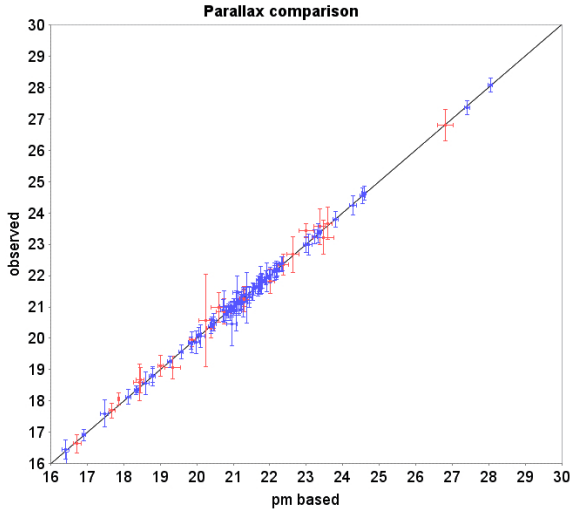

Fig. 11. Comparison between the parallaxes as measured and kinematically improved by means of the proper motion data. The blue data points use HIPPARCOS data as first epoch, the red data points use *Tycho-2* data instead.

value, considering the different size and composition of the radial velocity sample.

The weighted mean parallax for the 103 probable member stars (as projected on the line of sight towards the cluster centre) is

$$\varpi_c = 21.39 \pm 0.21 \text{ mas}, \quad (7)$$

in good agreement with earlier HIPPARCOS-based determination in fvl09, which gave a value of 21.53 ± 0.23 mas. The parallax is equivalent to a distance of 46.75 ± 0.46 pc and a distance modulus of 3.349 ± 0.021 mag. The error given is the *su* on the mean. The standard deviation is much larger, at about 8 mas, due to the size of the cluster relative to its distance. The mean position on the sky of the 103 selected stars is

$$\alpha_c = 66.^\circ85 = 4^h27.4^m,$$
$$\delta_c = 17.^\circ04 = 17^\circ2.4'. \quad (8)$$

The largest separation on the sky for a cluster member as found here is 17.2 degrees from the cluster centre, equivalent to 14.5 pc. There is an indication of more cluster members found at still larger distances from the centre, but whether these are actually bound to the cluster is unlikely and unclear from the data at this stage. For all numbers given above it should be realized that they are dependent on the initial values and criteria used for member selection, such as the maximum radius of the field and the internal velocity dispersion. However, those dependencies are small, as the figures shown here are the result of a converged iterative process, in which the assumed parallax, cluster centre position and space velocity vector were adjusted.

For the next step the reduced proper motions are derived as described in Appendix A.3. This allows to extract the differential parallax information from the proper motions, the so-called kinematically improved parallaxes, a process first described by Madsen (1999). Figure 11 shows the comparison between the parallaxes as published in the TGAS catalogue and the kinematically improved parallaxes, with the *su* error bars for both determinations. Including the proper motion data reduces the standard errors on the parallaxes by about a factor two to three, down to a level of 0.1 to 0.2 mas (Fig. 12), equivalent to relative errors below 1 per cent. A relative error on the parallax of 1 per cent

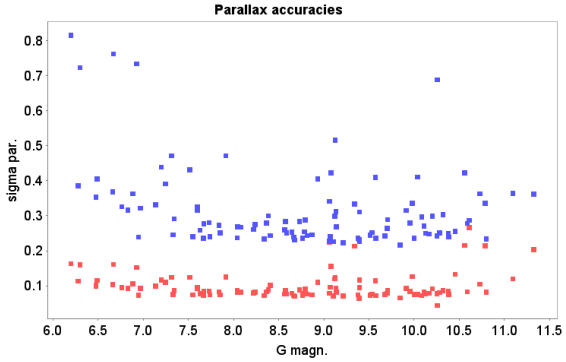

Fig. 12. Standard uncertainties on the parallax determinations. Blue dots: as derived from the TGAS catalogue; red dots: kinematically improved parallaxes using the cluster space velocity vector.

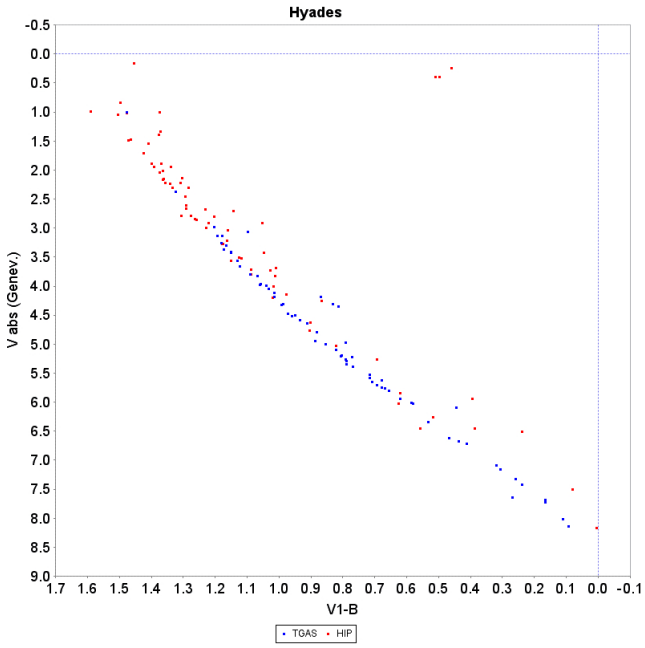

Fig. 13. Absolute magnitudes and colour indices in the Geneva photometry for cluster members, after applying distance moduli based on individual kinematically improved parallaxes. The red dots represent stars not present in the TGAS catalogue, but with similarly treated data in fvl09.

is almost equivalent to an uncertainty in the distance modulus of 0.02 mag. This shows in the HR diagram for the cluster in the form of a very narrow main sequence (Fig. 13). It is the reconstruction of a multitude of such sequences, for clusters of different age and composition, that will provide the detailed observational isochrones that may provide further insights into the many processes that are involved in producing theoretical isochrones.

The process of improving parallaxes by means of proper motion data in the Hyades is ultimately limited by the internal velocity dispersion in the cluster. This contributes on average an uncertainty at about the same 1 per cent level as the current determination of the parallaxes. In the calculations of the standard uncertainties on the kinematically improved parallaxes this has been taken into account in as far as possible. For future releases of the *Gaia* data, with improved accuracies for the parallaxes and proper motions, the process presented here can be inverted, and used to reconstruct the internal velocity dispersion throughout the cluster.

Table 3. Spatial densities in the Hyades cluster for 106 selected stars (before the final elimination of 3 possible members).

r_1	r_2	stars	log d
0	1	1	–0.62
1	2	10	–0.47
2	3	15	–0.72
3	4	14	–1.04
4	5	13	–1.29
5	6	10	–1.58
6	8	16	–1.89
8	11	12	–2.45
11	16	15	–2.89

Notes. r_1 and r_2 are the inner and outer radius in pc. d gives the density in number of stars per cubic parsec.

Table 3 gives the spatial densities for the 106 stars used in the current analysis. Considering the low number of stars and various selections that have been applied to the TGAS data, it seems a bit premature to further interpret and analyse the space density profile.

A full list of the source identifiers, cross matches with HD identifiers and the kinematically improved distance moduli is presented in Table D.1. It is these individual kinematically improved distance moduli that should be used in the construction of the Hyades HR diagram.

5. The nearby clusters

5.1. General considerations

For the following clusters, the mean parallax and proper motions have been determined while taking into account the local projection effects and the full covariance matrix for the astrometric solution of each member star. Membership selection was based on position, proper motion and parallax information, but will always be slightly ambiguous, and in particular for most of the younger clusters that are still close to, or even embedded into, an OB association. Because of the high levels of error correlations present in the astrometric parameters of the individual stars, the solution for the mean proper motion and parallax have to be done simultaneously, solving Eq. (A.3) after deconvolving with the square root of the inverse of the noise matrix. The noise matrix takes account of the correlations and standard uncertainties on the astrometric parameters as well as the internal velocity and parallax dispersions, all as described in Appendix A. Here we use a velocity dispersion of 0.6 km s^{-1} and a position dispersion along the line of sight of 5 pc was used. The outer radius of the cluster has been set at 15 pc. All results have a slight dependency on these assumptions, mostly where it affects membership selection.

Mean positions for the member stars, as an estimate for the projected position of the cluster centre, have been determined from the tangential projection of the member-star positions on the sky relative to an assumed position of the cluster centre (see Appendix B). The new centre was then obtained through deprojection on the sky. As corrections tend to be very small, this process generally converged rapidly through the iterations.

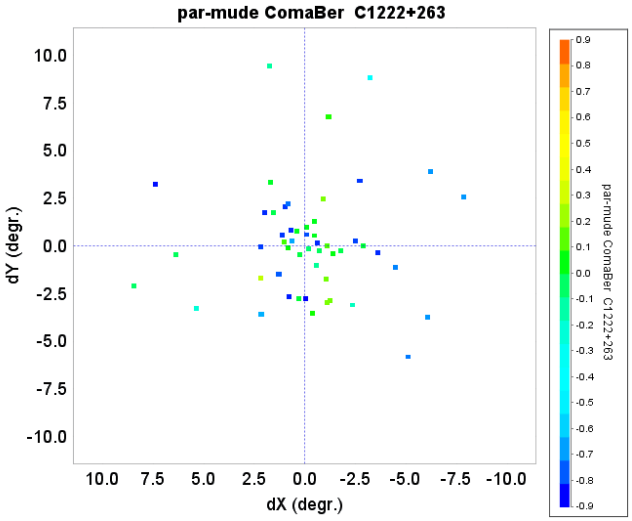

Fig. 14. Stars in the Coma Berenice cluster, colour coded according to the error-correlations between the parallax and proper motion in declination. The dark blue dots, representing strong negative error correlations, have first epoch *Tycho-2* data, the green dots, representing near-zero correlations, have first epoch HIPPARCOS data.

5.2. The Ursa Major moving group and the Coma Berenices cluster

Very little can be said here about the Ursa Major moving group. The brightest members of the group are not included in the TGAS catalogue, and a search for fainter members coinciding (in proper motion) with the local projection of the space velocity of the group showed no more than about three possible candidates. The Coma Berenices cluster is more interesting at this stage. It has first been analysed in the same way as the Hyades cluster. Starting with the HIPPARCOS solution for the cluster, a volume of 15 pc radius at a distance of 86.7 pc was initially searched. Likely cluster members were found to be restricted to within a radius of 13 pc only, and the distance had to be adjusted to 85.5 pc. Within that volume 142 stars are found.

In determining of the space velocity of the cluster, an additional "observation" was added for the mean radial velocity at the cluster centre in order to stabilize the solution, similar to the processing of the Hyades cluster. Assuming a radial velocity of -1.2 km s^{-1}, the space motion is found to be

$$\dot{\boldsymbol{R}} = \begin{bmatrix} -0.41 \pm 0.85 \\ 4.86 \pm 0.11 \\ -4.11 \pm 0.42 \end{bmatrix} \text{ km s}^{-1}, \tag{9}$$

as based on 44 stars identified as probable members. Of these, 25 have HIPPARCOS and 19 have *Tycho-2* first epoch data. The space motion is equivalent to the following values at the centre of the cluster:

$$\begin{aligned} v_{\mathrm{rad,c}} &= -\ 1.89 \pm 0.10 \text{ km s}^{-1}, \\ \mu_{\alpha*,\mathrm{c}} &= -12.04 \pm 0.15 \text{ mas yr}^{-1}, \\ \mu_{\delta,\mathrm{c}} &= -\ 8.97 \pm 0.19 \text{ mas yr}^{-1}. \end{aligned} \tag{10}$$

The weighted mean parallax for these stars is 11.69 ± 0.06 mas, which differs by 1.2σ from the determination in fvl09 (11.53 ± 0.12 mas). The parallax is equivalent to a distance of 85.5 ± 0.4 pc, and a distance modulus of 4.66 ± 0.01 mag. The distance moduli for individual stars in the cluster range from about 4.47 to 4.84, and individual parallaxes need to be taken into account when reconstructing absolute magnitudes. Compared with

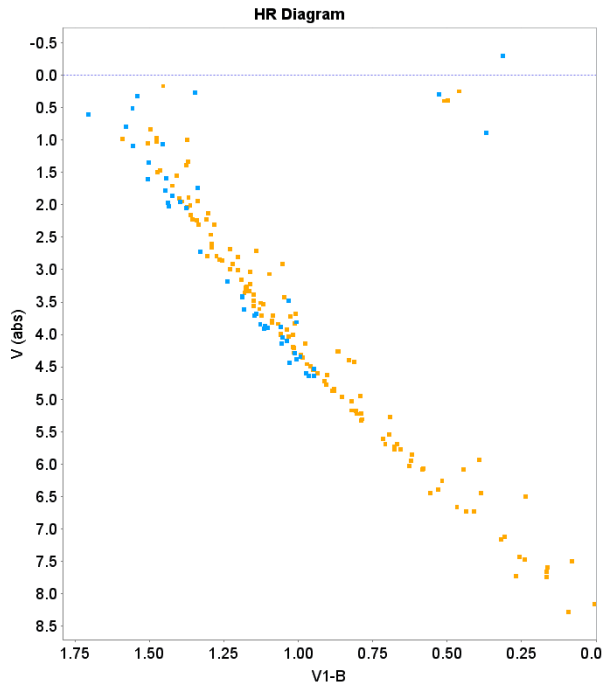

Fig. 15. HR diagram for the Coma Berenices cluster (light blue) compared with the Hyades cluster (orange-red). Geneva photometry.

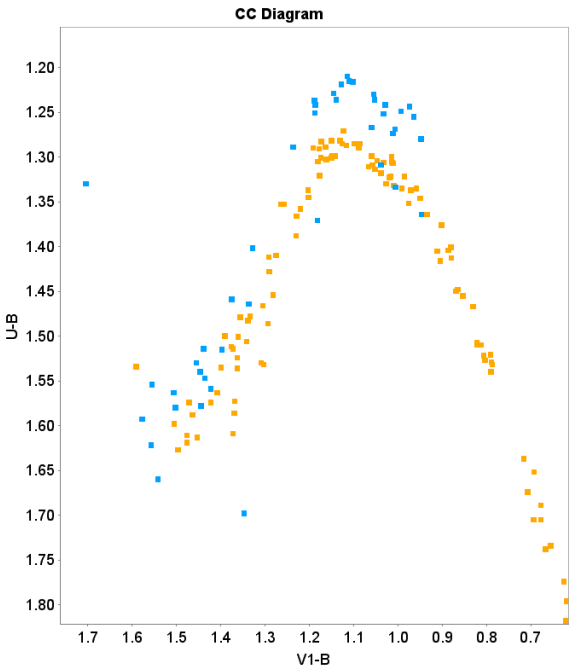

Fig. 16. Two colour diagram for the Coma Berenices cluster (light blue) compared with the Hyades (orange-red), showing the so-called Hyades anomaly.

isochrone fitting by Pinsonneault et al. (1998), who derived a distance modulus of 4.54 ± 0.04, there is still a difference of nearly 3σ. Even more discrepant is the MAP-based trigonometric parallax for the cluster by Gatewood (1995), which gave a parallax of 13.54 ± 0.54 mas, a difference in distance modulus (4.34 ± 0.09) of 0.3 mag. Also the parallax derived by Makarov (2003) is, at a value of 12.40 ± 0.17 mas off by 4σ, and in distance modulus by 0.13 mag.

The cluster centre is confirmed to be at

$$\alpha_c = 186\overset{\circ}{.}02 = 12^h24.08^m,$$
$$\delta_c = \ \ 25\overset{\circ}{.}95 = 25^\circ57'. \qquad (11)$$

All values are subject to minor adjustments depending on the exact selection criteria. They can be compared with the data presented in Table 6, which have been obtained with the weighted mean parallax and proper motion method as described in Appendix A. For this solution a field with a 10.4 degrees radius was investigated, containing 6717 stars, 52 of which were considered possible members of the Coma Ber cluster. Two of the 52 possible members were eliminated during the iterative solutions for the astrometric parameters of the cluster. For 786 stars and 28 cluster members in common with the HIPPARCOS catalogue, the weighted mean differences in the astrometric parameters are shown in Table 8. The differences are all well within the range of the formal *su* values, and are primarily due to slight differences in member selection. A full list of the 50 probable member stars is presented in Table D.2 and shown as a map in Fig. D.4. The HR diagram in Geneva photometry is shown in Fig. 15. As has been assessed before, these clusters are of closely the same age, with the impression of Coma Berenices cluster being slightly younger. Also in chemical composition they appear to be very similar (Heiter et al. 2014). However, there is a marked difference in the two-colour diagrams (Fig. 16) for late F and G stars, a difference which in field stars is directly related to luminosity differences in the sense that it would imply the Hyades stars to be more luminous at the same temperature than those in the Coma Berenices cluster. This is the so-called Hyades anomaly, first noted half a century ago by van Altena (1966).

5.3. The Praesepe cluster

The Praesepe cluster has been investigated over a 5.47 degrees radius field, an area for which 2082 stars are contained in the TGAS catalogue, 156 of which are also contained in the HIPPARCOS catalogue. 84 stars were selected as possible members of Praesepe, of which 5 were later eliminated in the iterative solutions for the astrometric parameters of the cluster. The weighted mean differences in this field between the TGAS and HIPPARCOS astrometric parameters for 146 stars (with a simple 5-parameter solution, excluding 10 stars with complex solutions), of which 23 are identified as probable cluster members, are summarized in Table 8.

There is a significant increase in the number of member stars with respect to the solution in fvl09, from 24 to 79 stars. Probable members are found projected up to 4.4 degrees from the cluster centre, equivalent to a distance of about 14 pc, much like what is observed in the Hyades. The Praesepe field shows generally strong to very strong correlations for the astrometric parameters of individual stars, in particular for stars for which *Tycho-2* first epoch data was used. These are the red points in Fig. 17.

As was noticed before in fvl09, the Praesepe and Hyades clusters appear to be very similar in composition and age. Figure 18 shows the combined HR diagram for the two clusters and the closely coinciding main sequences. In contrast, the main sequence of the Coma Ber cluster, considered to be of the same age as the Hyades, appears to be sub-luminous by about 0.1 to 0.15 mag with respect to the Hyades and Praesepe. This difference has increased slightly (by 0.06 mag) in the current analysis with respect to fvl09.

5.4. The Pleiades cluster

The Pleiades cluster has been investigated over a 6.7 degrees radius field, for which the TGAS catalogue contains 4996 stars,

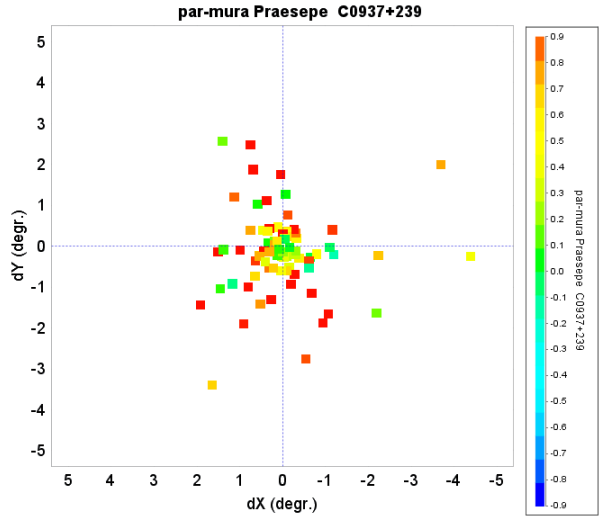

Fig. 17. Distribution of stars in the Praesepe cluster, colour coded according to the error-correlation factor between the parallax and the proper motion in right ascension for the individual solutions. The red dots, representing the highest correlations, belong to stars with *Tycho-2* first epoch positions.

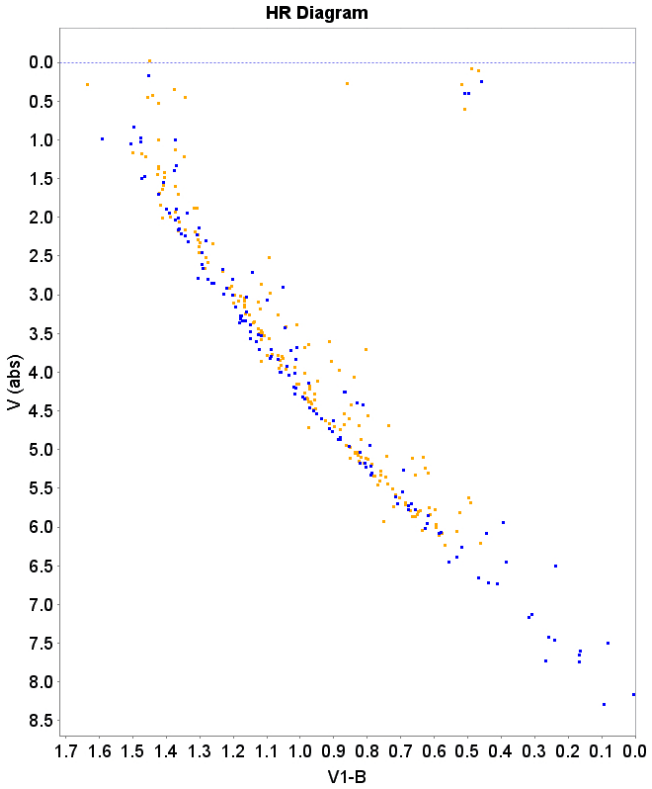

Fig. 18. HR diagram in Geneva photometry for the Hyades (blue dots) and Praesepe (orange dots) clusters. For the Hyades stars individual kinematically improved parallaxes were used, for the Praesepe stars the common cluster parallax. As was also observed in fvl09, the two main sequences accurately coincide.

160 of which were marked as possible cluster members. Within that area 325 stars are in common with the HIPPARCOS catalogue, and of these 285 have single-star 5-parameter astrometric solutions (44 of which are probable cluster members), and a *su* on the difference in parallax between the HIPPARCOS and TGAS solutions that is below 3 mas. For those stars the mean

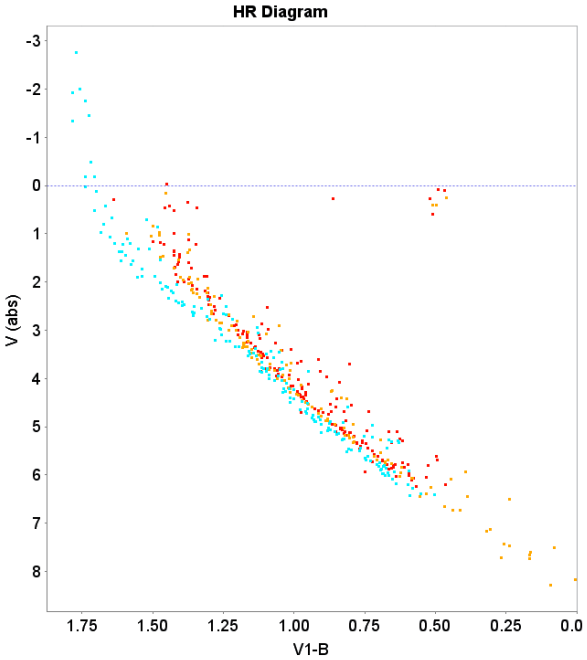

Fig. 19. Diagram for the Pleiades (light blue) compared with the Hyades and Praesepe clusters (orange, red) in Geneva photometry.

Table 4. Systematic differences (HIPPARCOS – TGAS) between the astrometric parameters for 134 stars in the Pleiades field.

Diff.	Mean	Stand.dev.	units
$d\varpi_c$	0.60 ± 0.12	1.27	mas
$d\mu_{\alpha*,c}$	0.22 ± 0.14	1.58	mas yr^{-1}
$d\mu_{\delta}$, c	0.01 ± 0.15	2.06	mas yr^{-1}

difference in the astrometric parameters between the HIPPARCOS and TGAS solutions are shown in Table 8. In a smaller field, at 4.5 degrees radius more compatible with the area of the sky used in the HIPPARCOS determination of the Pleiades parallax, the differences are as shown in Table 4.

From the TGAS catalogue we can identify 155 possible members, based on their proper motions, parallaxes and confirmed by consistency in the HR diagram. The mean parallax for 152 stars confirmed as Pleiades members in the subsequent iterations for the cluster astrometric solution is

$$\varpi_c = 7.48 \pm 0.03 \text{ mas}. \quad (12)$$

Details on the 152 probable Pleiades members are presented in Table D.3 in Appendix D.3.

The difference with the Pleiades parallax as derived in fvl09 is part of an overall parallax difference in that part of the sky between the HIPPARCOS and TGAS catalogues, for which there is currently no explanation. No such differences were observed between the three independent reductions of the HIPPARCOS data (the two reductions from which the first catalogue was constructed, and the new reduction). The current TGAS parallax for the Pleiades, dominated by fainter cluster members, agrees with other studies of the cluster distance that are also based on the fainter members of the cluster.

The HR diagram for the Pleiades is shown in comparison with the Hyades and Praesepe clusters in Fig. 19.

The differences in parallax for this field between the HIPPARCOS and TGAS solutions are not entirely random, but show correlations with brightness or colour (Fig. 20). From the

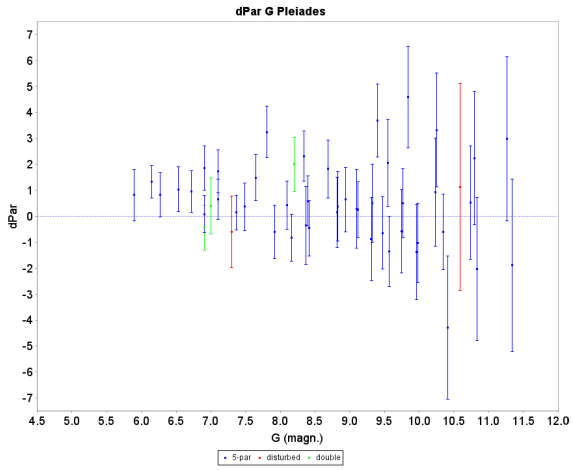

Fig. 20. Parallax differences between the HIPPARCOS and TGAS solutions as a function of the *Gaia G* magnitude for members of the Pleiades cluster.

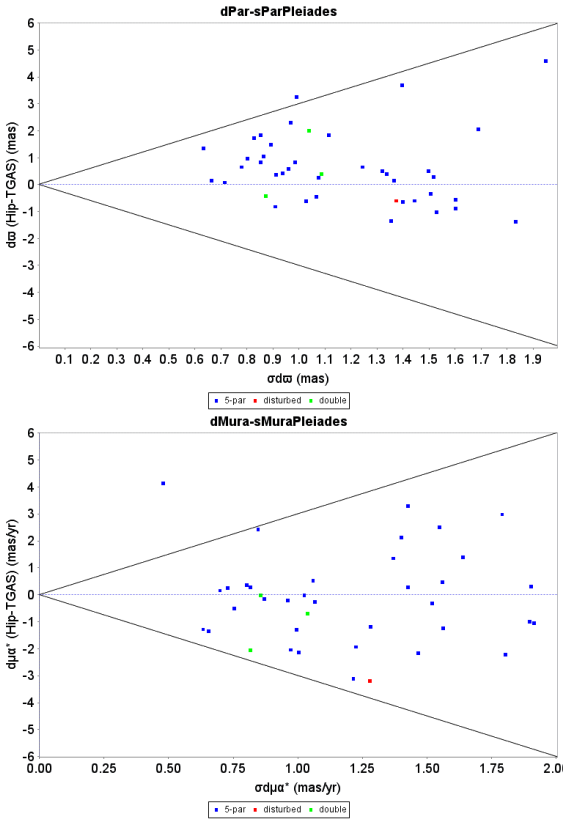

Fig. 21. Differences in parallax (*top*) and proper motion in Right Ascension (*bottom*) between the HIPPARCOS and TGAS solutions, for members of the Pleiades cluster, and as a function of the errors on the differences.

small volume of data and the strong correlation between brightness and colour it is not possible to distinguish which of these is the actual source of the correlation. This also affects comparisons between differences and their *su* values, as the latter are, for the HIPPARCOS solution in particular, strongly correlated with brightness.

It is noted that there is a similar difference in the proper motion in Right Ascension (Fig. 21), and that in the TGAS solution there is strong negative error correlation between the parallax and that component of the proper motion for stars with first

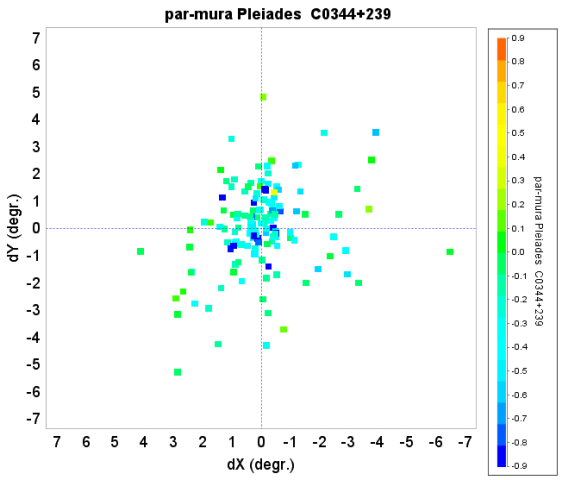

Fig. 22. Error correlation levels for Pleiades members as a function of position relative to the cluster centre. For reasons not understood, correlations appear to be stronger towards the cluster centre. The blue points, representing the negative correlation coefficients, all have *Tycho-2* first-epoch data. For stars with HIPPARCOS first epoch data (green points) the correlations are almost zero.

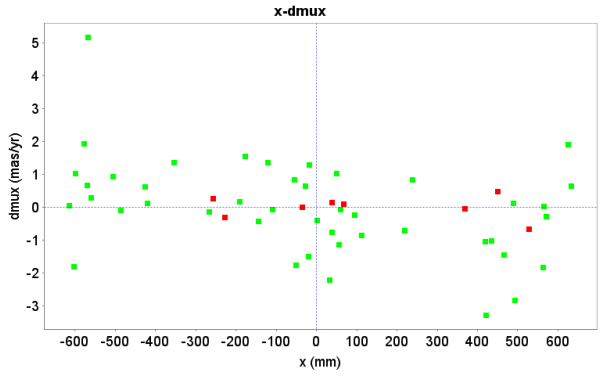

Fig. 23. A comparision between the proper motions in Right Ascension as measured from photographic plates (Vasilevskis et al. 1979) and as published in TGAS. The red dots represent stars with first epoch HIPPARCOS data, the green dots have first epoch *Tycho-2* data.

epoch data from *Tycho-2* (which dominate the parallax determination for the Pleiades), in particular towards the centre of the cluster (Fig. 22).

Another potentially interesting comparison is that with the high-accuracy differential, ground-based proper motion studies of the Pleiades, such as Vasilevskis et al. (1979), and the proper motions found in the TGAS catalogue. In both cases accuracies significantly better than 1 mas yr^{-1} are claimed. The epoch coverage in this ground-based study is 77 yrs (1899 to 1976, all taken with the same telescope at the same site), with good coverage up to the mid 1940s (which were used by Hertzsprung 1947 in his study of the Pleiades) and a large volume of data in 1975/76. Of the 146 stars in this study, 52 are contained in the TGAS catalogue, of which 8 have first epoch HIPPARCOS data. Scale corrections to the proper motions in Right Ascension (×0.90) and Declination (×1.05) as well as a colour dependence in Declination ($-0.43\ (B-V)$) had to be applied, after which a unit-weight standard deviation of 1.14 was obtained for the differences in proper motion, largely confirming the accuracies claimed in both Vasilevskis et al. (1979) and TGAS. When also considering the 44 stars with *Tycho-2* first epoch data the unit-weight standard deviation increases to 1.29, which may

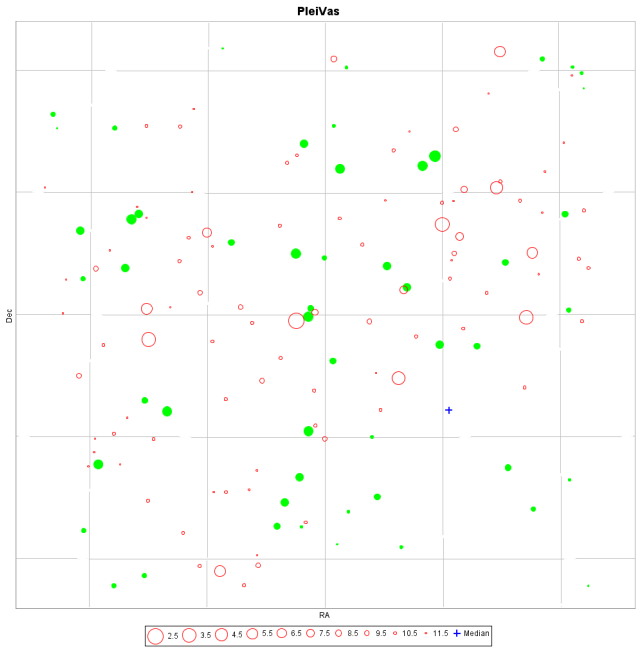

Fig. 24. Central area of the Pleiades cluster as defined by the brightest stars, showing as filled green circles all stars in this field that are included in TGAS and as open red circles those not included. The grid size is about 0.33 degrees. The cluster centre as defined by the cluster members in the TGAS catalogue, covering a much larger field, is indicated by the cross.

indicate a slight underestimate of the proper motion uncertainties for those stars in the TGAS catalogue.

Figure 24 shows the central field of the Pleiades cluster, as defined by the brightest stars, indicating which stars are included in TGAS. All the brightest stars are missing. These are the same stars that dominated by their weight the HIPPARCOS parallax and proper motion solution for the Pleiades. It is also noted that the cluster centre as determined based on the fainter stars in the cluster, is markedly offset from the mean position of the bright stars. However, a similar offset is not observed in a sample of 333 probable Pleiades cluster members as extracted from the URAT1 catalogue (Zacharias et al. 2015).

Although it may seem tempting to suggest that this has resolved the so-called Pleiades issue, there are still some unexplained, and quite serious, issues left. The systematic parallax difference at a level of 0.6 mas in the Pleiades field affects all stars in that field, not just those of the Pleiades cluster. This is relevant, as field stars in the same part of the sky have been observed to show no anomalous luminosities when applying HIPPARCOS parallaxes (Kim et al. 2016). It is a difference of which there has been no sign in comparisons between the three independent HIPPARCOS reductions (the two reductions that contributed to the 1997 catalogue, and the new reduction). Strongly correlated errors over an area of more than a degree in diameter are very difficult to explain because of the rapidly decreasing fraction of shared scans for pairs of stars with increasing separations on the sky. Differences between the 1997 and 2007 reductions only show localized features on a scale of 0.5 to 1.0 degrees on the sky. Those features could be attributed to smoothing over clanks and hits in the 1997 publication. It should be noted too that, unlike for *Gaia*, the basic angle for HIPPARCOS was observed to be only slowly evolving, and stable at the sub-mas level over 24 h periods, for almost the entire duration of the mission. Hits and clanks were very much less frequent for HIPPARCOS than they are for *Gaia*, and were in addition in the attitude reconstruction for the new reduction fully accounted for. For the *Gaia* GDR1 this is not yet the case. On the other hand, the apparent internal consistency of the TGAS data, such as shown for example by the distribution of negative parallaxes with respect to their formal errors, also does not leave much room for a discrepancy at the level observed for the Pleiades solutions.

5.4.1. HR diagrams of Pleiades and Praesepe

Main sequence fitting has long being considered a powerful tool to derive distances. In the *Gaia* era, when distances are known by direct measurements, it provides a powerful test-bed for stellar models. Having this goal in mind, we compare the HR diagrams of two of the most studied clusters, Pleiades and Praesepe with stellar models, focusing on the main sequence fitting. We make use of literature values for the cluster ages and extinctions that are well constrained and have been derived using independent methods.

In the case of the Pleiades, we assume an age of about 130 Myr that is derived using the lithium depletion boundary (Barrado y Navascués et al. 2004). We point out that the error budget is quite large, going from 120 to 150 Myr, depending on differences in the stellar models and on adopted photometry. The extinction $A_V = 0.1$ is by Stauffer et al. (1998) and the metal content is derived by high resolution spectroscopy, [Fe/H] = +0.03 (Soderblom et al. 2009).

Using a similar approach for Praesepe, we assume a metallicity from recent high resolution spectral analyses that have pointed in favour of super-solar values, going from [Fe/H] = +0.27 ± 0.10 (Pace et al. 2008), to [Fe/H] = +0.12 ± 0.04 (Boesgaard et al. 2013). We adopt an extinction of $A_V = 0.1$ (Taylor 2006). The age of Praesepe is less well constraint, since techniques such as lithium boundary depletion are not applicable to intermediate-age clusters. Stellar isochrones seem to suggest an age range of several hundred Myr, with the main-sequence turnoff giving an age of about 600 to 650 Myr for the most massive members (Fossati et al. 2008). Applying rotating stellar models, Brandt & Huang (2015) derive a best-fit age of about 800 Myr, in agreement with fvl09. Here we assume a conservative estimate of 600 Myr.

Figure 25 presents the HR diagram of the Pleiades in the $(B-V)$-M_V and $(V-I)$-M_V planes, using Stauffer et al. (2007) data corrected by the *Gaia* distance modulus and interstellar absorption. Only about 100 stars in common between *Gaia* and Stauffer et al. (2007) photometry were found. We compare the data with several sets of commonly used stellar models, either including stellar rotation (Ekström et al. 2012) or without (Baraffe et al. 2015; Chen et al. 2015).

Figure 26 presents the HR diagram of the Pleiades and Praesepe in the Geneva photometry (Rufener 1989) compared with Lejeune & Schaerer (2001) Geneva isochrone data base. This data set includes Schaller et al. (1992) stellar tracks for solar and super-solar metallicity that are of interest here. Although these stellar models make use of quite old prescriptions, we note that, concerning the main sequence, the combined effects of no rotational mixing and a stronger overshoot parameter $d_{\rm over}/H_P = 0.2$ (used in the '92 models) mimic the effect obtained in the more recent models (Ekström et al. 2012) including rotational mixing and an overshoot parameter of 0.1.

A discussion on the age of the Pleiades and Praesepe is outside the scope of the paper. Here we point out that broadly speaking the HR diagrams of Pleiades and Praesepe are reasonably fitted. The new Pleiades parallax seems to solve the discrepancy

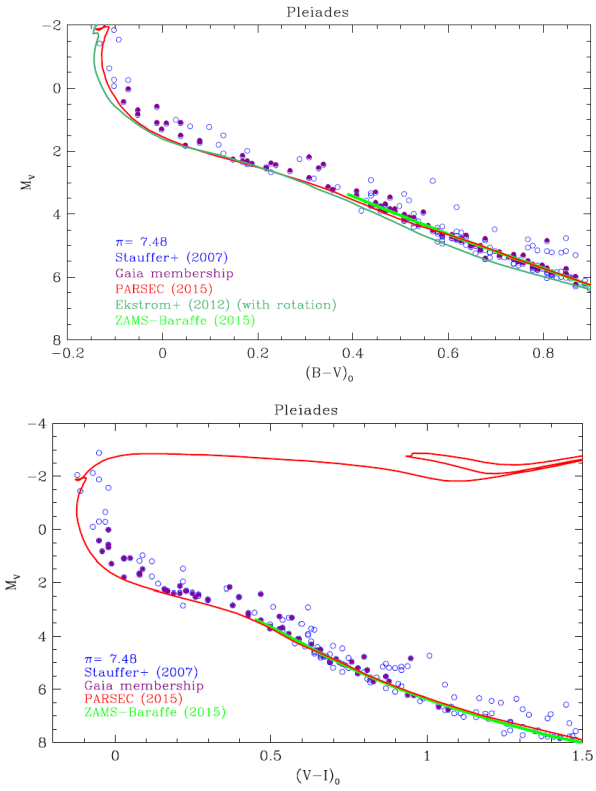

Fig. 25. M_V, $(B-V)_0$ HR diagram of the Pleiades, with several sets of commonly used isochrones (*top*). Filled dots: mebers confirmed with *Gaia* data; open dots: other cluster members. *Bottom panel* is the analogous in the M_V, $(V-I)_0$. We assume an age of 130 Myr, solar metallicity, $A_V = 0.1$.

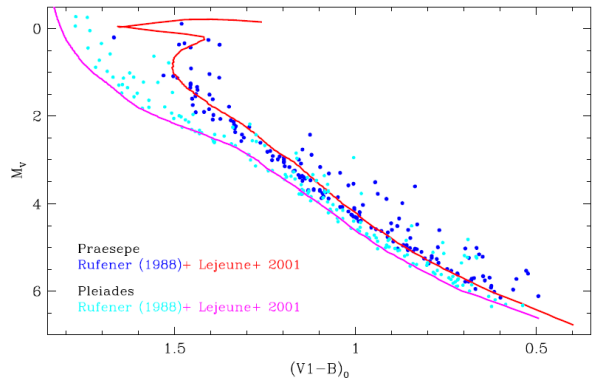

Fig. 26. M_V, $(V1-B)_0$ HR diagram of the Pleiades (cyan dots) and Praesepe (blue dots), compared with Geneva stellar models.

between HIPPARCOS distance and those estimated via HRD fitting (An et al. 2007). However, it is clear that even in the zero age main sequence region (in the magnitude range $M_V \sim 3-6$), the fit critically depends on the ingredients of the stellar models and is often far from optimal as already noticed by Bell et al. (2012).

5.5. The α Per cluster

The α Per cluster has been investigated over a 5.3 degrees radius field, an area for which 5475 stars are contained in the TGAS catalogue, 323 of which are also contained in the HIPPARCOS catalogue. The weighted mean differences in this field between

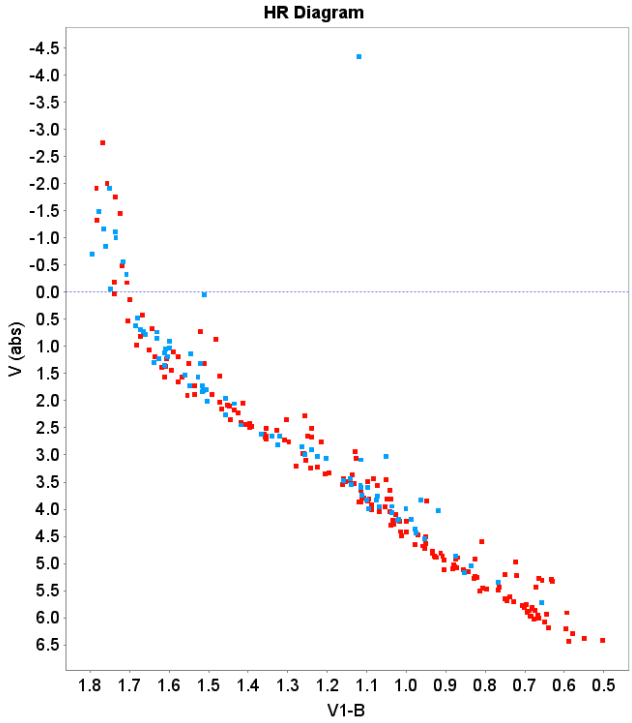

Fig. 27. Geneva photometry HR diagram for the α Per cluster (blue dots) compared with the data on the Pleiades cluster (red dots). Reddening corrections were applied for both clusters. Geneva photometry.

the TGAS and HIPPARCOS astrometric parameters for 295 stars (only those with a basic 5-parameter HIPPARCOS solution) of which 50 are identified as probable cluster members are summarized in Table 8.

The parallax as determined for the α Per cluster corresponds to a distance modulus of 6.17 ± 0.01, which is within 1σ of the distance modulus give in Pinsonneault et al. (1998). The difference with the parallax determination in fvl09 is also within one sigma. A list of member stars and a map of the cluster are presented in Appendix D.5. Figure 27 shows the Geneva photometry for stars in the α Per cluster that have been confirmed as cluster members from the TGAS or the HIPPARCOS astrometric data. The data is shown in comparison with the Pleiades cluster photometry.

There is no indication of increased scatter on the main sequence, at least compared to what is observed for Pleiades. This may contradict the suggested relatively high fraction of binary stars in the α Per cluster, as reported to by Sheikhi et al. (2016).

5.6. The cluster IC 2391

The cluster IC 2391 was examined over a 6.3 degrees radius field, in which 13 999 stars are contained in the TGAS catalogue, 45 of which were indicated as possible cluster members. Only a small fraction of those stars have HIPPARCOS first epoch data, 444 stars of which 8 are possible cluster members. The mean parallax and proper motion for the cluster are presented in Table 6. The list and maps of cluster members shown in Appendix D.6.

Figure 28 shows the error correlations for stars in the field of the cluster that have *Tycho-2* first epoch positions. There are substantial and systematic differences in error correlations between the astrometric parameters over the field of the cluster. Of particular interest here is that the brightest star in the field of IC 2391 is not a cluster member (fvl09). Three more stars indicated as

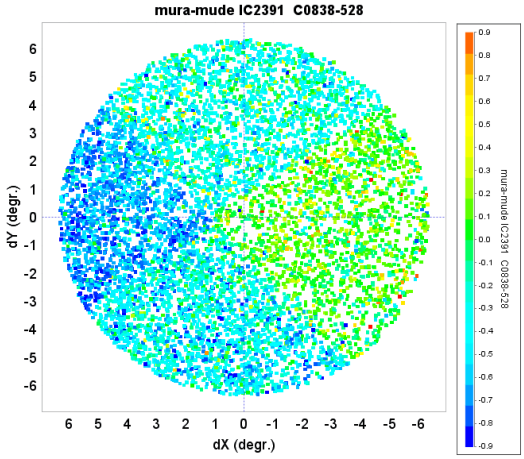

Fig. 28. Error correlations for the proper motion components in IC 2391, for stars with *Tycho-2* first epoch positions. The contributions of scans in different directions are clearly visible.

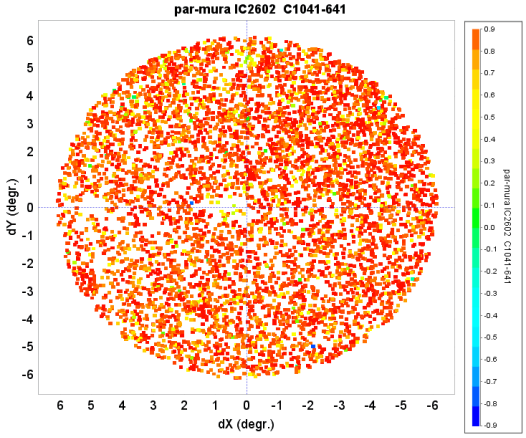

Fig. 29. Error correlations between the parallax and proper motion in Right Ascension in the field of IC 2602, for stars with first epoch positions from the *Tycho-2* catalogue.

members by Perry & Hill (1969) are also unlikely to be members as based on the parallax determinations in TGAS. They are HD 74582, 74955 and 75066. In proper motion these three stars do not deviate significantly from the cluster proper motion though. All three stars were also indicated as non-members in a spectroscopic follow-up study by Perry & Bond (1969). Compared to that paper, there are four stars for which the current astrometric solution reaches a different conclusion on membership. These are HD 74009 and 74195, which now do not appear to be cluster members based on their parallaxes, and HD 74169 and 74535 (rejected on spectral type criterion) which do appear to be members of IC 2391, as based on their proper motion and parallax. There are in addition 6 stars indicated as members in the photometric study that are not included in either the HIPPARCOS or the TGAS catalogue.

5.7. The cluster IC 2602

A field of 6.1 degrees radius was investigated, containing 20 762 stars, of which 70 were found to be possible cluster members. Of these stars 479 and 23 respectively have first epoch positions from the HIPPARCOS catalogue. The result of the astrometric solution for the cluster proper motion and parallax led to 4 more rejections and 66 probable members, the details for which are presented in Appendix D.7. Compared to the photometric study of Hill & Perry (1969) there is only one star now rejected as a cluster member, HD 93012. However, 6 of the member stars mentioned in that paper are not contained in the TGAS catalogue. Error correlations are particularly strong between parallax and proper motion in Right Ascension for stars with *Tycho-2* first-epoch positions. The field coverage shows some holes where bright stars are found (Fig. 29).

The HR diagram for IC 2391 and IC 2602, compared with the combined main sequence for the Hyades and Praesepe, is shown in Fig. 30. The main sequences for the two clusters coincide very well, confirming their very similar age.

5.8. The cluster Blanco 1

A field of 3.9 degrees radius was investigated for which 1169 stars are contained in the TGAS catalogue, 121 of which have first-epoch HIPPARCOS positions. Of these stars, 46 were marked as possible cluster members, of which 8 also have

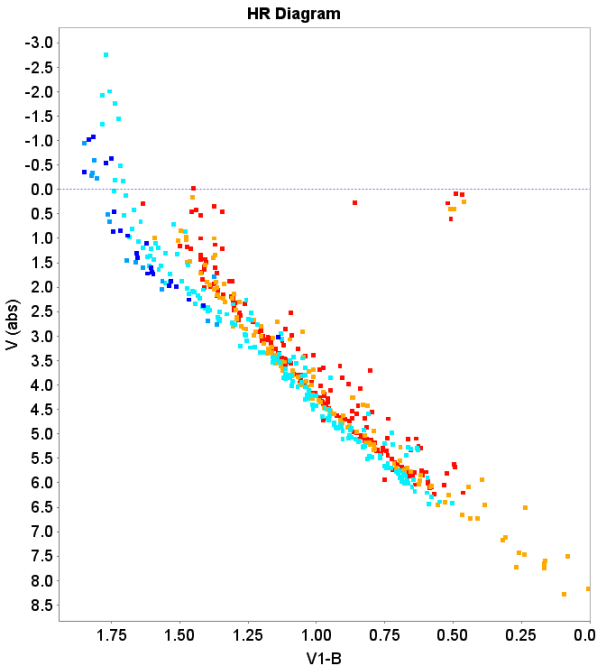

Fig. 30. Combined HR diagram for the Hyades and Praesepe (orange, red dots), Pleiades (light blue), IC 2391 (blue) and IC 2602 (dark blue dots). Only data for astrometrically confirmed cluster members is shown. Geneva photometric data.

HIPPARCOS data. The astrometric solution resulted in two further rejections, and the final selection details are presented in Appendix D.8. The parallax is just under 2σ less than what was found in fvl09, putting the cluster at around 232 pc, close to a recent estimate based on isochrone fitting (King & James 2015). The small number of members available in fvl09 led to a relatively large *su* on the parallax estimate.

The Geneva photometry for Blanco 1 contains 64 entries, of which 26 could be identified as cluster members in the TGAS or else the HIPPARCOS data, using information from Westerlund et al. (1988). Twelve non-members were found in the list, and the remainder of sources has not been identified as insufficient information was available. The HR diagram for Blanco 1, compared with other clusters, is shown in Fig. 31.

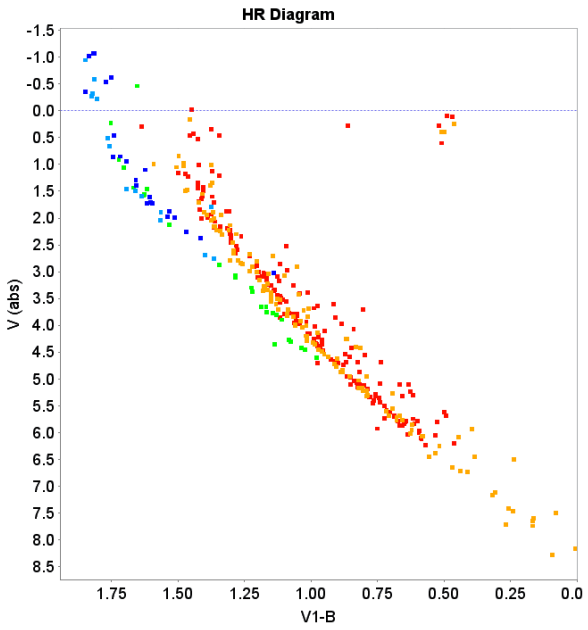

Fig. 31. HR diagram of Blanco 1 (green dots, only confirmed members) compared with the Hyades and Praesepe (orange, red dots) and IC 2391 and IC 2602 (blue dots). Geneva photometry.

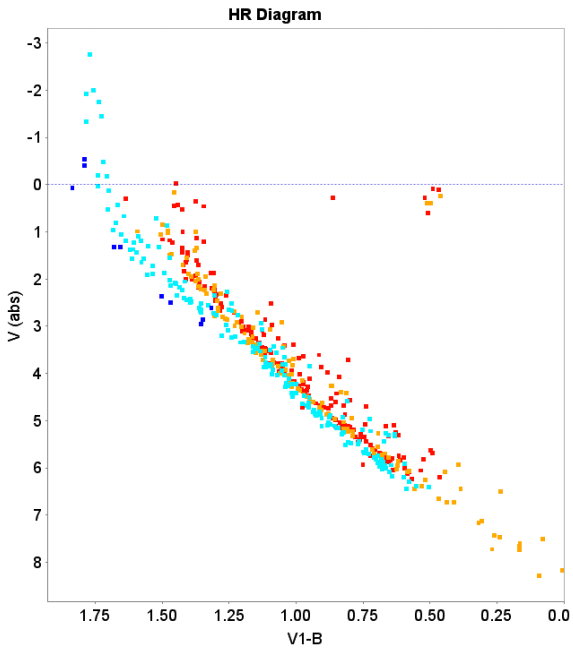

Fig. 32. Combined HR diagrams for the Hyades and Praesepe (orange, red), Pleiades (light blue) and confirmed members of NGC 2451A (dark blue), in Geneva photometry.

5.9. The cluster NGC 2451A

An extensive ground-based proper motion study of NGC 2451A was presented by Platais et al. (2001). The TGAS results cover only the brightest 5 mag of that study, where membership is close to unambiguous. Only NGC 2451A is covered, NGC 2451B, if it exists, is not an obvious feature in the proper motion or the parallax distributions in the field, and with its assumed distance, will anyway be eliminated from the analysis of NGC 2451A on the basis of the parallax selection criterion.

A field of 5 degrees radius was investigated, for which 7815 stars are contained in the TGAS catalogue. Of these, 247 have Hipparcos first epoch data. 39 stars were selected as possible cluster members, and of these 4 have Hipparcos first epoch data. Two of the possible members were later rejected in the cluster solution.

The parallax found is at 5.99 ± 0.11 mas slightly more than the 5.54 ± 0.11 mas determined from the Hipparcos data in fvl09. Taking into account a possible local calibration error of order 0.25 mas (see below), these results are in good agreement. On the other hand, the TGAS result for this cluster is closer to earlier results based on the first Hipparcos data publication, 5.30 ± 0.20 mas (van Leeuwen 1999). This shows how vulnerable these determinations can be to relatively large variations when only small numbers of stars are involved. The details for NGC 2451A are presented in Appendix D.9.

Figure 32 shows the HR diagram for NGC 2451A with respect to the Hyades, Praesepe and Pleiades clusters. The Geneva photometry gives 49 entries for NGC 2451A. Of these, only 10 could be confirmed as members of the cluster based on either TGAS or, for the brighter stars, Hipparcos astrometry, using HD identifiers or positions as given in Williams (1967). Around 12 stars could not be identified in either catalogue, and may still be members. The HR diagrams of the Pleiades and NGC 2451A have moved further apart with the TGAS parallaxes compared to fvl09.

Table 5. Star selection numbers in the fields of the more distant clusters.

Cluster	Rad.	N-T	N-H	n-T	n-H	Rej.
NGC 6475	3.2	2554	79	81	11	2
NGC 7092	2.7	3044	81	24	5	1
NGC 2516	2.6	1751	82	76	5	1
NGC 2232	3.7	1785	45	32	4	1
IC 4665	2.5	959	38	16	6	0
NGC 6633	2.2	1278	31	51	4	2
Coll 140	2.6	2984	59	32	3	1
NGC 2422	2.3	3204	46	39	2	2
NGC 3532	2.2	4304	76	140	4	8
NGC 2547	1.9	1152	42	36	8	2

Notes. Columns as follows, 1: cluster identifier; 2: field radius in degrees; 3, N-T: TGAS stars within the radius; 4, N-H: Hipparcos stars within the radius; 5, n-T: possible cluster members found in TGAS; 6, n-H: Hipparcos stars among the possible cluster members; 7, rej.: number of possible members rejected in astrometric parameter solution.

6. The more distant clusters

Table 5 gives an overview of the fields and their contents as these have been investigated for more distant clusters. The detailed astrometric solutions are presented in Table 6, while the details for each cluster can be found in Appendix D. A few clusters need special attention. For NGC 2422 the core of the cluster was essentially missing from the TGAS catalogue (see Fig. 33).

The field of NGC 6633 is crossed by 4 diagonal "empty" lines, which may have affected the selection. A similar situation, though less severe, is found for NGC 3532.

The Hipparcos data for the same clusters has mostly been obtained with a significantly smaller sample of stars (see Table 8), but also often using the brightest stars that are not included in TGAS, leaving a generally small overlap between the two solutions. Despite that, there is in most cases a good agreement. The main exception is NGC 2547.

Table 6. Overview of the results.

Name	α (degr)	ϖ	$\mu_{\alpha*}$	μ_δ	c_{12}	c_{23}	nMemb
ClustId	δ (degr)	σ_ϖ	$\sigma_{\mu\alpha*}$	$\sigma_{\mu\delta}$	c_{13}	r(max)°	st.dev.
Hyades	66.85	21.39	104.92	–28.00	0.	0.	103
C0424+157	17.04	0.21	0.12	0.09	0.	17.2	1.00
ComaBer	185.983	11.73	–12.14	–8.90	0.14	0.32	50
C1222+263	26.093	0.05	0.14	0.16	–0.07	9.42	0.86
Pleiades	56.438	7.48	20.38	–45.39	–0.17	–0.03	152
C0344+239	23.844	0.03	0.07	0.08	0.02	6.49	1.10
Praesepe	130.081	5.47	–36.06	–13.15	0.40	0.06	79
C0937+201	19.675	0.05	0.07	0.08	–0.05	4.36	1.09
alphaPer	52.069	5.91	23.06	–25.36	–0.29	–0.01	116
C0318+484	49.060	0.03	0.06	0.07	0.09	5.11	1.04
IC 2391	130.059	6.97	–24.15	23.83	0.53	–0.04	43
C0838-528	–52.818	0.13	0.16	0.25	–0.01	6.16	1.82
IC 2602	159.809	6.74	–17.67	11.06	0.36	–0.19	66
C1041-641	–64.496	0.05	0.09	0.13	0.05	5.35	1.18
Blanco 1	0.855	4.34	18.20	2.66	–0.46	0.07	43
C0001-302	–30.079	0.11	0.12	0.11	–0.44	3.77	1.41
NGC 2451A	115.799	5.59	–21.82	15.59	0.63	0.13	37
C0743-378	–38.579	0.11	0.11	0.16	–0.01	4.70	1.38
NGC 6475	268.530	3.57	3.10	–5.32	0.01	0.37	78
C1750-348	–34.849	0.02	0.06	0.04	0.10	2.37	0.62
NGC 7092	323.437	2.99	–7.34	–19.94	–0.58	0.09	23
C2130+482	48.438	0.12	0.11	0.13	0.21	2.14	1.30
NGC 2516	119.490	3.01	–4.06	11.16	0.77	–0.07	84
C0757-607	–60.688	0.10	0.07	0.08	0.05	2.54	1.60
NGC 2232	97.149	3.00	–4.34	–1.71	0.32	–0.32	31
C0624-047	–5.111	0.06	0.10	0.08	–0.06	2.64	0.86
IC 4665	266.618	2.83	–0.78	–8.37	–0.12	0.19	16
C1743+057	5.583	0.05	0.07	0.06	0.09	1.92	0.60
NGC 6633	276.956	2.41	1.45	–1.78	–0.36	0.45	48
C1825+065	6.749	0.04	0.06	0.05	–0.03	2.01	0.73
Coll 140	111.028	2.86	–8.36	4.95	0.70	–0.21	31
C0722-321	–32.168	0.11	0.09	0.10	–0.26	2.53	1.08
NGC 2422	114.054	2.28	–6.80	0.99	0.61	–0.25	37
C0734-143	–14.142	0.09	0.08	0.08	–0.33	2.20	1.01
NGC 3532	166.258	2.42	–10.65	5.27	0.60	–0.03	132
C1104-584	–58.726	0.04	0.04	0.04	0.27	2.19	0.96
NGC 2547	122.824	2.75	–8.92	4.07	0.60	0.00	34
C0809-491	–49.197	0.08	0.07	0.09	–0.10	1.59	1.04

In addition to these clusters, the possible existence of a cluster associated with δ Cep (de Zeeuw et al. 1999; Majaess et al. 2012) was looked into. Although there are around 18 stars detected within a 5 degrees radius around δ Cep, with similar distances and proper motions, these stars do not show any noticeable clustering in their distribution on the sky or the distribution of proper motions. The average parallax for these 18 stars is slightly larger than the measured parallax for δ Cep in fvl09.

7. Summary of results

We have determined and examined the astrometric data for 19 open clusters, ranging from the Hyades at just under 47 pc to IC 2422 at nearly 440 pc. The results are summarized in Table 6. Overall the agreement with a similar study using the HIPPARCOS data is better than expected. There is one exception which remains unexplained, which is the Pleiades cluster. Whether the difference originates in the TGAS data or in the HIPPARCOS data, it remains at this stage unresolved. The differences between the current solution and fvl09 are shown in Table 7 and Fig. 34. Without taking into account as additional noise local parallax zeropoint variations of 0.3 mas, as suggested in Lindegren et al. (2016), the unit weight standard deviation of the differences of the differences between the two solutions is 1.45. An additional noise at a level of 0.25 mas brings this down to 1.01. When excluding the Pleiades determinations, a smaller additional noise of 0.14 mas is required, which would make the Pleiades result stand out by 4.5 times the *su* of the parallax differences between the TGAS and HIPPARCOS solutions.

The main result, and unique to the *Gaia* data, is that we seem to detect cluster members, bound or escaped, often still at nearly 15 pc from the cluster centre. With its complete survey, the *Gaia*

Table 7. Comparison between the HIPPARCOS and TGAS parallax determinations.

Cluster	N(TH)	N(TT)	ϖ_T	$\sigma\varpi$	$\Sigma\varpi$	N(Hip)	ϖ_H	$\sigma\varpi$	$\Delta\varpi$	$\sigma\Delta\varpi$
Hyades	88	22	21.39	0.21	0.33	150	21.53	0.23	–0.22	0.40
Coma Ber	28	22	11.73	0.05	0.25	27	11.53	0.12	+0.20	0.28
Pleiades	51	101	7.48	0.03	0.25	53	8.32	0.13	–0.85	0.28
Praesepe	24	55	5.47	0.05	0.25	24	5.49	0.18	–0.02	0.31
α Per	51	65	5.91	0.03	0.25	50	5.80	0.10	0.09	0.27
IC 2391	8	35	6.97	0.13	0.28	11	6.90	0.12	–0.03	0.30
IC 2602	23	43	6.74	0.05	0.25	15	6.73	0.09	0.02	0.27
Blanco 1	8	35	4.34	0.11	0.27	13	4.83	0.27	–0.50	0.38
NGC 2451A	4	33	5.59	0.11	0.27	14	5.45	0.11	0.14	0.29
NGC 6475	11	67	3.57	0.02	0.25	20	3.70	0.14	–0.13	0.29
NGC 7092	5	18	2.99	0.12	0.28	7	3.30	0.19	–0.31	0.34
NGC 2516	6	78	3.01	0.10	0.27	11	2.92	0.10	0.09	0.29
NGC 2232	4	27	3.00	0.06	0.26	6	2.84	0.18	0.16	0.32
IC 4665	6	10	2.83	0.05	0.25	7	2.81	0.27	0.02	0.37
NGC 6633	4	43	2.41	0.04	0.25	6	2.67	0.32	–0.26	0.41
Coll 140	4	27	2.86	0.11	0.27	9	2.66	0.13	0.20	0.30
NGC 2422	2	35	2.28	0.09	0.27	7	2.52	0.21	–0.24	0.34
NGC 3532	4	128	2.42	0.04	0.25	6	2.43	0.24	–0.01	0.35
NGC 2547	8	26	2.75	0.08	0.26	8	2.11	0.17	0.64	0.31

Notes. The meaning of the columns is as follows: N(TH): number of stars in the TGAS solution with HIPPARCOS first epoch data; N(TT): number of stars in the TGAS solution with *Tycho-2* first epoch data; ϖ_T: TGAS parallax for the cluster; $\sigma\varpi$: formal *su* on ϖ_T; $\Sigma\varpi$: *su* including calibration uncertainty of 0.25 mas; N(Hip): number of stars in the HIPPARCOS solution; ϖ_H: HIPPARCOS parallax for the cluster; $\sigma\varpi$: formal *su* on ϖ_H; $\Delta\varpi = \varpi_T - \varpi_H$; $\sigma\Delta\varpi$: *su* on the parallax difference.

Table 8. Comparisons between TGAS and HIPPARCOS astrometric parameters in cluster fields.

Cluster	N	$\Delta\varpi$	UWSD	$\Delta\mu_{\alpha*}$	UWSD	$\Delta\mu_\delta$	UWSD
ComaBer	28	−0.14 ± 0.22	1.44	−0.08 ± 0.40	2.77	0.17 ± 0.34	3.69
ComaBer	758	−0.01 ± 0.05	1.22	0.14 ± 0.05	1.42	0.21 ± 0.04	1.73
Pleiades	44	0.72 ± 0.17	1.05	0.28 ± 0.30	1.80	0.28 ± 0.19	1.36
Pleiades	241	0.36 ± 0.09	1.30	0.25 ± 0.11	1.65	−0.22 ± 0.11	2.08
Praesepe	23	0.19 ± 0.21	1.18	0.77 ± 0.32	1.87	0.02 ± 0.21	1.77
Praesepe	123	0.30 ± 0.13	1.35	−0.07 ± 0.13	1.36	−0.32 ± 0.11	1.79
alphaPer	50	−0.41 ± 0.14	1.20	−0.24 ± 0.15	1.60	−0.72 ± 0.18	2.06
alphaPer	245	−0.05 ± 0.07	1.24	−0.08 ± 0.08	1.63	−0.38 ± 0.08	1.72
IC 2391	7	0.03 ± 0.33	1.50	0.29 ± 0.25	1.66	−0.18 ± 0.33	2.29
IC 2391	390	−0.05 ± 0.04	1.19	0.18 ± 0.05	1.76	−0.06 ± 0.04	1.67
IC 2602	19	−0.01 ± 0.15	1.17	0.12 ± 0.12	1.11	0.28 ± 0.19	2.13
IC 2602	394	0.03 ± 0.04	1.29	0.18 ± 0.06	2.05	0.01 ± 0.05	1.77
Blanco 1	8	−0.26 ± 0.39	1.15	0.16 ± 0.35	1.03	−0.11 ± 0.34	1.60
Blanco 1	98	0.14 ± 0.16	1.41	0.10 ± 0.15	1.46	0.08 ± 0.28	4.18
NGC 2451A	4	−0.20 ± 0.24	0.69	−0.28 ± 0.31	2.70	−0.41 ± 0.37	2.68
NGC 2451A	224	0.00 ± 0.05	1.16	0.05 ± 0.04	1.54	0.11 ± 0.05	1.41
NGC 6475	11	0.23 ± 0.22	0.93	−1.02 ± 0.31	1.33	0.35 ± 0.15	1.09
NGC 6475	64	0.13 ± 0.14	1.04	−0.54 ± 0.26	1.78	0.23 ± 0.11	1.44
NGC 7092	5	0.05 ± 0.26	1.03	0.08 ± 0.17	0.90	0.15 ± 0.51	2.87
NGC 7092	63	−0.01 ± 0.10	1.22	−0.01 ± 0.12	1.69	−0.10 ± 0.14	2.20
NGC 2516	5	0.27 ± 0.21	0.95	0.47 ± 0.30	1.84	0.43 ± 0.19	1.15
NGC 2516	64	0.11 ± 0.09	1.18	0.46 ± 0.11	1.56	−0.04 ± 0.13	1.75
NGC 2232	3	−0.56 ± 0.23	0.55	0.18 ± 0.20	0.55	−0.11 ± 0.19	0.62
NGC 2232	41	0.19 ± 0.17	1.36	−0.04 ± 0.33	3.19	0.12 ± 0.19	2.20
IC 4665	6	0.35 ± 0.35	1.00	−0.46 ± 0.98	3.36	0.13 ± 0.36	1.83
IC 4665	28	−0.48 ± 0.18	0.96	0.46 ± 0.25	1.85	0.16 ± 0.16	1.77
NGC 6633	4	0.50 ± 0.43	0.93	−0.56 ± 0.62	1.54	0.13 ± 0.07	0.18
NGC 6633	25	−0.29 ± 0.22	1.32	−0.38 ± 0.31	2.17	0.59 ± 0.20	1.59
Coll 140	3	0.24 ± 0.83	2.10	−0.31 ± 0.31	1.23	−0.32 ± 0.20	0.67
Coll 140	52	0.12 ± 0.12	1.09	0.11 ± 0.20	2.99	0.30 ± 0.19	2.16
NGC 2422	2	1.46 ± 0.55	0.72	0.29 ± 0.24	0.38	0.10 ± 0.66	1.16
NGC 2422	33	0.24 ± 0.20	1.31	0.09 ± 0.18	1.66	0.26 ± 0.14	1.54
NGC 3532	4	0.32 ± 0.50	1.40	0.47 ± 0.13	0.38	−0.29 ± 0.43	1.49
NGC 3532	63	−0.04 ± 0.11	1.15	0.37 ± 0.17	2.23	−0.07 ± 0.16	2.33
NGC 2547	8	−0.72 ± 0.20	0.80	−0.20 ± 0.27	1.23	−0.07 ± 0.28	1.36
NGC 2547	48	−0.26 ± 0.14	1.50	0.49 ± 0.18	2.39	−0.09 ± 0.10	1.52

Notes. For each cluster: first line for cluster members, second line for the remaining stars in the field of the cluster. Only stars with clean 5-parameter solutions in the HIPPARCOS catalogue were used. For each value is given the mean, error on the mean and unit-weight standard deviation of the differences.

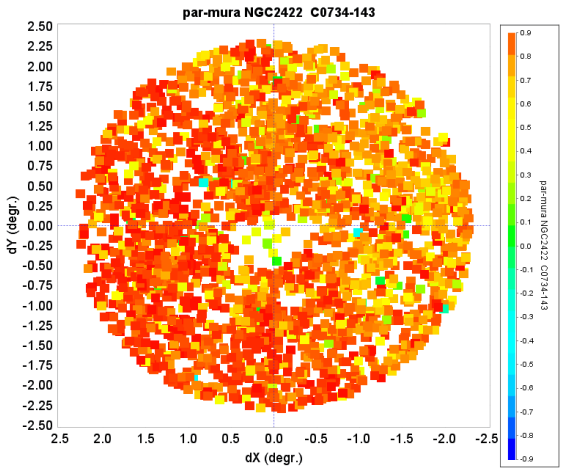

Fig. 33. Correlation levels between parallax and proper motion in Right Ascension for the field of NGC 2422, showing the hole in the centre where the cluster core is situated. Data points are for stars with *Tycho-2* first epoch positions.

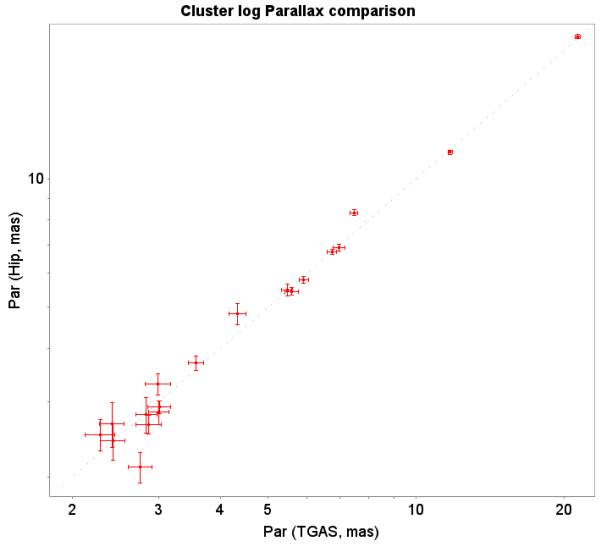

Fig. 34. Comparison between the cluster parallaxes as determined by the HIPPARCOS and TGAS analyses.

mission can detect these potential cluster members from the combined parallax and proper motion data, and future releases will further supplement this with radial velocity measurements. Without the parallax as an additional distinction the contrast of the cluster members from the field stars is much more difficult and uncertain.

There were assumptions still to be made for the current reductions. The one most affecting the results concerns properties of the internal velocities. Once proper motion and parallax accuracies for a significant group of stars are down to the 0.01 mas level it will become possible to examine for example the internal structure of the Pleiades cluster, and describe the distribution of positions and velocities of stars in the cluster. Being able to do so for clusters of different ages, such as Hyades, Coma Ber and the Pleiades, can then provide data that can be directly compared with *N*-body simulations.

The results for the Hyades confirmed what had earlier been observed in the Pleiades too, that the main sequence for a population that is homogeneous in age and composition can in fact be very narrow. This contrasts sharply with the width of the main sequence for field stars, in particular in the region of late G to early B stars. With future releases of the *Gaia* data and its application to star clusters of different ages and chemical composition, it should become possible to reach a better understanding of the broad distribution of the field stars.

8. Conclusions

The *Gaia* data, like the HIPPARCOS data before, can not be validated or invalidated by results derived for the open clusters. A limited set of conclusions can be drawn from internal consistency of the data, and the most important one is the agreement between the parallaxes of the Hyades stars as measured and as derived from the proper motions. This agreement is, however, limited by the internal velocity dispersion of the cluster. The proper motion comparison with ground-based differential data in the Pleiades field is also reassuring. The overall agreement for the parallaxes of the 19 clusters investigated here with the earlier study (fvl09) based on the new reduction of the HIPPARCOS data is more than satisfactory, and an indication that earlier estimates for an additional local noise on the TGAS parallaxes of 0.3 mas may have been slightly overestimated.

Although questions remain on the one discrepancy between the HIPPARCOS and TGAS results, as well as on the *su* levels of the current determination, the overall results are very promising for future releases, when parallaxes and proper motions at similar and higher accuracies will come available for much larger numbers of stars, extending over a wider range of magnitudes. Future releases should also gradually become less complicated to use, with error correlation levels between astrometric parameters reduced, and also modelling errors in the attitude solution becoming much less significant.

Acknowledgements. This work has made use of results from the European Space Agency (ESA) space mission *Gaia*, the data from which were processed by the *Gaia* Data Processing and Analysis Consortium (DPAC). Funding for the DPAC has been provided by national institutions, in particular the institutions participating in the *Gaia* Multilateral Agreement. The *Gaia* mission website is http://www.cosmos.esa.int/gaia. The authors are current or past members of the ESA *Gaia* mission team and of the *Gaia* DPAC. This work has financially been supported by: the Algerian Centre de Recherche en Astronomie, Astrophysique et Géophysique of Bouzareah Observatory; the Austrian FWF Hertha Firnberg Programme through grants T359, P20046, and P23737; the BELgian federal Science Policy Office (BELSPO) through various PROgramme de Développement d'Expériences scientifiques (PRODEX) grants; the Brazil-France exchange programmes FAPESP-COFECUB and CAPES-COFECUB; the Chinese National Science Foundation through grant NSFC 11573054; the Czech-Republic Ministry of Education, Youth, and Sports through grant LG 15010; the Danish Ministry of Science; the Estonian Ministry of Education and Research through grant IUT40-1; the European Commission's Sixth Framework Programme through the European Leadership in Space Astrometry (ELSA) Marie Curie Research Training Network (MRTN-CT-2006-033481), through Marie Curie project PIOF-GA-2009-255267 (SAS-RRL), and through a Marie Curie Transfer-of-Knowledge (ToK) fellowship (MTKD-CT-2004-014188); the European Commission's Seventh Framework Programme through grant FP7-606740 (FP7-SPACE-2013-1) for the *Gaia* European Network for Improved data User Services (GENIUS) and through grant 264895 for the *Gaia* Research for European Astronomy Training (GREAT-ITN) network; the European Research Council (ERC) through grant 320360 and through the European Union's Horizon 2020 research and innovation programme through grant agreement 670519 (Mixing and Angular Momentum tranSport of massIvE stars – MAMSIE); the European Science Foundation (ESF), in the framework of the *Gaia* Research for European Astronomy Training Research Network Programme (GREAT-ESF); the European Space Agency in the framework of the *Gaia* project; the European Space Agency Plan for European Cooperating States (PECS) programme through grants for Slovenia; the Czech Space Office through ESA PECS contract 98058; the Academy of Finland; the Magnus Ehrnrooth Foundation; the French Centre National de la Recherche Scientifique (CNRS) through action "Défi MASTODONS"; the French Centre National d'Études Spatiales (CNES); the French L'Agence Nationale de la Recherche (ANR) investissements d'avenir Initiatives D'EXcellence

(IDEX) programme PSL* through grant ANR-10-IDEX-0001-02; the Région Aquitaine; the Université de Bordeaux; the French Utinam Institute of the Université de Franche-Comté, supported by the Région de Franche-Comté and the Institut des Sciences de l'Univers (INSU); the German Aerospace Agency (Deutsches Zentrum für Luft- und Raumfahrt e.V., DLR) through grants 50QG0501, 50QG0601, 50QG0602, 50QG0701, 50QG0901, 50QG1001, 50QG1101, 50QG140, 50QG1401, 50QG1402, and 50QG1404; the Hungarian Academy of Sciences through Lendület Programme LP2014-17; the Hungarian National Research, Development, and Innovation Office through grants NKFIH K-115709 and PD-116175; the Israel Ministry of Science and Technology through grant 3-9082; the Agenzia Spaziale Italiana (ASI) through grants I/037/08/0, I/058/10/0, 2014-025-R.0, and 2014-025-R.1.2015 to INAF and contracts I/008/10/0 and 2013/030/I.0 to ALTEC S.p.A.; the Italian Istituto Nazionale di Astrofisica (INAF); the Netherlands Organisation for Scientific Research (NWO) through grant NWO-M-614.061.414 and through a VICI grant to A. Helmi; the Netherlands Research School for Astronomy (NOVA); the Polish National Science Centre through HARMONIA grant 2015/18/M/ST9/00544; the Portugese Fundação para a Ciência e a Tecnologia (FCT) through grants PTDC/CTE-SPA/118692/2010, PDCTE/CTE-AST/81711/2003, and SFRH/BPD/74697/2010; the Strategic Programmes PEst-OE/AMB/UI4006/2011 for SIM, UID/FIS/00099/2013 for CENTRA, and UID/EEA/00066/2013 for UNINOVA; the Slovenian Research Agency; the Spanish Ministry of Economy MINECO-FEDER through grants AyA2014-55216, AyA2011-24052, ESP2013-48318-C2-R, and ESP2014-55996-C2-R and MDM-2014-0369 of ICCUB (Unidad de Excelencia María de Maeztu); the Swedish National Space Board (SNSB/Rymdstyrelsen); the Swiss State Secretariat for Education, Research, and Innovation through the ESA PRODEX programme, the Mesures d'Accompagnement, and the Activités Nationales Complémentaires; the Swiss National Science Foundation, including an Early Postdoc.Mobility fellowship; the United Kingdom Rutherford Appleton Laboratory; the United Kingdom Science and Technology Facilities Council (STFC) through grants PP/C506756/1 and ST/I00047X/1; and the United Kingdom Space Agency (UKSA) through grants ST/K000578/1 and ST/N000978/1.

References

An, D., Terndrup, D. M., Pinsonneault, M. H., et al. 2007, ApJ, 655, 233
Arenou, F., Luri, X., Babusiaux, C., et al. 2017, A&A, 599, A50 (*Gaia SI*)
Baraffe, I., Homeier, D., Allard, F., & Chabrier, G. 2015, A&A, 577, A42
Barrado y Navascués, D., Stauffer, J. R., & Jayawardhana, R. 2004, ApJ, 614, 386
Bell, C. P. M., Naylor, T., Mayne, N. J., Jeffries, R. D., & Littlefair, S. P. 2012, MNRAS, 424, 3178
Boesgaard, A. M., Roper, B. W., & Lum, M. G. 2013, ApJ, 775, 58
Brandt, T. D., & Huang, C. X. 2015, ApJ, 807, 24
Chen, Y., Bressan, A., Girardi, L., et al. 2015, MNRAS, 452, 1068
Cummings, J. D., Deliyannis, C. P., Maderak, R. M., & Steinhauer, A. 2017, AJ, 153, 128
de Bruijne, J. H. J., Hoogerwerf, R., & de Zeeuw, P. T. 2001, A&A, 367, 111
de Zeeuw, P. T., Hoogerwerf, R., de Bruijne, J. H. J., Brown, A. G. A., & Blaauw, A. 1999, AJ, 117, 354
Detweiler, H. L., Yoss, K. M., Radick, R. R., & Becker, S. A. 1984, AJ, 89, 1038
Ekström, S., Georgy, C., Eggenberger, P., et al. 2012, A&A, 537, A146
ESA 1997, The HIPPARCOS and Tycho catalogues, Astrometric and photometric star catalogues derived from the ESA HIPPARCOS Space Astrometry Mission (Noordwijk, Netherlands: ESA Publications Division), ESA SP, 1200
Fabricius, C., Makarov, V. V., Knude, J., & Wycoff, G. L. 2002, A&A, 386, 709
Fossati, L., Bagnulo, S., Landstreet, J., et al. 2008, A&A, 483, 891
Gaia Collaboration (Brown, A. G. A., et al.) 2016a, A&A, 595, A2 (*Gaia SI*)
Gaia Collaboration (Prusti, T., et al.) 2016b, A&A, 595, A1 (*Gaia SI*)
Gatewood, G. 1995, ApJ, 445, 712
Górski, K. M., Hivon, E., Banday, A. J., et al. 2005, ApJ, 622, 759
Heiter, U., Soubiran, C., Netopil, M., & Paunzen, E. 2014, A&A, 561, A93
Hertzsprung, E. 1947, Annalen van de Sterrewacht te Leiden, 19, A1
Hill, G., & Perry, C. L. 1969, AJ, 74, 1011
Høg, E., Fabricius, C., Makarov, V. V., et al. 2000, A&A, 355, L27
Kharchenko, N. V., Piskunov, A. E., Schilbach, E., Röser, S., & Scholz, R.-D. 2016, A&A, 585, A101
Kim, B., An, D., Stauffer, J. R., et al. 2016, ApJS, 222, 19
King, P. A. S., & James, D. 2015, in AAS Meeting Abstracts, 225, 247.26
Lejeune, T., & Schaerer, D. 2001, A&A, 366, 538
Lindegren, L., Lammers, U., Bastian, U., et al. 2016, A&A, 595, A4
Madsen, S. 1999, in Harmonizing Cosmic Distance Scales in a Post-HIPPARCOS Era, eds. D. Egret, & A. Heck, ASP Conf. Ser., 167, 78
Majaess, D., Turner, D., & Gieren, W. 2012, ApJ, 747, 145
Makarov, V. V. 2003, AJ, 126, 2408
Netopil, M., Paunzen, E., Heiter, U., & Soubiran, C. 2016, A&A, 585, A150
Pace, G., Pasquini, L., & François, P. 2008, A&A, 489, 403
Perry, C. L., & Bond, H. E. 1969, PASP, 81, 629
Perry, C. L., & Hill, G. 1969, AJ, 74, 899
Perryman, M. A. C., Turon, C., Arenou, F., et al. 1989, in The HIPPARCOS mission, Pre-launch status, Vol. II: The Input Catalogue, 2
Perryman, M. A. C., Brown, A. G. A., Lebreton, Y., et al. 1998, A&A, 331, 81
Pinsonneault, M. H., Stauffer, J., Soderblom, D. R., King, J. R., & Hanson, R. B. 1998, ApJ, 504, 170
Platais, I., Kozhurina-Platais, V., Barnes, S., et al. 2001, AJ, 122, 1486
Risquez, D., van Leeuwen, F., & Brown, A. G. A. 2013, A&A, 551, A19
Robichon, N., Arenou, F., Mermilliod, J.-C., & Turon, C. 1999, A&A, 345, 471
Rufener, F. 1989, A&AS, 78, 469
Schaller, G., Schaerer, D., Meynet, G., & Maeder, A. 1992, A&AS, 96, 269
Sheikhi, N., Hasheminia, M., Khalaj, P., et al. 2016, MNRAS, 457, 1028
Soderblom, D. R., Laskar, T., Valenti, J. A., Stauffer, J. R., & Rebull, L. M. 2009, AJ, 138, 1292
Stauffer, J. R., Schild, R., Barrado y Navascués, D., et al. 1998, ApJ, 504, 805
Stauffer, J. R., Hartmann, L. W., Fazio, G. G., et al. 2007, ApJS, 172, 663
Taylor, B. J. 2006, AJ, 132, 2453
van Altena, W. F. 1966, AJ, 71, 482
van Leeuwen, F. 1999, A&A, 341, L71
van Leeuwen, F. 2007, A&A, 474, 653
van Leeuwen, F. 2009, A&A, 497, 209
Vasilevskis, S., van Leeuwen, F., Nicholson, W., & Murray, C. A. 1979, A&AS, 37, 333
Westerlund, B. E., Lundgren, K., Pettersson, B., Garnier, R., & Breysacher, J. 1988, A&AS, 76, 101
Williams, P. M. 1967, Monthly Notes of the Astronomical Society of South Africa, 26, 30
Zacharias, N., Finch, C., Subasavage, J., et al. 2015, AJ, 150, 101

[1] Institute of Astronomy, University of Cambridge, Madingley Road, Cambridge CB3 0HA, UK
e-mail: fvl@ast.cam.ac.uk
[2] INAF–Osservatorio astronomico di Padova, Vicolo Osservatorio 5, 35122 Padova, Italy
[3] Institut de Ciències del Cosmos, Universitat de Barcelona (IEEC-UB), Martí Franquès 1, 08028 Barcelona, Spain
[4] Lund Observatory, Department of Astronomy and Theoretical Physics, Lund University, Box 43, 22100 Lund, Sweden
[5] Astronomisches Rechen-Institut, Zentrum für Astronomie der Universität Heidelberg, Mönchhofstr. 12–14, 69120 Heidelberg, Germany
[6] Scientific Support Office, Directorate of Science, European Space Research and Technology Centre (ESA/ESTEC), Keplerlaan 1, 2201 AZ Noordwijk, The Netherlands
[7] Leiden Observatory, Leiden University, Niels Bohrweg 2, 2333 CA Leiden, The Netherlands
[8] GEPI, Observatoire de Paris, PSL Research University, CNRS, Univ. Paris Diderot, Sorbonne Paris Cité, 5 Place Jules Janssen, 92190 Meudon, France
[9] Max Planck Institute for Astronomy, Königstuhl 17, 69117 Heidelberg, Germany
[10] Department of Astronomy, University of Geneva, Chemin des Maillettes 51, 1290 Versoix, Switzerland
[11] Mission Operations Division, Operations Department, Directorate of Science, European Space Research and Technology Centre (ESA/ESTEC), Keplerlaan 1, 2201 AZ Noordwijk, The Netherlands
[12] Lohrmann Observatory, Technische Universität Dresden, Mommsenstraße 13, 01062 Dresden, Germany
[13] European Space Astronomy Centre (ESA/ESAC), Camino bajo del Castillo, s/n, Urbanizacion Villafranca del Castillo, Villanueva de la Cañada, 28692 Madrid, Spain
[14] Laboratoire Lagrange, Université Nice Sophia-Antipolis, Observatoire de la Côte d'Azur, CNRS, CS 34229, 06304 Nice Cedex, France
[15] CNES Centre Spatial de Toulouse, 18 avenue Edouard Belin, 31401 Toulouse Cedex 9, France
[16] Institut d'Astronomie et d'Astrophysique, Université Libre de Bruxelles CP 226, Boulevard du Triomphe, 1050 Brussels, Belgium

[17] F.R.S.-FNRS, rue d'Egmont 5, 1000 Brussels, Belgium
[18] INAF–Osservatorio Astrofisico di Arcetri, Largo Enrico Fermi 5, 50125 Firenze, Italy
[19] Telespazio Vega UK Ltd for ESA/ESAC, Camino bajo del Castillo, s/n, Urbanizacion Villafranca del Castillo, Villanueva de la Cañada, 28692 Madrid, Spain
[20] Laboratoire d'astrophysique de Bordeaux, Université de Bordeaux, CNRS, B18N, allée Geoffroy Saint-Hilaire, 33615 Pessac, France
[21] Instituut voor Sterrenkunde, KU Leuven, Celestijnenlaan 200D, 3001 Leuven, Belgium
[22] Department of Astrophysics/IMAPP, Radboud University Nijmegen, PO Box 9010, 6500 GL Nijmegen, The Netherlands
[23] Mullard Space Science Laboratory, University College London, Holmbury St Mary, Dorking, Surrey RH5 6NT, UK
[24] INAF–Osservatorio Astrofisico di Torino, via Osservatorio 20, 10025 Pino Torinese (TO), Italy
[25] Niels Bohr Institute, University of Copenhagen, Juliane Maries Vej 30, 2100 Copenhagen Ø, Denmark
[26] Centre for Electronic Imaging, Department of Physical Sciences, The Open University, Walton Hall MK7 6AA Milton Keynes, UK
[27] ALTEC S.p.a, Corso Marche, 79, 10146 Torino, Italy
[28] INAF–Osservatorio Astronomico di Bologna, via Ranzani 1, 40127 Bologna, Italy
[29] Serco Gestión de Negocios for ESA/ESAC, Camino bajo del Castillo, s/n, Urbanizacion Villafranca del Castillo, Villanueva de la Cañada, 28692 Madrid, Spain
[30] Department of Astronomy, University of Geneva, Chemin d'Ecogia 16, 1290 Versoix, Switzerland
[31] STFC, Rutherford Appleton Laboratory, Harwell, Didcot, OX11 0QX, UK
[32] Gaia DPAC Project Office, ESAC, Camino bajo del Castillo, s/n, Urbanizacion Villafranca del Castillo, Villanueva de la Cañada, 28692 Madrid, Spain
[33] SYRTE, Observatoire de Paris, PSL Research University, CNRS, Sorbonne Universités, UPMC Univ. Paris 06, LNE, 61 avenue de l'Observatoire, 75014 Paris, France
[34] National Observatory of Athens, I. Metaxa and Vas. Pavlou, Palaia Penteli, 15236 Athens, Greece
[35] IMCCE, Observatoire de Paris, PSL Research University, CNRS, Sorbonne Universités, UPMC Univ. Paris 06, Univ. Lille, 77 av. Denfert-Rochereau, 75014 Paris, France
[36] Royal Observatory of Belgium, Ringlaan 3, 1180 Brussels, Belgium
[37] Institut d'Astrophysique Spatiale, Université Paris XI, UMR 8617, CNRS, Bâtiment 121, 91405 Orsay Cedex, France
[38] Institute for Astronomy, Royal Observatory, University of Edinburgh, Blackford Hill, Edinburgh EH9 3HJ, UK
[39] HE Space Operations BV for ESA/ESAC, Camino bajo del Castillo, s/n, Urbanizacion Villafranca del Castillo, Villanueva de la Cañada, 28692 Madrid, Spain
[40] Institut d'Astrophysique et de Géophysique, Université de Liège, 19c, Allée du 6 Août, 4000 Liège, Belgium
[41] Área de Lenguajes y Sistemas Informáticos, Universidad Pablo de Olavide, Ctra. de Utrera, km 1. 41013 Sevilla, Spain
[42] Observatoire Astronomique de Strasbourg, Université de Strasbourg, CNRS, UMR 7550, 11 rue de l'Université, 67000 Strasbourg, France
[43] Kavli Institute for Cosmology, University of Cambridge, Madingley Road, Cambride CB3 0HA, UK
[44] Aurora Technology for ESA/ESAC, Camino bajo del Castillo, s/n, Urbanizacion Villafranca del Castillo, Villanueva de la Cañada, 28692 Madrid, Spain
[45] Laboratoire Univers et Particules de Montpellier, Université Montpellier, Place Eugène Bataillon, CC72, 34095 Montpellier Cedex 05, France
[46] Department of Astrophysics, Astronomy and Mechanics, National and Kapodistrian University of Athens, Panepistimiopolis, Zografos, 15783 Athens, Greece
[47] Department of Physics and Astronomy, Division of Astronomy and Space Physics, Uppsala University, Box 516, 75120 Uppsala, Sweden
[48] Università di Catania, Dipartimento di Fisica e Astronomia, Sezione Astrofisica, via S. Sofia 78, 95123 Catania, Italy
[49] INAF–Osservatorio Astrofisico di Catania, via S. Sofia 78, 95123 Catania, Italy
[50] Universidade da Coruña, Facultade de Informática, Campus de Elviña S/N, 15071 A Coruña, Spain
[51] CENTRA, Universidade de Lisboa, FCUL, Campo Grande, Edif. C8, 1749-016 Lisboa, Portugal
[52] University of Helsinki, Department of Physics, PO Box 64, University of Helsinki, 00014 Helsinki, Finland
[53] Finnish Geospatial Research Institute FGI, Geodeetinrinne 2, 02430 Masala, Finland
[54] Isdefe for ESA/ESAC, Camino bajo del Castillo, s/n, Urbanizacion Villafranca del Castillo, Villanueva de la Cañada, 28692 Madrid, Spain
[55] ASI Science Data Center, via del Politecnico SNC, 00133 Roma, Italy
[56] Institut UTINAM UMR 6213, CNRS, OSU THETA Franche-Comté Bourgogne, Université Bourgogne Franche-Comté, 25000 Besançon, France
[57] Dpto. de Inteligencia Artificial, UNED, c/ Juan del Rosal 16, 28040 Madrid, Spain
[58] Elecnor Deimos Space for ESA/ESAC, Camino bajo del Castillo, s/n, Urbanizacion Villafranca del Castillo, Villanueva de la Cañada, 28692 Madrid, Spain
[59] Thales Services for CNES Centre Spatial de Toulouse, 18 avenue Edouard Belin, 31401 Toulouse Cedex 9, France
[60] EURIX S.r.l., via Carcano 26, 10153 Torino, Italy
[61] University of Vienna, Department of Astrophysics, Türkenschanzstraße 17, 1180 Vienna, Austria
[62] Department of Physics and Astronomy, The Johns Hopkins University, 3400 N Charles St, Baltimore, MD 21218, USA
[63] ON/MCTI-BR, rua Gal. José Cristino 77, 20921-400 Rio de Janeiro, RJ, Brazil
[64] OV/UFRJ-BR, Ladeira Pedro Antônio 43, 20080-090 Rio de Janeiro, RJ, Brazil
[65] Faculdade Ciencias, Universidade do Porto, Departamento Matematica Aplicada, rua do Campo Alegre, 687 4169-007 Porto, Portugal
[66] Instituto de Astrofísica e Ciências do Espa co, Universidade de Lisboa Faculdade de Ciências, Campo Grande, 1749-016 Lisboa, Portugal
[67] Departamento de Astrofísica, Centro de Astrobiología (CSIC-INTA), ESA-ESAC. Camino Bajo del Castillo s/n., 28692 Villanueva de la Cañada, Madrid, Spain
[68] Department of Physics and Astronomy, University of Leicester, University Road, Leicester LE1 7RH, UK
[69] University of Oviedo, Campus Universitario, 33203 Gijón, Spain
[70] University of Cádiz, Avd. De la universidad, Jerez de la Frontera, 11002 Cádiz, Spain
[71] Kapteyn Astronomical Institute, University of Groningen, Landleven 12, 9747 AD Groningen, The Netherlands
[72] Consorci de Serveis Universitaris de Catalunya, C/ Gran Capità, 2-4 3rd floor, 08034 Barcelona, Spain
[73] University of Turin, Department of Computer Sciences, Corso Svizzera 185, 10149 Torino, Italy
[74] INAF–Osservatorio Astronomico di Roma, via di Frascati 33, 00078 Monte Porzio Catone (Roma), Italy
[75] CRAAG – Centre de Recherche en Astronomie, Astrophysique et Géophysique, Route de l'Observatoire, BP 63 Bouzareah, 16340 Algiers, Algeria
[76] Universiteit Antwerpen, Onderzoeksgroep Toegepaste Wiskunde, Middelheimlaan 1, 2020 Antwerpen, Belgium
[77] Department of Physics and Astronomy, University of Padova, via Marzolo 8, 35131 Padova, Italy
[78] INAF–Osservatorio Astronomico di Teramo, via Mentore Maggini, 64100 Teramo, Italy

[79] INAF–Osservatorio Astronomico di Capodimonte, via Moiariello 16, 80131 Napoli, Italy
[80] Instituto de Astronomia, Geofìsica e Ciências Atmosféricas, Universidade de São Paulo, rua do Matão, 1226, Cidade Universitaria, 05508-900 São Paulo, SP, Brazil
[81] Department of Geosciences, Tel Aviv University, 6997801 Tel Aviv, Israel
[82] Astronomical Institute Anton Pannekoek, University of Amsterdam, PO Box 94249, 1090 GE Amsterdam, The Netherlands
[83] Leibniz Institute for Astrophysics Potsdam (AIP), An der Sternwarte 16, 14482 Potsdam, Germany
[84] ATOS for CNES Centre Spatial de Toulouse, 18 avenue Edouard Belin, 31401 Toulouse Cedex 9, France
[85] School of Physics and Astronomy, Tel Aviv University, 6997801 Tel Aviv, Israel
[86] UNINOVA – CTS, Campus FCT-UNL, Monte da Caparica, 2829-516 Caparica, Portugal
[87] Laboratoire Géoazur, Université Nice Sophia-Antipolis, UMR 7329, CNRS, Observatoire de la Côte d'Azur, 250 rue A. Einstein, 06560 Valbonne, France
[88] RHEA for ESA/ESAC, Camino bajo del Castillo, s/n, Urbanizacion Villafranca del Castillo, Villanueva de la Cañada, 28692 Madrid, Spain
[89] Astronomical Institute, Academy of Sciences of the Czech Republic, Fričova 298, 25165 Ondřejov, Czech Republic
[90] Barcelona Supercomputing Center – Centro Nacional de Supercomputación, c/ Jordi Girona 29, Ed. Nexus II, 08034 Barcelona, Spain
[91] Department of Mechanical Engineering, University of La Rioja, c/San José de Calasanz, 31, 26004 Logroño, La Rioja, Spain
[92] ETSE Telecomunicación, Universidade de Vigo, Campus Lagoas-Marcosende, 36310 Vigo, Galicia, Spain
[93] SRON, Netherlands Institute for Space Research, Sorbonnelaan 2, 3584CA Utrecht, The Netherlands
[94] Faculty of Mathematics and Physics, University of Ljubljana, Jadranska ulica 19, 1000 Ljubljana, Slovenia
[95] Physics Department, University of Antwerp, Groenenborgerlaan 171, 2020 Antwerp, Belgium
[96] Harvard-Smithsonian Center for Astrophysics, 60 Garden Street, Cambridge, MA 02138, USA
[97] Institut de Physique de Rennes, Université de Rennes 1, 35042 Rennes, France
[98] Shanghai Astronomical Observatory, Chinese Academy of Sciences, 80 Nandan Rd, 200030 Shanghai, PR China
[99] CSC Danmark A/S, Retortvej 8, 2500 Valby, Denmark
[100] Las Cumbres Observatory Global Telescope Network, Inc., 6740 Cortona Drive, Suite 102, Goleta, CA 93117, USA
[101] Astrophysics Research Institute, Liverpool John Moores University, L3 5RF, UK
[102] Konkoly Observatory, Research Centre for Astronomy and Earth Sciences, Hungarian Academy of Sciences, Konkoly Thege Miklós út 15-17, 1121 Budapest, Hungary
[103] Baja Observatory of University of Szeged, Szegedi út III/70, 6500 Baja, Hungary
[104] Laboratoire AIM, IRFU/Service d'Astrophysique, CEA/DSM, CNRS, Université Paris Diderot, Bât 709, CEA-Saclay, 91191 Gif-sur-Yvette Cedex, France
[105] INAF–Osservatorio Astronomico di Trieste, via G.B. Tiepolo 11, 34143 Trieste, Italy
[106] Laboratoire de l'Accélérateur Linéaire, Université Paris-Sud, CNRS/IN2P3, Université Paris-Saclay, 91898 Orsay Cedex, France
[107] École polytechnique fédérale de Lausanne, SB MATHAA STAP, MA B1 473 (Bâtiment MA), Station 8, 1015 Lausanne, Switzerland
[108] INAF/IASF-Bologna, via P. Gobetti 101, 40129 Bologna, Italy
[109] Technical University of Madrid, José Gutiérrez Abascal 2, 28006 Madrid, Spain
[110] EQUERT International for CNES Centre Spatial de Toulouse, 18 avenue Edouard Belin, 31401 Toulouse Cedex 9, France
[111] AKKA for CNES Centre Spatial de Toulouse, 18 avenue Edouard Belin, 31401 Toulouse Cedex 9, France
[112] Villanova University, Dept. of Astrophysics and Planetary Science, 800 E Lancaster Ave, Villanova, PA 19085, USA
[113] Vitrociset Belgium for ESA/ESAC, Camino bajo del Castillo, s/n, Urbanizacion Villafranca del Castillo, Villanueva de la Cañada, 28692 Madrid, Spain
[114] Fork Research, rua do Cruzado Osberno, Lt. 1, 9 esq., 1900-174 Lisboa, Portugal
[115] APAVE SUDEUROPE SAS for CNES Centre Spatial de Toulouse, 18 avenue Edouard Belin, 31401 Toulouse Cedex 9, France
[116] Spanish Virtual Observatory, 2869 Madrid, Spain
[117] Fundación Galileo Galilei – INAF, Rambla José Ana Fernández Pérez 7, 38712 Breña Baja, Santa Cruz de Tenerife, Spain
[118] INSA for ESA/ESAC, Camino bajo del Castillo, s/n, Urbanizacion Villafranca del Castillo, Villanueva de la Cañada, 28692 Madrid, Spain
[119] Dpto. Arquitectura de Computadores y Automática, Facultad de Informática, Universidad Complutense de Madrid, C/ Prof. José García Santesmases s/n, 28040 Madrid, Spain
[120] H H Wills Physics Laboratory, University of Bristol, Tyndall Avenue, Bristol BS8 1TL, UK
[121] Stellar Astrophysics Centre, Aarhus University, Department of Physics and Astronomy, 120 Ny Munkegade, Building 1520, 8000 Aarhus C, Denmark
[122] Applied Physics Department, University of Vigo, 36310 Vigo, Spain
[123] HE Space Operations BV for ESA/ESTEC, Keplerlaan 1, 2201AZ Noordwijk, The Netherlands
[124] Warsaw University Observatory, Al. Ujazdowskie 4, 00-478 Warszawa, Poland
[125] Instituto de Astrofísica de Canarias, 38205 La Laguna, Tenerife, Spain
[126] Universidad de La Laguna, Departamento de Astrofísica, 38206 La Laguna, Tenerife, Spain
[127] RHEA for ESA/ESTEC, Keplerlaan 1, 2201AZ Noordwijk, The Netherlands
[128] Max Planck Institute for Solar System Research, Justus-von-Liebig-Weg 3, 37077 Göttingen, Germany
[129] SISSA (Scuola Internazionale Superiore di Studi Avanzati), via Bonomea 265, 34136 Trieste, Italy
[130] Instituto Nacional de Pesquisas Espaciais/Ministério da Ciencia Tecnologia, Avenida dos Astronautas 1758, 12227-010 São José Dos Campos, Brazil
[131] Argelander Institut für Astronomie der Universität Bonn, Auf dem Hügel 71, 53121 Bonn, Germany
[132] European Southern Observatory (ESO), Karl-Schwarzschild-Straße 2, 85748 Garching bei München, Germany
[133] Laboratory of Optics, Lasers and Systems, Faculty of Sciences, University of Lisbon, Campus do Lumiar, Estrada do Paço do Lumiar, 22, 1649-038 Lisboa, Portugal
[134] Department of Physics and Astronomy, Notre Dame University, Louaize, PO Box 72, Zouk Mikaël, Lebanon
[135] University of Nova Gorica, Vipavska 13, 5000 Nova Gorica, Slovenia
[136] Max Planck Institute for Extraterrestrial Physics, OPINAS, Gießenbachstraße, 85741 Garching, Germany
[137] NASA/IPAC Infrared Science Archive, California Institute of Technology, Mail Code 100-22, 770 South Wilson Avenue, Pasadena, CA 91125, USA
[138] Center of Applied Space Technology and Microgravity (ZARM), c/o Universität Bremen, Am Fallturm 1, 28359 Bremen, Germany
[139] RHEA System for ESA/ESOC, Robert Bosch Straße 5, 64293 Darmstadt, Germany
[140] Tartu Observatory, 61602 Tõravere, Estonia
[141] Sydney Institute for Astronomy, School of Physics A28, The University of Sydney, 2006 Sydney, Australia
[142] Slovak Organisation for Space Activities, Zamocka 18, 85101 Bratislava, Slovak Republic
[143] National Astronomical Observatories, CAS, 100012 Beijing, PR China

[144] US Naval Observatory, Astrometry Department, 3450 Massachusetts Ave. NW, Washington, DC 20392-5420, USA
[145] European Southern Observatory (ESO), Alonso de Córdova 3107, Vitacura, Casilla 19001, Santiago de Chile, Chile
[146] Airbus Defence and Space SAS, 31 rue des Cosmonautes, 31402 Toulouse Cedex 4, France
[147] EJR-Quartz BV for ESA/ESTEC, Keplerlaan 1, 2201 AZ Noordwijk, The Netherlands
[148] The Server Labs for ESA/ESAC, Camino bajo del Castillo, s/n, Urbanizacion Villafranca del Castillo, Villanueva de la Cañada, 28692 Madrid, Spain
[149] Astronomical Observatory Institute, Faculty of Physics, A. Mickiewicz University, ul. Słoneczna 36, 60-286 Poznań, Poland
[150] CS Systèmes d'Information for CNES Centre Spatial de Toulouse, 18 avenue Edouard Belin, 31401 Toulouse Cedex 9, France
[151] Directorate of Science, European Space Research and Technology Centre (ESA/ESTEC), Keplerlaan 1, 2201 AZ Noordwijk, The Netherlands
[152] Praesepe BV for ESA/ESAC, Camino bajo del Castillo, s/n, Urbanizacion Villafranca del Castillo, Villanueva de la Cañada, 28692 Madrid, Spain
[153] Sorbonne Universités UPMC et CNRS, UMR 7095, Institut d'Astrophysique de Paris, 75014 Paris, France
[154] GMV for ESA/ESAC, Camino bajo del Castillo, s/n, Urbanizacion Villafranca del Castillo, Villanueva de la Cañada, 28692 Madrid, Spain
[155] Institute of Theoretical Physics and Astronomy, Vilnius University, Sauletekio al. 3, 10222 Vilnius, Lithuania
[156] S[&]T Corporation, PO Box 608, 2600 AP Delft, The Netherlands
[157] Department of Space Studies, Southwest Research Institute (SwRI), 1050 Walnut Street, Suite 300, Boulder, Colorado 80302, USA
[158] Deutsches Zentrum für Luft- und Raumfahrt, Institute of Space Systems, Am Fallturm 1, 28359 Bremen, Germany
[159] University of Applied Sciences Munich, Karlstr. 6, 80333 Munich, Germany
[160] Dipartimento di Fisica, Università di Roma Tor Vergata, via della Ricerca Scientifica 1, 00133 Rome, Italy
[161] Department of Physics and Astronomy, University of the Western Cape, Robert Sobukwe Road, 7535 Bellville, Cape Town, South Africa
[162] INAF – Istituto di Radioastronomia, via Gobetti 101, 40129 Bologna, Italy
[163] Department of Physics, Florida International University, 11200 SW 8th Street, Miami, FL 33199, USA
[164] Hamburger Sternwarte, Gojenbergsweg 112, 21029 Hamburg, Germany

Appendix A: Combined astrometric solutions

A.1. Observations and noise contributions

In the combined astrometric solution the observed parallaxes and proper motions are compared with predicted ones, based on the assumed parallax and space motion of the cluster centre, and the position of the star on the sky relative to the projection of the cluster centre. This forms the common solution which provides an update to the proper motion of the cluster.

The correction for the parallax offset $\mathrm{d}\varpi_i$ along the line of sight of the observed parallax is reflected in the proper motion for each star i:

$$\begin{bmatrix} 1 \\ \mu_{\alpha*,c}/\varpi_c \\ \mu_{\delta,c}/\varpi_c \end{bmatrix} \cdot \mathrm{d}\varpi_i. \tag{A.1}$$

In reality this contribution is only significant for the nearby clusters. The complete observation equations for the cluster parallax and proper motion corrections are as follows:

$$\begin{bmatrix} 1 & 0 & 0 & 1 \\ 0 & 1 & 0 & \mu_{\alpha*,c}/\varpi_c \\ 0 & 0 & 1 & \mu_{\delta,c}/\varpi_c \end{bmatrix} \cdot \begin{bmatrix} \mathrm{d}\varpi_c \\ \mathrm{d}\mu_{\alpha*,c} \\ \mathrm{d}\mu_{\delta,c} \\ \mathrm{d}\varpi_i \end{bmatrix} = \begin{bmatrix} \delta\varpi_i \\ \delta\mu_{\alpha*,i} \\ \delta\mu_{\delta,i} \end{bmatrix} + \sqrt{\mathsf{N}_i}\,\boldsymbol{\epsilon}. \tag{A.2}$$

Where the index c refers to the cluster parameters, N_i is the noise covariance matrix for the astrometric parameters of star i (see below), and each element of the vector ϵ has expectation value 0 and sigma of one. The value of $\delta\varpi_i$ is the difference between the assumed cluster parallax and the observed parallax for star i. The values of $\delta\mu_{\alpha*,i}$ and $\delta\mu_{\delta,i}$ are the differences between the observed and predicted proper motion assuming the parallax to be the same as the cluster. This way, the expression in Eq. (A.1) allows for a compensation of the relative distance of a star, as based on the parallax and proper motion measurements. However, due to the still fairly limited accuracies of both proper motions and parallaxes for individual stars, the inclusion of the relative parallax corrections (Eq. (A.1)) creates a near-singularity in the solution when also the cluster parallax is solved for. There are therefore, at this stage, two types of solutions, one for the cluster parallax,

$$\begin{bmatrix} \mathsf{I}_3 \end{bmatrix} \cdot \begin{bmatrix} \mathrm{d}\varpi_c \\ \mathrm{d}\mu_{\alpha*,c} \\ \mathrm{d}\mu_{\delta,c} \end{bmatrix} = \begin{bmatrix} \delta\varpi_i \\ \delta\mu_{\alpha*,i} \\ \delta\mu_{\delta,i} \end{bmatrix} + \sqrt{\mathsf{N}_i}\,\boldsymbol{\epsilon}, \tag{A.3}$$

and one for the differential parallaxes within the cluster,

$$\begin{bmatrix} 0 & 0 & 1 \\ 1 & 0 & \mu_{\alpha*,c}/\varpi_c \\ 0 & 1 & \mu_{\delta,c}/\varpi_c \end{bmatrix} \cdot \begin{bmatrix} \mathrm{d}\mu_{\alpha*,c} \\ \mathrm{d}\mu_{\delta,c} \\ \mathrm{d}\varpi_i \end{bmatrix} = \begin{bmatrix} \delta\varpi_i \\ \delta\mu_{\alpha*,i} \\ \delta\mu_{\delta,i} \end{bmatrix} + \sqrt{\mathsf{N}_i}\,\boldsymbol{\epsilon}. \tag{A.4}$$

Only when both the parallaxes and proper motions reach a higher accuracy it may become possible to combine the two solutions.

Two noise matrices are associated with the observations. The first is the covariance matrix N_a for the astrometric parameter determination as applicable to each individual member. The second is the noise on the proper motions introduced by the internal velocity dispersion, N_v. The sum of these two contributions is given by N_i. If the matrix U_i is an upper-triangular square root of N_i, then we can normalize the noise on the observation equations by multiplying both sides of Eq. (A.3) by the upper-triangular inverse of U_i:

$$\begin{bmatrix} \mathsf{U}_i^{-1} \end{bmatrix} \cdot \begin{bmatrix} \mathrm{d}\varpi_c \\ \mathrm{d}\mu_{\alpha*,c} \\ \mathrm{d}\mu_{\delta,c} \end{bmatrix} = \mathsf{U}_i^{-1} \cdot \begin{bmatrix} \delta\varpi_i \\ \delta\mu_{\alpha*} \\ \delta\mu_{\delta} \end{bmatrix} + \boldsymbol{\epsilon}. \tag{A.5}$$

Equations of the type Eq. (A.5) are the input observation equations for the cluster astrometric parameters solution. The matrix U^{-1} is referred to as the weight matrix, and is a square root of the normal equations. It has the same dimensions as the observation equations. A similar procedure can be applied to Eq. (A.4).

The first component of N_i can be reconstructed from the data provided in the *Gaia* DR1 TGAS records, where the standard errors σ and correlation coefficients c for the astrometric parameter solution are given. Here we are only concerned about the parallax and proper motion determinations. The 3 by 3 matrix N_a is then given as:

$$\mathsf{N}_a = \begin{bmatrix} \sigma_1^2 & c_{12}\sigma_1\sigma_2 & c_{13}\sigma_1\sigma_3 \\ c_{12}\sigma_1\sigma_2 & \sigma_2^2 & c_{23}\sigma_2\sigma_3 \\ c_{13}\sigma_1\sigma_3 & c_{23}\sigma_2\sigma_3 & \sigma_3^2 \end{bmatrix}, \tag{A.6}$$

where the indices 1–3 stand for parallax, proper motion in right ascension and proper motion in declination respectively. The values for $c_{i,j}$ are provided with the astrometric data as the correlation coefficients for the astrometric parameters.

The noise matrix for the internal velocity dispersion is given by:

$$\mathsf{N}_v = \begin{bmatrix} 0 & 0 & 0 \\ 0 & \sigma_v^2 & 0 \\ 0 & 0 & \sigma_v^2 \end{bmatrix}, \tag{A.7}$$

where σ_v is equivalent to an internal velocity dispersion of 0.6 km s^{-1} ($\kappa = 4.74047$, the transformation factor from mas yr^{-1} to km s^{-1}):

$$\sigma_v = 0.6 \cdot \varpi_c/\kappa \ \text{ mas s}^{-1}, \tag{A.8}$$

which is roughly equivalent to what has been observed in the Pleiades and Hyades. The assumptions concerning this internal velocity dispersion can significantly affect the outcome of the cluster parallax due to the strong correlation coefficients in N_a. It is a value that is going to be dependent on stellar mass and distance from the cluster centre, but these are considerations that become possible to implement with future releases of the *Gaia* data. The current data is still too complicated to determine and implement such dependencies.

When solving Eq. (A.3) the parallax dispersion has to be taken into account. This again is a somewhat uncertain quantity, that will differ from cluster to cluster. The dispersion in actual distance for an "average cluster" is assumed to be 0.003 kpc. In first approximation this will give a parallax dispersion $\sigma_\varpi \approx \varpi^2\sigma_r$. At a parallax of, say, 8 mas, this implies a parallax dispersion of just under 0.2 mas. The noise matrix contribution is simply

$$\mathsf{N}_\varpi = \begin{bmatrix} \sigma_\varpi^2 & 0 & 0 \\ 0 & 0 & 0 \\ 0 & 0 & 0 \end{bmatrix}. \tag{A.9}$$

For any individual star the measured proper motion may be further disturbed by unresolved orbital motion, but these have to be resolved with increase in the data volume and epoch coverage.

A.2. Projection effects

If we consider the centre of the cluster to be represented by the vector $\boldsymbol{R}$, then the cluster space velocity is given by the derivative of this vector, $\dot{\boldsymbol{R}}$. Expressed in equatorial coordinates, these vectors have the following familiar expressions:

$$\boldsymbol{R} = R \cdot \begin{bmatrix} \cos\alpha\cos\delta \\ \sin\alpha\cos\delta \\ \sin\delta \end{bmatrix} \tag{A.10}$$

and

$$\dot{\boldsymbol{R}} = \begin{bmatrix} \cos\alpha\cos\delta & -\sin\alpha & -\cos\alpha\sin\delta \\ \sin\alpha\cos\delta & \cos\alpha & -\sin\alpha\sin\delta \\ \sin\delta & 0 & \cos\delta \end{bmatrix} \cdot \begin{bmatrix} \dot{R} \\ R\,\dot{\alpha}\cos\delta \\ R\,\dot{\delta} \end{bmatrix}. \quad \text{(A.11)}$$

The vector on the right-hand side of Eq. (A.11) relates directly to the proper motion and radial velocity of the cluster:

$$\begin{bmatrix} \dot{R} \\ R\,\dot{\alpha}\cos\delta \\ R\,\dot{\delta} \end{bmatrix} = \begin{bmatrix} V_{\rm rad} \\ \kappa\mu_{\alpha*}/\varpi \\ \kappa\mu_{\delta}/\varpi \end{bmatrix}. \quad \text{(A.12)}$$

Similarly, the projection of the cluster space motion on the observed parameters of a cluster member (index i) can be expressed as:

$$\begin{bmatrix} V_{{\rm rad},i} \\ \kappa\mu_{\alpha*,i}/\varpi_i \\ \kappa\mu_{\delta,i}/\varpi_i \end{bmatrix} = \begin{bmatrix} \cos\alpha_i\cos\delta_i & \sin\alpha_i\cos\delta_i & \sin\delta_i \\ -\sin\alpha_i & \cos\alpha_i & 0 \\ -\cos\alpha_i\sin\delta_i & -\sin\alpha_i\sin\delta_i & \cos\delta_i \end{bmatrix} \cdot \dot{\boldsymbol{R}}. \quad \text{(A.13)}$$

An approximation of these equations for distant clusters, with small differences between the position of the cluster centre and those of the member stars, can be found in fvl09. Equation (A.13) is used to provide predicted values for the proper motions.

A.3. Transformation to reduced proper motions

For further analysis the reference system can be rotated such that one component of the proper motion is aligned with the cluster proper motion, while the other is perpendicular to it. This system of reduced proper motions is particularly useful for analysing the Hyades and other nearby systems. The shared cluster motion for any cluster member is in the direction of the convergent point (α_t, δ_t), the position of which is set by the direction of the space motion vector $\dot{\boldsymbol{R}}$ of the cluster:

$$\hat{\dot{\boldsymbol{R}}} = \begin{bmatrix} \cos\alpha_t\cos\delta_t \\ \sin\alpha_t\cos\delta_t \\ \sin\delta_t \end{bmatrix}. \quad \text{(A.14)}$$

The transformation of the positional reference system to the new coordinates (ρ, τ), with the pole at the convergent point, is given by:

$$\begin{bmatrix} \cos\rho\cos\tau \\ \sin\rho\cos\tau \\ \sin\tau \end{bmatrix} = \begin{bmatrix} \cos\alpha_t\sin\delta_t & \sin\alpha_t\sin\delta_t & -\cos\delta_t \\ -\sin\alpha_t & \cos\alpha_t & 0 \\ \cos\alpha_t\cos\delta_t & \sin\alpha_t\cos\delta_t & \sin\delta_t \end{bmatrix} \cdot \hat{\boldsymbol{R}}. \quad \text{(A.15)}$$

For the rotation of the proper motions to the new system the local orientation of the equatorial coordinates needs to be reconstructed.

The vector product of the direction to the source, $\hat{\boldsymbol{R}}$ and the direction of the convergent point is a vector $\boldsymbol{u}$ in the plane tangential to the direction of source and perpendicular to the direction of the convergent point as seen from the source. In that same plane the vectors

$$\boldsymbol{p} = \begin{bmatrix} -\sin\alpha \\ \cos\alpha \\ 0 \end{bmatrix} \quad \text{(A.16)}$$

and

$$\boldsymbol{q} = \begin{bmatrix} -\cos\alpha\sin\delta \\ -\sin\alpha\sin\delta \\ \cos\delta \end{bmatrix} \quad \text{(A.17)}$$

describe the direction, from the source, of right ascension and declination respectively (see also Eq. (A.11)). Thus, the inner products

$$\cos\phi = \hat{\boldsymbol{u}} \cdot \boldsymbol{p} \quad \text{(A.18)}$$

and

$$\cos(90-\phi) = \sin\phi = \hat{\boldsymbol{u}} \cdot \boldsymbol{q} \quad \text{(A.19)}$$

define the orientation angle ϕ needed for the transformation of the proper motions. The proper motions in the new coordinate system are

$$\begin{aligned} \mu_{\rho\cos\tau} &= \cos\phi\,\mu_{\alpha\cos\delta} - \sin\phi\,\mu_{\delta} \\ \mu_{\tau} &= \sin\phi\,\mu_{\alpha\cos\delta} + \cos\phi\,\mu_{\delta}. \end{aligned} \quad \text{(A.20)}$$

The transformation of the weight matrix U^{-1} is having the same form:

$$\mathsf{W} = \mathsf{U}^{-1} \cdot \begin{bmatrix} 1 & 0 & 0 \\ 0 & \cos\phi & \sin\phi \\ 0 & -\sin\phi & \cos\phi \end{bmatrix}, \quad \text{(A.21)}$$

which transforms the application of the standard errors and correlations to the new system. Note that the weight matrix W is no longer upper triangular. The predicted projected cluster proper motion has only one component, in the τ direction. It is zero in the ρ direction. Thus, the vector $\boldsymbol{s}$ in Eq. (A.4) is simplified to

$$\boldsymbol{s}' \cdot {\rm d}\varpi_i = \begin{bmatrix} 1 \\ 0 \\ \mu_{\tau,c}/\varpi_c \end{bmatrix} \cdot {\rm d}\varpi_i \quad \text{(A.22)}$$

and the observation equations become

$$\mathsf{W}_i \cdot \begin{bmatrix} 0 & 0 & 1 \\ 1 & 0 & 0 \\ 0 & 1 & \mu_{\tau,c}/\varpi_c \end{bmatrix} \cdot \begin{bmatrix} {\rm d}\mu_{\rho\cos\tau,c} \\ {\rm d}\mu_{\tau,c} \\ {\rm d}\varpi_i \end{bmatrix} = \mathsf{W}_i \cdot \begin{bmatrix} \delta\varpi_i \\ \delta\mu_{\rho\cdot} \\ \delta\mu_{\tau} \end{bmatrix} + \boldsymbol{\epsilon}. \quad \text{(A.23)}$$

The proper motion in the τ direction is primarily a function of the parallax of the star (relative to the mean cluster parallax) and the angular separation from the convergent point, and can as such be used to derive differential parallaxes of cluster members (Madsen 1999). These are referred to as the kinematically improved parallaxes. The added uncertainty is in the internal velocity dispersion of the cluster members.

The observed proper motion dispersion in the ρ direction, after correcting for observational standard errors, provides a potential measure for the internal velocity dispersion in the cluster. This reduced proper motion solution, which can be seen as the inverse of the convergent point cluster parallax determination (see also see Madsen 1999; van Leeuwen 2009), is only useful in that context. For solving the cluster parallax and proper motion it is better to use Eq. (A.3) and staying that way closer to the original observations.

Appendix B: Tangential projection and de-projection

The tangential projection is used here as a simple tool to determine cluster centre positions, based on the average of the positions of all selected member stars. Just for reference, the equations are given here. Using the subscripts i and c for the star and

the cluster centre respectively, and $\Delta\alpha_i \equiv (\alpha_i - \alpha_c)$, the projection is:

$$x_i = \frac{\sin\Delta\alpha_i \cos\delta_i}{\sin\delta_i \sin\delta_c + \cos\delta_i \cos\delta_c \cos\Delta\alpha_i},$$
$$y_i = \frac{\sin\delta_i \cos\delta_c - \cos\delta_i \sin\delta_c \cos\Delta\alpha_i}{\sin\delta_i \sin\delta_c + \cos\delta_i \cos(\delta_c) \cos\Delta\alpha_i}. \quad \text{(B.1)}$$

For the inverse derivation, first derive

$$w_i = \sin\delta_i \sin\delta_c + \cos\delta_i \cos\delta_c \cos\Delta\alpha_i = \frac{1}{\sqrt{1 + x_i^2 + y_i^2}} \quad \text{(B.2)}$$

and similarly

$$u_i = \sin\delta_i \cos\delta_c - \cos\delta_i \sin\delta_c \cos\Delta\alpha_i = y_i \cdot w_i \quad \text{(B.3)}$$

and

$$v_i = \sin\Delta\alpha_i \cos\delta_i = x_i w_i. \quad \text{(B.4)}$$

Combine Eqs. (B.2) and (B.3) to give

$$\sin\delta_i = u_i \cos\delta_c + w_i \sin\delta_c$$
$$\cos\delta_i \cos\Delta\alpha_i = -u_i \sin\delta_c + w_i \cos\delta_c. \quad \text{(B.5)}$$

Equations (B.4) and (B.5) are all that is needed to recover (α_c, δ_c).

Appendix C: Three-dimensional distance from cluster centre

If the vector towards the star is given by $\boldsymbol{R}_s$ and for the cluster centre as $\boldsymbol{R}_c$, then the position of the star within the cluster is given by

$$\boldsymbol{r} = \boldsymbol{R}_s - \boldsymbol{R}_c. \quad \text{(C.1)}$$

The angular separation ρ of the star from the centre of the cluster is given by

$$\cos\rho = \varpi_c \varpi_s \boldsymbol{R}_c \cdot \boldsymbol{R}_s, \quad \text{(C.2)}$$

where ϖ_c is the assumed parallax for the cluster centre, and ϖ_s the observed parallax for the star. The length of $\boldsymbol{r}$ is given by

$$r = \|\boldsymbol{r}\| = \sqrt{\frac{1}{\varpi_c^2} + \frac{1}{\varpi_s^2} - \frac{2\cos\rho}{\varpi_c \varpi_s}}. \quad \text{(C.3)}$$

Along the line of sight, the *su* on r is dominated by the relative error on the stellar parallax:

$$\sigma_r = \frac{\partial r}{\partial \varpi_s} \sigma_{\varpi,s} = \frac{|\varpi_s \cos\rho/\varpi_c - 1|}{r\varpi_s^3} \sigma_{\varpi,s}. \quad \text{(C.4)}$$

The *su* σ_r leads to a "stretched out" appearance of the cluster along the line of sight. For clusters much more distant than the Hyades, the parallax of the star can be expressed as $\varpi_s = \varpi_c + \Delta\varpi_s$, with $\Delta\varpi_s \ll \varpi_c$. In addition, $\cos\rho \approx 1$, which gives in first approximation (expressed in the parallax of the cluster):

$$\sigma_r \approx \frac{\sigma_{\varpi,s}}{r\varpi_c^3} \frac{|\Delta\varpi_s|}{\varpi_c}. \quad \text{(C.5)}$$

Also, $\Delta\varpi_s \approx \varpi_c^2 r \cos\theta$, where θ is measured from the line of sight through the cluster centre. Substituting gives

$$\sigma_r \approx \frac{\sigma_{\varpi,s} \cos\theta}{\varpi_c^2}. \quad \text{(C.6)}$$

Thus, in Eq. (C.4) the error σ_r effectively scales with the distance of the cluster squared, which makes it at this stage only just applicable to the Hyades.

Appendix D: Selected stars

Here we present the tables with the selected members for the different clusters, and other information that may be of interest. Cross identifications with HD numbers were obtained from the HIPPARCOS or *Tycho-2* identifiers in the TGAS records, and the cross matches of those identifiers with the HD catalogue as provided by ESA (1997) and Fabricius et al. (2002). Positions in the tables are in the ICRS, at epoch 2015.0. Further *Gaia* data on the sources in the tables can be extracted from the *Gaia* archive[3], using the option "file", providing a file with source identifiers. The option "Tycho-Gaia Astrometric Solution" should be selected.

[3] https://gea.esac.esa.int/archive/

D.1. The Hyades cluster

For the Hyades cluster the individual distance moduli, as based on the combined information from the parallax measurement and the proper motion, are included in Table D.1. Figure D.2 shows the distribution of the members as projected on the sky.

Table D.1. Identifiers, positions and distance moduli for members of the Hyades cluster.

SourceId	HD	α (degr)	δ (degr)	G	dm	SourceId	HD	α (degr)	δ (degr)	G	dm
68000018174329600		53.2094	23.6920	8.568	3.12	3307645127438373888	286789	66.7269	13.1381	9.999	3.41
71487325460694912		54.7836	28.3821	10.259	3.73	3312709374919349248	28205	66.9000	15.5891	7.247	3.37
3277270534605393920		57.0502	7.1463	10.129	2.81	3306922954457367936	28237	66.9424	11.7364	7.331	3.32
43789768566924416		57.6046	17.2464	9.126	3.41	3310903736305456512	285830	66.9464	14.4177	9.138	3.45
66482348530642176	283066	57.7637	23.9035	9.705	3.05	3307844860597241088	28258	67.0189	13.8679	8.764	3.40
67351752990540544	283044	58.1715	25.8042	10.457	3.27	3312921374502681984	285804	67.0458	16.4708	10.381	3.15
38354676428572288	286363	58.7566	12.4855	9.676	3.31	48061405596787712	28291	67.1555	19.7405	8.384	3.39
43538289638888064	285252	58.7777	16.9984	8.674	3.05	3314109912215994112	28344	67.2017	17.2853	7.671	3.32
170457596891797760	281459	60.2819	33.1958	9.394	3.30	3314212063714381056	28406	67.3769	17.8630	6.764	3.33
50327292903510144		60.9132	19.4549	9.701	3.40	151379146007107200	283704	67.3786	26.6713	8.933	3.79
50298121485861120		61.3575	19.4420	10.728	3.37	3314213025787054592	285773	67.3822	17.8930	8.669	3.29
45367052352895360	25825	61.5677	15.6980	7.666	3.36	3312951748510907648	28462	67.4910	16.6727	8.786	3.26
45159897490770816	285507	61.7556	15.3349	9.954	3.26	3305871821341047808	28608	67.7387	10.7517	6.886	3.36
45567507066546048	285482	61.9305	16.5187	9.512	3.30	144171228809559808	28593	67.8159	20.1330	8.341	3.31
3304337452864501120	286554	62.1116	12.1918	10.589	3.32	3307815001984777088	28635	67.8727	13.9034	7.600	3.65
53942246617146240	284155	62.1514	23.7684	9.120	3.36	3312564033223630720	285876	67.9691	15.4994	10.381	3.29
3300315439330018304		62.4563	9.3055	9.533	2.76	3307504218151520256	286839	68.1073	13.1132	10.382	3.34
46975431705914112	26345	62.6770	18.4231	6.477	3.34	3410640882737635200	285836	68.1710	19.1133	10.039	3.61
3311514205777562496	26756	63.6073	14.6250	8.238	3.45	3312644881687518976	28805	68.2481	15.8189	8.407	3.36
3304412597612195328	26767	63.6141	12.4353	7.840	3.39	144377799556207488	284552	68.4054	21.1507	10.110	3.19
52813460492850304	26737	63.6272	22.4517	6.925	3.92	3313259165090609280	28878	68.4086	16.7624	9.080	3.45
149005266040519808	26736	63.6352	23.5747	7.851	3.27	3410453484725565312	285837	68.4251	19.0139	10.166	3.39
3300934223858467072	26784	63.6436	10.7014	6.945	3.27	3307528029449757056	28911	68.4448	13.2518	6.489	3.32
3311492799660064384	285625	63.7939	14.3984	10.802	3.39	3312602344331419136	28977	68.6345	15.8275	9.342	3.57
3312197930211158784	285590	63.8909	15.7062	10.320	3.27	3312575681175439616	28992	68.6476	15.5045	7.739	3.31
49365082792386816	26874	63.9273	20.8197	7.600	3.50	3309956850635519488	29159	69.0224	15.6839	9.071	3.51
3312136494998639872	26911	63.9434	15.4006	6.199	3.32	3282171745125201792	26911	69.4931	4.6698	10.788	3.42
52548237672091392	284253	64.1400	21.9073	8.867	3.54	146677874804442240	29419	69.7142	23.1497	7.343	3.19
45789299177700352	27130	64.4128	16.9477	8.047	3.34	3307992332594320640	286929	69.9628	12.7284	9.577	3.16
47620260916592384	27149	64.5082	18.2567	7.313	3.35	146698078328904064	284574	70.0247	23.3044	9.107	3.86
148946064212226944	284303	64.5454	23.2845	9.063	3.65	148183862135533952	283810	70.0389	25.5921	9.978	3.25
3312281664893305728	285690	64.5808	16.0882	9.215	3.27	3281064262038614912		71.5787	3.6364	10.282	3.28
49005576847854080	27250	64.7421	19.9065	8.363	3.32	3309006597711379328	30246	71.6270	15.4719	8.082	3.36
47345005052090880	27282	64.7839	17.5246	8.220	3.37	3412605297699792512	284785	71.7877	20.8821	9.392	3.14
3283285790922135424		65.2677	3.2688	9.064	2.86	3413146910255989248	284653	71.8595	23.0508	10.203	3.68
49231663928585344	27524	65.3823	21.0397	6.661	3.42	3405127244241184256	27524	72.2156	15.9475	9.397	3.88
47541096078933376	27534	65.3849	18.4174	6.670	3.39	147182172683187712	283882	72.3045	24.8026	9.134	3.45
3311024785663873920	27561	65.3954	14.4097	6.477	3.45	3405113740864365440	30589	72.3842	15.8886	7.550	3.40
145325544220443904	27732	65.8435	21.3789	8.586	3.49	3405988677241799040	286085	72.5033	16.4119	10.087	3.49
3312025581763840512	285749	65.8559	15.7630	9.914	3.07	3404812680839290368	30712	72.6413	15.0833	7.517	3.36
3311148824319241472	27771	65.8852	14.6704	8.814	3.33	3405220084257276416	30738	72.7026	16.2103	7.135	3.48
3310820620098473728	286734	65.9772	14.0520	10.252	3.17	3404850785786832512	30809	72.8470	15.4334	7.728	3.92
3313630078465745280	27835	66.0537	16.3788	8.039	3.76	3406943087694799744	284930	73.0984	18.9968	9.846	3.51
145373372976256512	27808	66.0613	21.7361	6.969	3.16	3408463506117452544	31236	73.7435	19.4853	6.278	3.99
3314079503847287424	285720	66.0711	18.0028	9.571	3.31	3392446817156214784	31609	74.4566	14.0021	8.647	3.68
3313947699887831808	27848	66.0932	17.0788	6.828	3.51	3239389678968988288		75.2040	4.7332	9.377	3.58
3313662892016181504	27859	66.1185	16.8861	7.627	3.27	3391728561185367168	27859	75.4005	13.9329	10.612	3.12
3312783557591565440	27991	66.4060	15.9409	6.297	3.38	3407518510233429248	27991	75.7799	19.0178	11.096	3.66
3311179335766914944		66.5200	15.0413	11.326	3.42	3391712034151625984	32347	75.7822	13.7306	8.729	3.63
145293177350363264	28033	66.5775	21.4703	7.201	3.37	3407121827053483776	240648	76.5752	17.8163	8.574	3.63
3313689417734366720	28099	66.6676	16.7468	7.916	3.30	3387381641964995712	242780	80.1062	11.6098	8.795	3.71
144534720481849856	284455	66.6989	21.2347	10.560	3.19						

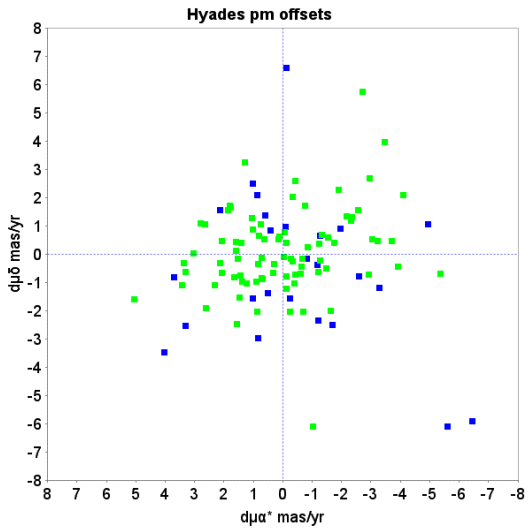

Fig. D.1. Offsets between measured proper motions and the predicted values as based on the measured parallax, position on the sky and space velocity vector of the cluster. The main noise contribution is likely to be the internal velocity dispersion.

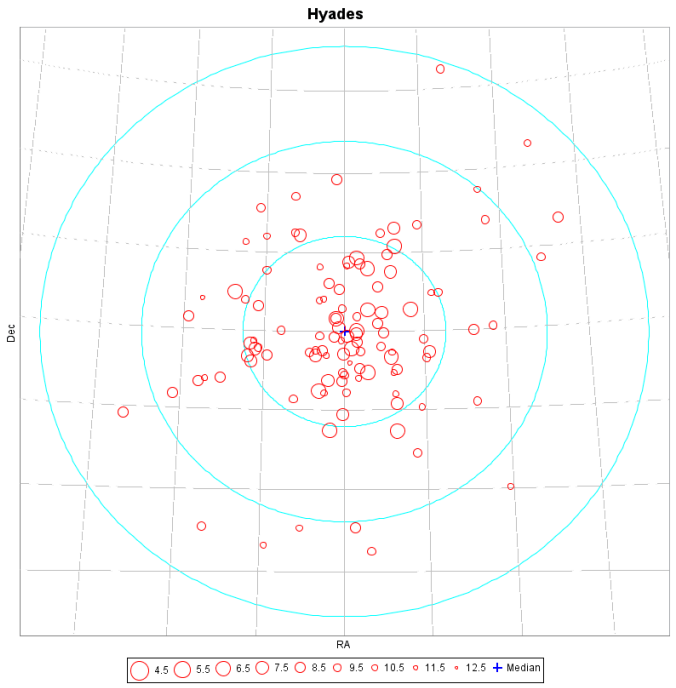

Fig. D.2. A map of the Hyades members as identified from the TGAS catalogue. The coordinate grid is at 5 degrees intervals, the three concentric circles are at 5, 10 and 15 pc from the cluster centre at the cluster distance.

D.2. Coma Berenices

Table D.2. Identifiers and positions for members of the Coma Berenices cluster.

SourceId	HD	α (degr)	δ (degr)	G	SourceId	HD	α (degr)	δ (degr)	G
4019588595869297792		177.1570	28.2751	10.243	4008681509241392256		185.9242	26.6015	9.187
4020237891845231872		178.8889	29.7282	11.285	3953816566210308864		185.9467	23.2457	11.242
3999244366580288512		180.6109	20.1230	9.711	4008364334496501504	108102	186.2593	25.5606	8.073
4002921030384951936		181.0969	24.8206	9.892	3953772070349122816	108154	186.3437	23.2290	8.505
4003439518837094272		181.9904	25.5865	11.070	4009051048227419520	108226	186.4664	26.7766	8.276
4003559674841400320	105863	182.7807	25.9901	9.442	4008790017295714688		186.7126	26.2671	11.514
4013188785360910336		182.8965	29.3790	11.019	4008867670304423424		186.7760	26.8457	9.732
4003406533487752832		183.2218	26.2504	11.091	3953787429152384256		186.8361	23.3298	10.118
4001595500398414848	106293	183.4329	22.8880	8.029	4008390928933851264	108486	186.9098	25.9121	6.724
4002565304013314944	106691	184.0348	25.7603	8.041	4009300946604526208		186.9512	28.1944	9.536
4002550288811032832	106946	184.4621	25.5713	7.821	4009295139808743936		187.0879	28.0405	10.164
4016309611677805568	107053	184.6211	32.7489	6.702	4008777029313889152	108642	187.1589	26.2269	6.556
3953951874859947904	107067	184.6507	23.1200	8.602	3960008294143258240		187.4205	24.5207	9.501
4008571351920493440	107131	184.7584	26.0083	6.492	4009041083903247488	108976	187.7628	27.7303	8.489
3953900747569804928	107168	184.8299	23.0346	6.307	4010969146262166144	109069	187.9606	29.3141	7.527
4002172366045267072	107214	184.8681	24.2842	8.886	1518264342066234368		188.1294	35.3312	9.467
4010203989248653184	107276	184.9609	28.4643	6.681	4010481375416160000		188.2525	27.7124	10.925
4008525241151501824	107399	185.1898	25.7658	8.956	3958685993971916672		188.3333	22.4065	10.099
4008553484856786048		185.3150	26.1539	11.144	3959212282084332544	109307	188.3925	24.2829	6.328
4008227720176880384	107513	185.3614	24.9970	7.393	3960681298339257728		188.4254	25.9427	10.312
4008706729289355520	107583	185.4542	26.5491	9.177	3955895055503655552	111154	191.7780	22.6168	8.284
4009518100151157248	107611	185.4839	27.3095	8.454	3958022919740939904	111878	193.0483	25.3735	8.787
3953625835302703488	107685	185.6031	22.4641	8.461	1464103808031348480		194.4035	28.9791	10.071
4008433603729046784	107793	185.7849	25.8513	8.995	3956998690300563200	113037	195.1465	23.6517	8.195
4008744250123486720	107877	185.9208	26.9799	8.312					

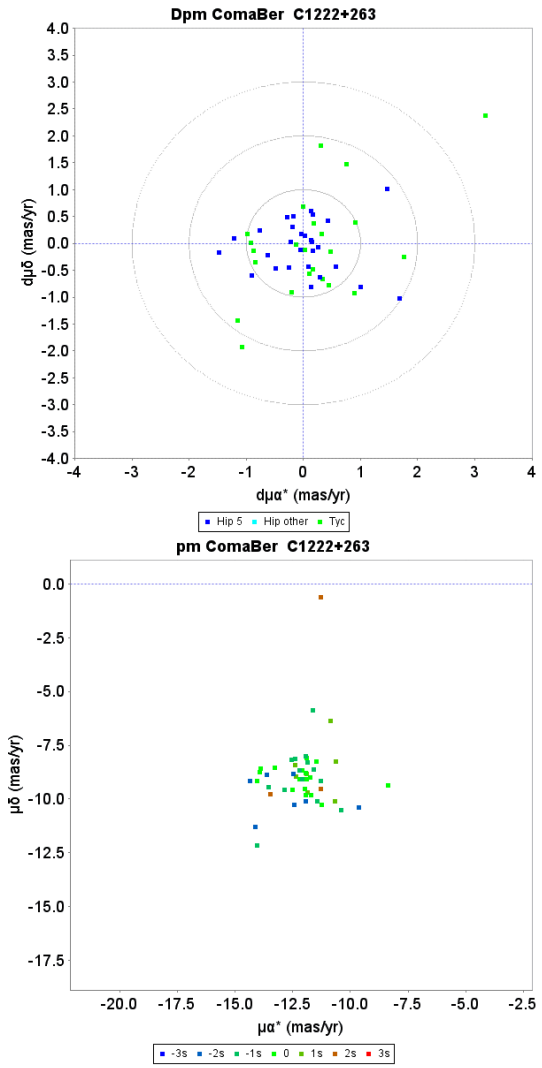

Fig. D.3. Proper motion charts for the Coma Ber cluster. *Top*: unit weight residual proper motions. Green dots have first epoch *Tycho-2* data, the dark blue dots have HIPPARCOS first epoch 5-parameter solutions. The concentric circles represent 1–3σ *su* levels. *Bottom*: actual proper motion distribution, where the colour indicate the difference from the cluster parallax in *su* units.

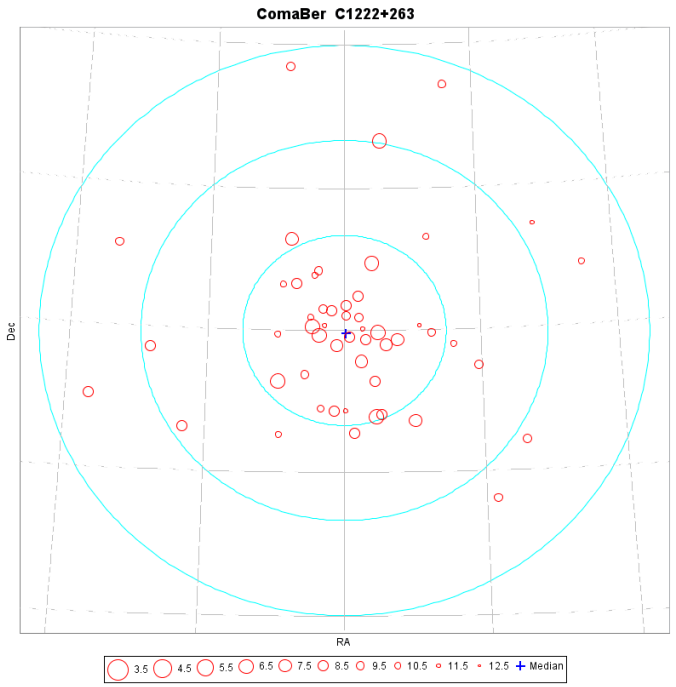

Fig. D.4. A map of members of the Coma Ber cluster as identified from the TGAS catalogue. The coordinate grid is at 5 degrees intervals, the three concentric circles are at 5, 10 and 15 pc from the cluster centre at the cluster distance.

D.3. The Pleiades

Table D.3. Identifiers and positions for members of the Pleiades cluster.

SourceId	HD	α (degr)	δ (degr)	G	SourceId	HD	α (degr)	δ (degr)	G
62413983709539584	20420	49.4574	22.8320	7.567	65221483571888128	23409	56.4652	24.0387	7.840
118078787089883392		52.0463	27.3070	10.529	66798492484311936	23432	56.4771	24.5543	5.815
117672070866974976	21510	52.2364	26.3084	8.315	69872039800655744	23430	56.4965	25.3984	8.022
68897838137902208		52.4100	24.5103	11.809	66786500935624320	23441	56.5122	24.5277	6.456
69335615566555904	21744	52.8166	25.2553	8.084	70049473488842112		56.5397	26.1387	11.423
61519668439604992		52.8682	21.8217	8.745	64981927476000128		56.5751	23.4865	10.275
69643753698133376		52.8902	26.2653	10.512	63289916519862656		56.5807	20.8796	11.261
61554646652580736		53.2744	22.1341	11.136	65231482255770112	23489	56.6138	24.2548	7.365
67680850564641792		53.3080	23.0062	11.586	69847610026687104	282952	56.6141	25.1353	10.342
69250231614573056		53.5076	24.8807	10.663	65008693712182656	23512	56.6426	23.6238	8.013
68097015715726208		53.5306	24.3443	9.394	65199974375696512	282975	56.6571	23.7875	9.997
67799185503558016	22146	53.7445	23.5300	8.764	64808204638390912	23514	56.6601	22.9196	9.265
67618281484716544		53.8822	22.8234	9.688	66838452861270272	282954	56.6617	24.9595	10.051
71296663272200320		54.0353	27.3428	9.168	64952824777149440	23513	56.6667	23.1101	9.260
64575726648969600	22444	54.3503	22.3508	9.034	64899017426872960		56.6962	22.9144	10.291
64671899556831360		54.5942	22.4995	9.884	66789868189090816	23568	56.7476	24.5199	6.828
68444873706967808		54.7370	24.5696	10.331	64979728452744192		56.7560	23.4948	11.209
68250260148846720	22627	54.7881	24.3676	9.692	65212103363335296	23585	56.7677	23.9950	8.313
64313218247427456	22637	54.8051	21.8431	7.291	66729257611496704	23584	56.7920	24.2765	9.334
68254245878512384		54.8062	24.4663	10.172	66715273197982848	23607	56.8307	24.1389	8.238
65113559634339200	22680	54.9217	23.2907	9.763	69964879813013248	23598	56.8371	25.5257	9.663
68593342136568448	22702	54.9633	25.1947	8.728	65017627244152064	23632	56.8375	23.8032	7.025
71371258264471424		55.0129	27.7403	9.468	66715101399291392	23629	56.8378	24.1161	6.328
70941383577307392		55.0241	26.1962	10.942	64898364591843712	23610	56.8455	22.9219	8.118
68334235349446528		55.1281	24.4871	11.420	65207705316826752	23631	56.8518	23.9145	7.306
70190245337962368		55.1495	26.1512	10.897	65007078804476928	23643	56.8619	23.6781	7.753
65119160271381248		55.2103	23.4183	10.591	66729876086786944	23642	56.8728	24.2881	6.833
65120465942548864	22887	55.3458	23.4867	9.037	69948249699646720	23664	56.9452	25.3855	8.259
65150943028579200		55.3660	23.7081	10.894	64913448517448192		56.9506	23.2179	10.875
70108469159560448		55.4008	25.6191	9.899	66724447247218048	23733	57.0566	24.3182	8.188
65027591568709632	22977	55.5198	22.8584	9.023	66939848447027584	23732	57.0704	25.2149	9.066
64317994252099840		55.6001	21.4733	9.664	63948214747182848	23792	57.1640	21.9248	8.280
64449729487990912		55.6002	22.4210	10.157	64933755122821120	23791	57.1830	23.2596	8.320
63144712265008512	23028	55.6245	20.1498	8.340	64114241002810496	23852	57.2970	22.6093	7.713
68310561489710336	23061	55.7297	24.4929	9.330	66506331628024832	23863	57.3009	23.8866	8.113
68317605236065408		55.7624	24.6696	11.588	66746437479801088	23872	57.3201	24.3959	7.537
69896469573892224		55.8068	25.2699	11.850	66745612851296256	23873	57.3407	24.3808	6.637
65063703653090176		55.8523	23.2258	10.281	66555981449928832	23886	57.3584	24.2475	7.957
69904097435804672		55.8631	25.3874	11.110	64930490947667840	23912	57.3864	23.3802	9.010
64380632054140416		55.8798	22.1582	10.171	64109911675780224	23913	57.4092	22.5333	7.028
65232100731054592		55.8832	23.6739	10.574	64928601162063744		57.4143	23.2899	10.938
65233784358231168		55.8935	23.7617	11.121	64929391436043264	23924	57.4206	23.3414	8.093
65089336018173440		55.9073	23.5358	10.514	66453486350431232	23923	57.4315	23.7117	6.196
65184924810275968	23157	55.9231	23.6490	7.844	66980358578521856	23935	57.4706	25.6473	9.388
69876712724339456		55.9515	25.0042	11.358	64053561704835584	23950	57.4796	22.2440	6.073
65289275335247872		55.9614	24.2473	11.035	64924409273987712		57.4855	23.2184	10.091
68306094723718528	23194	56.0012	24.5568	8.037	66558249192653952	23948	57.4859	24.3488	7.562
65086587239103616		56.0026	23.5438	10.766	66507465499396224	23964	57.4920	23.8485	6.828
68296886313838848		56.0149	24.5041	10.458	66960258131598720	23975	57.5737	25.3794	9.483
65072431026899712		56.0468	23.3791	11.133	64172034082472448		57.5889	23.0962	11.102
68322140721525760		56.0581	24.7792	10.528	70506870326054656		57.5889	27.1442	11.088
70252676982016768		56.0641	26.3310	10.798	65677368580114560		57.7144	23.3289	12.084
69811635379765760		56.0838	24.7960	10.407	66969672699893248	24086	57.7765	25.5945	8.983
65272817021006848	23247	56.0982	24.1325	8.932	66480939781378048		57.8204	23.8264	11.976
65292230272755200	23246	56.1073	24.3945	8.133	66657411397616128	24132	57.8635	24.5185	8.744
69811944617410688	23269	56.1699	24.8183	9.693	66863054431798272		57.9186	24.9830	10.643
69945810158924672		56.1800	25.8753	11.347	63730305286697600		57.9255	21.6682	11.220
69917635172718720		56.1832	25.4991	11.744	66471215975411200	24194	57.9870	23.9018	9.910
63378976961208704	23290	56.1870	20.7478	8.606	67369654414221952	24178	57.9893	25.9987	7.653
64879398017459072	23289	56.2136	23.2687	8.858	50905051903831680		58.0034	19.5967	10.265
70234878637524480		56.2210	26.1418	12.012	66570549979009280		58.3489	24.0648	11.150
64739244643463552	23312	56.2456	22.0323	9.322	51619115986889472		58.3703	20.9072	11.553
63052044051306112		56.2570	19.5592	9.264	65819961494790400	24463	58.5900	24.0755	9.554
65194648616227840		56.2637	23.8392	11.597	66581957412169728		58.6052	24.3599	10.758
69840875517213184		56.2668	25.2577	10.482	51742467447748224		58.6161	21.3895	10.713
65188085906203520	23326	56.2721	23.7025	8.859	51674916201705344		58.8832	21.0793	10.843
65275497080596480	23325	56.2773	24.2633	8.527	65308413709777664	24655	59.0163	22.2268	8.944
70242781377368704		56.2843	26.2923	11.183	65309100904545280		59.0464	22.2210	11.241
69864308858778112		56.3141	25.2893	10.939	65754128236100096		59.1093	23.7841	11.049
69819400680743808	23351	56.3370	24.9219	8.901	65437640685532288	24711	59.1173	23.1501	8.289
69819022723623296	23352	56.3506	24.8858	9.524	51717109960976896		59.3132	21.5156	11.420
65222205126393984	23361	56.3590	24.0350	8.013	49809491645958528		59.4573	18.5622	11.160
71729527256889216	23336	56.3648	28.6685	7.405	51452746133437696		59.5072	20.6766	9.249
63502259702709888	23388	56.3834	21.2465	7.731	65776736943479808	24899	59.5872	24.0809	7.224
64798686990854400	23402	56.4163	22.6943	7.802	51694741770737152		59.5902	21.2575	11.180
69922239378409088		56.4381	25.5956	9.938	53783848223326976		60.9341	22.9441	9.491
64956123312029952	23410	56.4535	23.1470	6.920	51861420861864448	284215	62.2309	20.3858	9.232

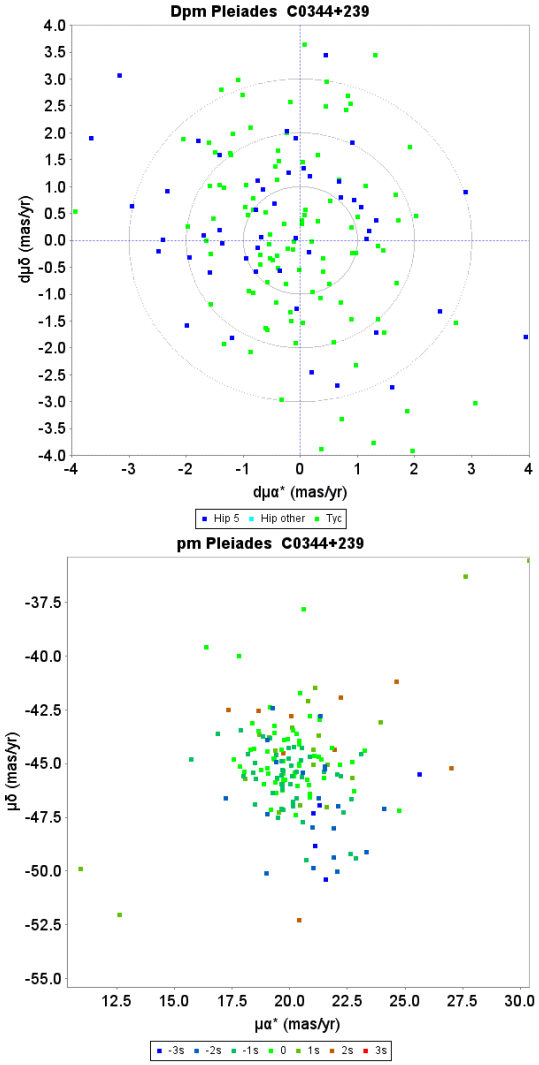

Fig. D.5. Proper motion charts for the Pleiades cluster. *Top*: unit weight residual proper motions. Green dots have first epoch *Tycho-2* data, the dark blue dots have HIPPARCOS first epoch 5-parameter solutions. The concentric circles represent 1–3σ *su* levels. *Bottom*: actual proper motion distribution, where the colour indicate the difference from the cluster parallax in *su* units.

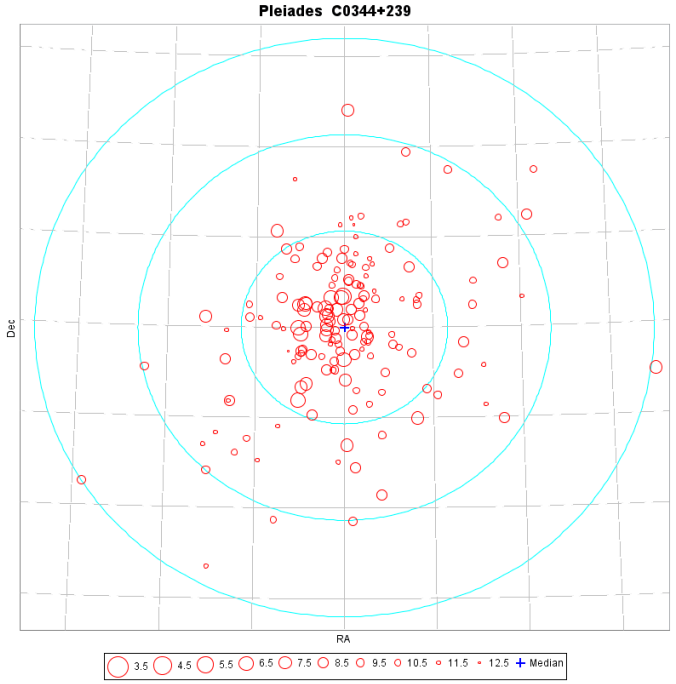

Fig. D.6. A map of members of the Pleiades cluster as identified from the TGAS catalogue. The coordinate grid is at 2 degrees intervals, the three concentric circles are at 5, 10 and 15 pc from the cluster centre at the cluster distance.

D.4. The Praesepe cluster

Table D.4. Identifiers and positions for members of the Praesepe cluster.

SourceId	HD	α (degr)	δ (degr)	G	SourceId	HD	α (degr)	δ (degr)	G
663386973364333056	70297	125.4596	19.4890	8.681	661291132403077760	73731	130.1124	19.5448	6.272
676256482090436480		126.1375	21.7394	9.823	661199907297724416	73746	130.1372	19.1943	8.601
662925625157936256		127.7309	19.5554	10.606	661300546971382016	73785	130.1799	19.7193	6.800
662215546804136064		127.8039	18.1536	9.718	664424637463005824	73798	130.2185	20.2665	8.420
664683125774748032		128.7483	21.0969	10.988	661246018066598656	73819	130.2344	19.5803	6.741
662794164798230016	72779	128.8309	19.5900	6.362	661319547906689024	73818	130.2371	19.9348	8.633
664376430751104512		128.8667	20.1963	10.141	661305838371084288	73854	130.2943	19.8295	8.930
662849896293859712	72846	128.9376	19.7711	7.461	661401358443742720	73872	130.3072	19.9219	8.348
659539232422905472		128.9771	18.1493	10.676	661224577591160448		130.3267	19.2604	10.074
659343622432367360		129.1157	17.9148	10.610	659472230933525760		130.3812	18.5006	10.221
664286476955590016	73081	129.2583	19.6047	9.035	661252993093483392		130.4261	19.6605	9.445
664282663024631808		129.3663	19.5625	9.556	661424070230823040		130.4324	20.2268	10.302
664281494793527936	73175	129.4195	19.5184	8.214	661221760091324544		130.4394	19.2672	10.006
661277457228117504		129.4441	19.4383	10.473	661396754238802816	73974	130.4585	19.8741	6.583
659771023218259072	73210	129.4447	19.2672	6.696	661422764560767360	73993	130.4713	20.1594	8.462
658465868556261888		129.5320	17.0506	9.640	664486794229860864		130.4967	20.9186	11.075
661281752195411328	73397	129.6955	19.5009	8.906	661233133164719616	74028	130.5269	19.4112	7.924
664323276234817664	73430	129.7648	19.9997	8.282	661344183839101952		130.5644	19.6876	9.738
664330835377270912	73429	129.7716	20.1171	9.265	661412490998994176	74058	130.5899	20.1816	9.109
661288624142170368	73449	129.7753	19.6768	7.374	660909189551857664		130.6532	18.3888	9.951
661284019938140032	73450	129.7877	19.5923	8.448	661235985023012864		130.6695	19.5431	9.636
659439073785562240		129.7955	18.1759	10.091	661329958907430272		130.6849	19.5799	9.555
661207019764473344		129.8006	19.1156	10.396	664845303740260992	74135	130.7209	20.8192	8.753
664344819790782592		129.8123	20.2107	11.074	661043845366041984		130.7746	19.4375	9.738
659687494694306688		129.8979	18.8768	10.542	661015910898910080	74186	130.7792	19.0683	9.398
661311439008441600	73575	129.9276	19.7784	6.601	664963020203495552		130.8439	21.6716	10.349
661210730616213248	73576	129.9359	19.2752	7.630	661386240158893568		130.8979	20.1895	9.968
664452949887595136	73597	129.9762	20.5602	9.214	665276415377154688		130.9115	22.2692	11.963
661268248817325312	73619	129.9906	19.5414	7.493	658628905514597376		131.0497	17.9021	9.780
661206573087872256	73641	129.9918	19.2016	9.346	661872464816550144	74547	131.3110	20.9975	9.366
664329186109826944	73616	129.9931	20.1582	8.818	660953994650380416	74589	131.3354	18.8753	8.382
661324701867480576	73617	129.9960	20.0314	9.114	665004698566151168		131.3663	21.6535	10.364
664328911231920896	73640	130.0052	20.1356	9.536	661779796602531712		131.3769	20.5901	9.690
664547885844673792	73639	130.0320	21.0627	9.212	661156854545540480	74718	131.5643	19.7091	8.324
661322056167588736	73666	130.0476	19.9711	6.619	665104341807795584	74740	131.6203	22.3521	8.165
661323636715553152		130.0638	19.9942	8.741	660288790115813632	74780	131.6385	18.7609	9.056
661290754445957248	73711	130.0752	19.5319	7.516	610194902914961664		131.8087	16.3964	10.461
661217911800624384	73712	130.0838	19.3489	6.698	660225911794604416		132.0071	18.6771	10.185
661297076637809024	73710	130.0919	19.6699	6.097	660204402598397312		132.1158	18.3455	11.207
661419259867455488		130.0928	20.1067	9.919					

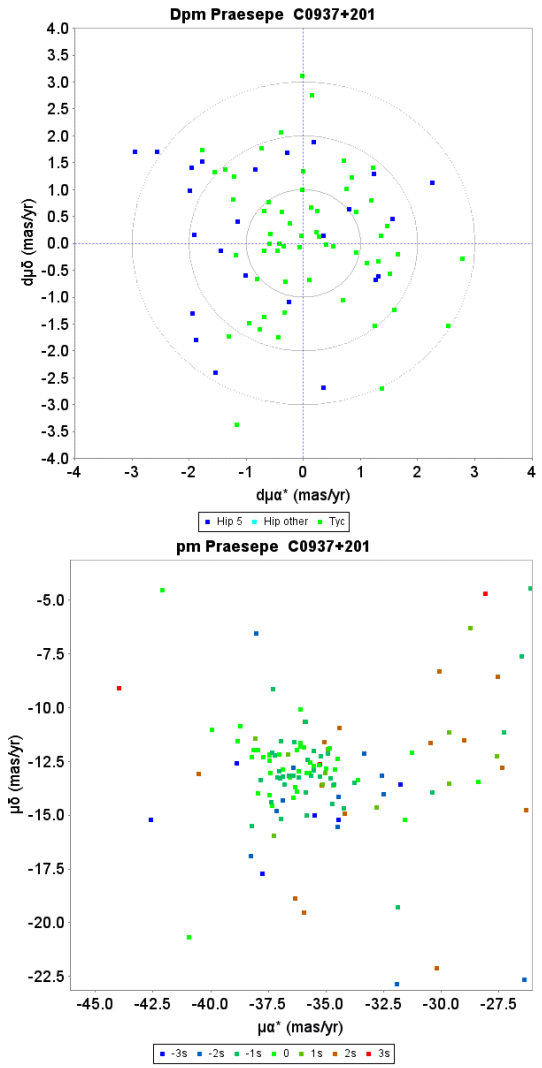

Fig. D.7. Proper motion charts for the Praesepe cluster. *Top*: unit weight residual proper motions. Green dots have first epoch *Tycho-2* data, the dark blue dots have HIPPARCOS first epoch 5-parameter solutions. The concentric circles represent 1–3σ *su* levels. *Bottom*: actual proper motion distribution, where the colour indicate the difference from the cluster parallax in *su* units.

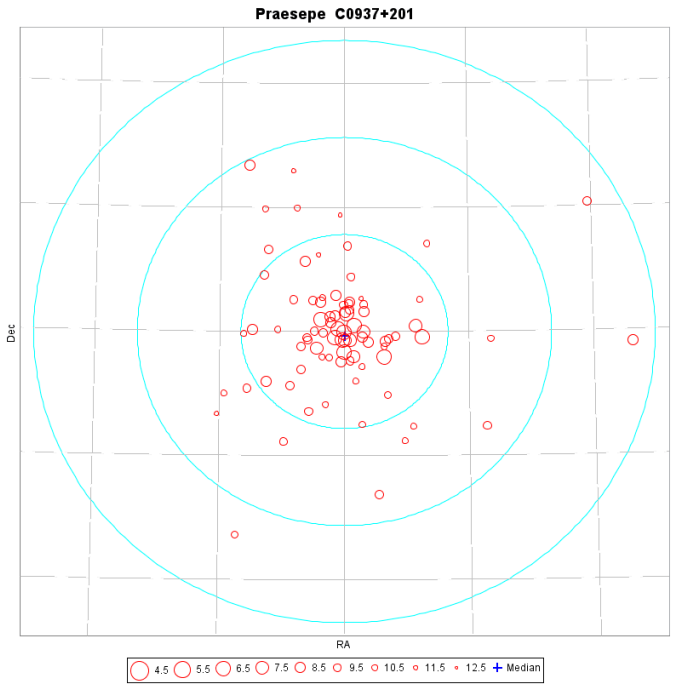

Fig. D.8. A map of members of the Praesepe cluster as identified from the TGAS catalogue. The coordinate grid is at 2 degrees intervals, the three concentric circles are at 5, 10 and 15 pc from the cluster centre at the cluster distance.

D.5. The α Per cluster

Table D.5. Identifiers and positions for members of the α Per cluster.

SourceId	HD	α (degr)	δ (degr)	G	SourceId	HD	α (degr)	δ (degr)	G
439191432859770624	18280	44.4756	48.8786	8.676	249203176564080000	21239	51.9068	48.2728	8.344
436211962508592000		46.9603	49.1082	9.953	441415504364607360		51.9077	48.9912	10.370
440153471174320768	19268	47.0162	52.2134	6.337	441582114738266368	21238	51.9125	49.5998	6.963
436802640772120960		47.6742	50.5255	10.872	441585722510785408		51.9794	49.7602	10.474
445951986261569280	19624	47.9289	52.1634	6.899	249126519989327872	21279	51.9826	47.7358	7.269
436786663491188096		47.9585	50.3796	9.586	441597954577636608	21302	52.0776	49.9528	8.100
435152789212540800	19767	48.1779	47.8385	8.896	441401932267956096		52.1314	48.9408	9.623
436392282414665344	19805	48.2720	49.0093	7.966	441815142481538048		52.1446	50.2668	9.904
436345965487346560		48.4522	48.9864	11.932	441519064618374656	21345	52.1584	49.3875	8.409
436422244105716480	19893	48.4599	49.5688	7.156	249212797292342400	21398	52.2820	48.3028	7.390
436499553517681024		48.8483	49.4402	9.975	441493775848573440		52.3541	48.9624	10.111
436461517287294464		49.0967	49.6258	9.863	249164418780724224		52.3595	48.2031	9.793
436455126375970304		49.1625	49.4523	11.573	242888956163684096	21455	52.3597	46.9378	6.186
442841914544333696	20191	49.2047	51.2181	7.195	441494188165433216		52.4454	49.0094	9.047
436536249718223744		49.2479	49.9265	10.190	249222383659342336	21527	52.5807	48.4992	8.754
436482064410835968		49.5074	49.6440	9.583	248924965763985280	21553	52.6418	47.6281	8.723
436493849800482048		49.5221	49.9060	9.778	249149025617941248	21551	52.6541	48.1035	5.859
442576794801933312	20344	49.5998	50.5556	8.014	441550125819632768	21600	52.8113	49.7061	8.582
435242914806781184		49.6143	47.3542	11.253	249331785065507968		52.8709	48.9911	9.919
442556556916042496		49.6822	50.3862	10.105	441560399381392768	21619	52.8759	49.9020	8.729
436477460205283584	20391	49.6867	49.7699	7.952	248960218855540736	21641	52.8882	47.8623	6.790
436477013528685184		49.7098	49.7311	10.920	441532499273859840		52.9358	49.5367	9.493
435641144174237568	20475	49.9241	48.9135	9.093	249278355672330624	21672	52.9749	48.7350	6.635
435609670653875328	20487	49.9470	48.6278	7.659	249267120037890432		52.9760	48.5272	10.272
442609127315775744	20510	50.0262	50.9687	7.070	249267875952132736		52.9827	48.5837	8.207
442921800934903424	20537	50.0988	51.6183	7.299	441558440876307584		52.9948	49.8701	9.089
435429007149649920		50.3761	48.4938	9.060	442265083255962624	232804	53.1330	51.4895	10.037
435647638163950848		50.4177	49.1201	9.443	248077998211731840		53.1944	46.7008	9.705
441653239394337024		50.4944	49.2148	9.081	248886001820685184	21855	53.3429	47.4219	8.199
242950116497972608		50.7646	46.3341	11.393	241699525101944576		53.3994	44.8708	10.210
435341561615535360		50.9181	47.9581	9.806	442041985477060480		53.4957	50.8821	9.747
442750826879003648	20842	50.9300	51.7703	7.871	249282100885527040	21931	53.5542	48.6174	7.392
435422581877640704	20863	50.9474	48.6043	7.002	247787692782638976		53.5747	45.7300	11.278
441645233577061248	20919	51.0801	49.2212	8.903	249282341403694592		53.5901	48.6599	8.756
441454914984502656	20931	51.1253	49.1398	7.891	442036934595519872		53.7711	50.9124	11.047
441371523899475840		51.1964	48.4116	9.742	249765198807892736		53.7866	49.7442	10.947
441436601243976448		51.2073	48.8716	11.361	248192106902849408	22136	53.9938	47.0909	6.900
243137067835529344		51.2298	47.4149	9.598	249087281167662464		54.1329	48.6545	9.944
441696326507978752	20969	51.2683	49.7953	8.953	249475649291238784		54.2297	48.8285	9.916
441480409912850432	20986	51.2919	49.2514	8.157	444862507681846016	22222	54.2836	53.9832	8.456
441481165827089024	21005	51.3365	49.3161	8.403	248229524660290688	22401	54.5651	47.5769	7.472
243190978263909632		51.3729	47.9672	9.140	249408682161136000	22440	54.6464	48.5934	8.585
441849158625581568		51.4070	50.3215	9.913	443683693773493504	22603	55.1440	52.0083	9.076
243068657596900224	21046	51.4071	47.0205	8.903	443627412522052992		55.1938	51.6344	11.372
441463607998311808	21071	51.4892	49.1206	6.106	244833442477429888		55.2741	45.7937	10.070
249199878029198208	21092	51.5444	48.2216	8.489	248624661649191296		55.3585	48.1450	10.213
441356921010671232	21091	51.5454	48.3839	7.525	251450990648112128	232823	55.4209	51.2764	9.306
441486044909931136		51.5928	49.4270	11.097	248376137662086784	23219	56.3649	47.6602	7.198
243096832581342848	21122	51.6362	47.2663	8.166	244788843539087104		56.3727	45.7420	11.511
249180396057550848		51.6634	47.8822	9.494	245189890404732160		56.4311	46.3011	11.820
441901694662492928	21117	51.6645	50.8464	7.633	244596497721602176	23287	56.4719	45.5998	7.602
441383171850821888		51.6700	48.7768	9.596	251154431747668096	23255	56.4783	50.4191	9.352
441780164270958464		51.6831	49.9094	10.672	248480453827267456		56.6770	48.0868	10.413
441405917997620352		51.7089	48.7921	10.164	250324850223865472		56.7326	49.6907	10.449
249180567856242048	21152	51.7095	47.9160	7.721	251516652110388992	23452	56.9172	51.5287	7.320
441405780558667264		51.7637	48.7869	9.808	251087224100861952		57.1336	50.0471	10.128
249197404128036480	21181	51.7717	48.2054	6.857	249956685626486144		57.9157	48.3759	9.619
441901282346949760	232793	51.8090	50.8788	10.016	246596887329673728		58.9503	47.0402	10.480

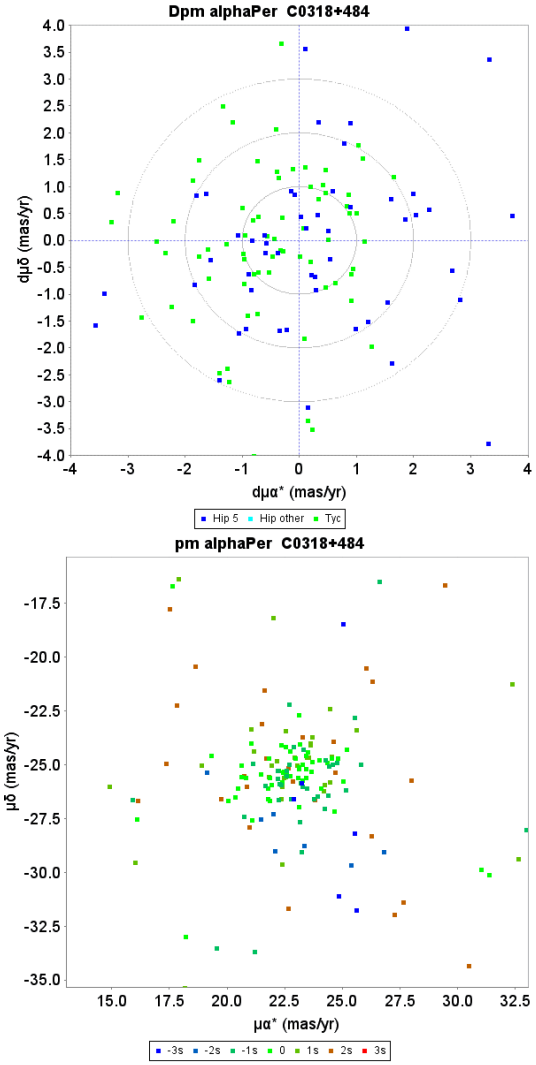

Fig. D.9. Proper motion charts for the α Per cluster. *Top*: unit weight residual proper motions. Green dots have first epoch *Tycho-2* data, the dark blue dots have HIPPARCOS first epoch 5-parameter solutions. The concentric circles represent 1–3σ *su* levels. *Bottom*: actual proper motion distribution, where the colour indicate the difference from the cluster parallax in *su* units.

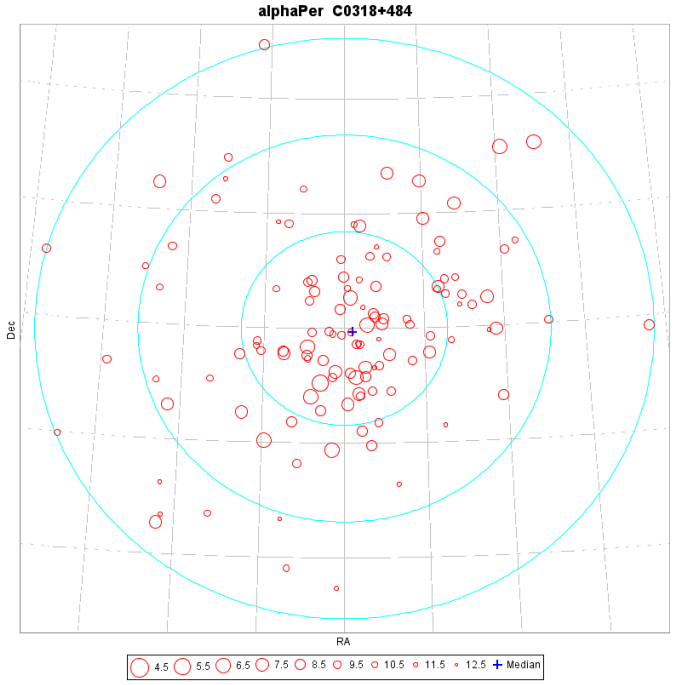

Fig. D.10. A map of members of the α Per cluster as identified from the TGAS catalogue. The coordinate grid is at 2 degrees intervals, the three concentric circles are at 5, 10 and 15 pc from the cluster centre at the cluster distance.

D.6. The cluster IC 2391

Table D.6. Identifiers and positions for members of the cluster IC 2391.

SourceId	HD	α (degr)	δ (degr)	G	SourceId	HD	α (degr)	δ (degr)	G
5513364924200650752	68276	122.3267	–51.0123	7.620	5317906150880166528	74374	130.3446	–53.6358	9.367
5319716806015487488	70560	125.0151	–53.9216	9.253	5318499818442087936	74516	130.5413	–52.9676	7.395
5515719116036643072		126.4811	–47.5548	11.003	5317887321743547264	74561	130.5757	–53.9022	9.236
5515330266875244544		127.0046	–48.6839	9.923	5317884435525524224		130.7515	–53.9020	10.841
5321517668619002240		127.1900	–52.0907	10.247	5318486074546754048	74678	130.7643	–53.0779	7.664
5316373981428187904	72323	127.3967	–55.4168	7.703	5318536995675325952	74714	130.8244	–52.6030	9.014
5515501481453454208	72516	127.8404	–47.4435	8.627	5318702128577954816	74734	130.8866	–52.0037	7.881
5321225473403915136		128.5853	–52.8346	10.115	5318316096918509568		130.9678	–53.2332	9.579
5318069600154320384		129.1009	–54.0182	10.000	5318512256667367040		131.0216	–52.8880	10.546
5322839178517948800	73462	129.1030	–50.2554	9.325	5316501971457325952		131.0555	–57.2547	11.133
5321190151592875904	73777	129.4459	–52.8700	9.510	5329039874346093056		131.0715	–48.5083	9.301
5318077502894130944		129.4647	–53.7626	11.159	5318521671232021632		131.1088	–52.7089	11.214
5318077915210988928	73904	129.5995	–53.7217	7.658	5318630900840369152		131.4129	–52.4331	9.714
5321582711603786880	74044	129.8187	–52.3137	8.442	5318296271349488640		131.4496	–53.4306	10.048
5318113546259668864	74071	129.8492	–53.4397	5.539	5318229269859699072		131.5635	–53.7562	10.190
5321795845062877312		129.9808	–51.3655	10.042	5317423293481147264		131.8926	–54.4835	11.827
5318117325830884224	74169	129.9972	–53.2609	7.241	5318412682141952512	75466	132.0007	–52.8501	6.305
5318567953805446400	74145	130.0067	–52.7034	8.468	5317551352220546048	76472	133.5550	–53.3850	9.393
5318096125872352768		130.0258	–53.6352	10.255	5325336375583055232		134.0447	–49.4907	10.068
5318554106825052160	74275	130.2020	–52.8018	7.294	5317261802706432000	76840	134.1002	–54.3225	9.186
5318093239654329472		130.2044	–53.6292	10.773	5303472346348134656		135.5162	–58.1471	11.095
5317797574106967552		130.2551	–54.5172	10.279					

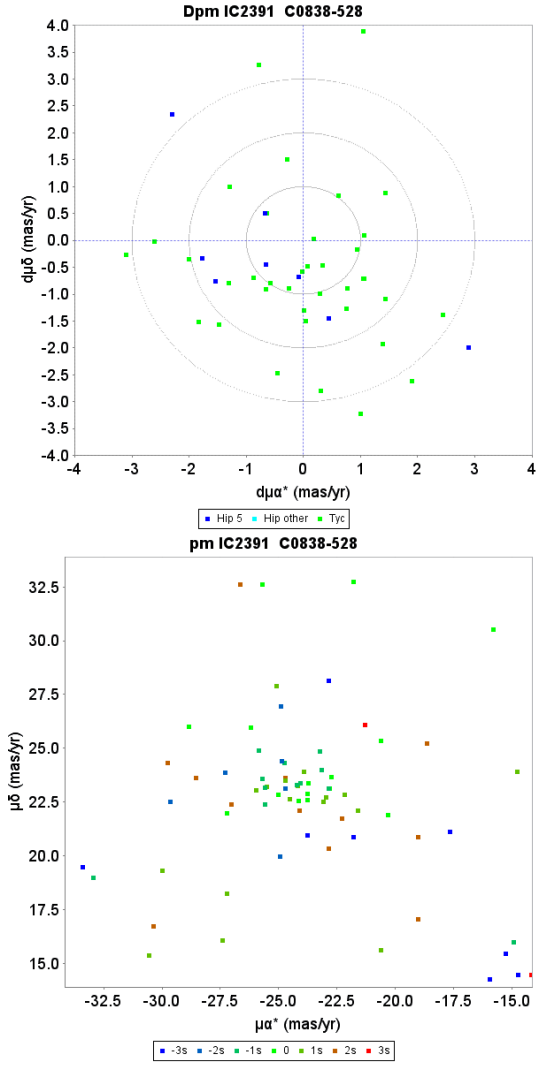

Fig. D.11. Proper motion charts for the cluster IC 2391. *Top*: unit weight residual proper motions. Green dots have first epoch *Tycho-2* data, the dark blue dots have HIPPARCOS first epoch 5-parameter solutions. The concentric circles represent 1–3σ *su* levels. *Bottom*: actual proper motion distribution, where the colour indicate the difference from the cluster parallax in *su* units.

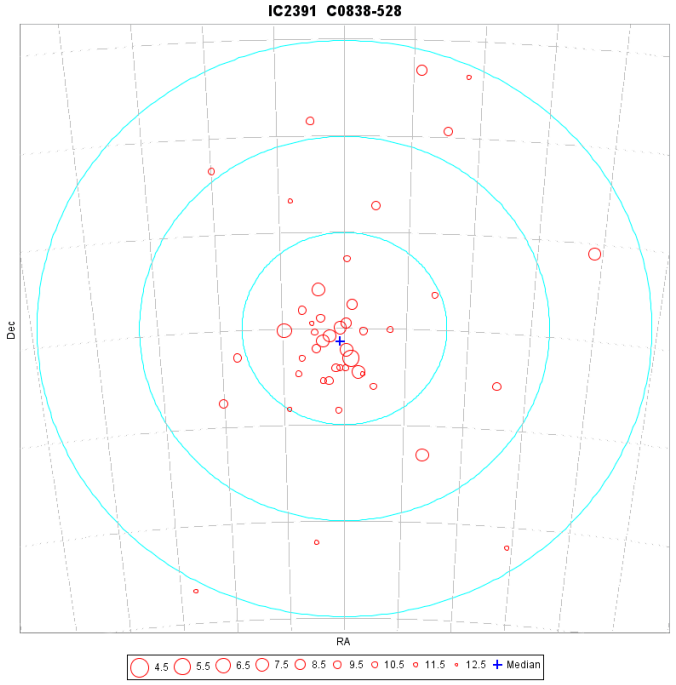

Fig. D.12. A map of members of the cluster IC 2391 as identified from the TGAS catalogue. The coordinate grid is at 2 degrees intervals, the three concentric circles are at 5, 10 and 15 pc from the cluster centre at the cluster distance.

D.7. The cluster IC 2602

Table D.7. Identifiers and positions for members of the cluster IC 2602.

SourceId	HD	α (degr)	δ (degr)	G	SourceId	HD	α (degr)	δ (degr)	G
5246562414765401472	87713	151.1418	–64.6477	6.947	5239689092704584704	92664	160.0475	–65.1002	5.568
5246170163993645056	88386	152.2842	–65.7982	9.002	5239251727594949120	310144	160.1382	–65.9278	10.629
5256461077433424896	88307	152.2888	–60.4162	8.073	5239772689945600128	92715	160.1753	–64.6531	6.834
5244883529229180928		152.3408	–67.6105	11.150	5239869103371472000	92783	160.2766	–64.4743	6.740
5252566023132496256	307557	152.9157	–63.2241	9.439	5239883946781824256	92837	160.3962	–64.1063	7.183
5252392884409210624	88980	153.4413	–63.8999	8.677	5239823782876560512	92966	160.6047	–64.3988	7.287
5245507295921159680	309933	153.7489	–65.8036	9.571	5239725548384560128	92989	160.6599	–64.6779	7.600
5245462112865217024	89903	155.0783	–66.0636	7.534	5239660367966484736		160.7508	–65.5049	10.958
5251495957802232448	90020	155.3235	–65.1956	7.333	5239858726733859968	93098	160.8727	–64.0684	7.605
5245270626044873344	90083	155.4193	–66.1127	8.219	5241458584871666176	307912	161.0135	–63.1726	9.555
5253053725257383424		155.4318	–62.2425	11.126	5239701565287189120	307979	161.2482	–65.0386	10.619
5232616277998058752	90456	156.0607	–68.1295	7.683	5242010093028921856		161.3487	–61.7751	11.182
5251663495883800448	90731	156.6849	–64.3517	7.448	5239801689564803072	93424	161.3913	–64.7038	8.105
5252084918078077952	90837	156.8759	–63.5232	8.280	5239809557944885888	93517	161.5411	–64.5955	7.844
5251470943909316096		157.0373	–64.5052	10.302	5239849896277704960		161.5616	–64.0494	10.484
5252077668171627648		157.1300	–63.7376	11.170	5239498739751922432	310131	161.6374	–65.4550	10.694
5253965770155144704	91042	157.2239	–61.1637	9.478	5239843196128730368	93648	161.7879	–64.2646	7.841
5251238225402532352	91144	157.3580	–65.8758	8.785	5241357189281206656	93874	162.1746	–63.8330	8.179
5251888517809705216		157.3863	–63.8209	11.157	5239626420542800512		162.4515	–64.7745	11.286
5233181908011057536	310053	157.5378	–66.5259	10.061	5239637759256457472	94174	162.6916	–64.4794	7.734
5251845946093877632	307802	157.7811	–64.1819	9.412	5241909865679004288		162.7754	–62.6092	10.616
5251991356506637568	91451	157.9370	–63.4894	9.095	5241082311374967296		163.5722	–64.6809	11.416
5251880511990665216	307793	157.9753	–63.8144	10.189	5241132579670834816	94684	163.6177	–63.9726	8.931
5251765681750027520		158.4151	–64.7811	11.404	5239525196750143616		163.7080	–65.4460	11.618
5251822100435455744	91906	158.7351	–64.1339	7.483	5241066608973054080	308100	164.0480	–64.8004	10.312
5239891677722958976		159.5734	–64.1351	10.393	5241109696086432640	308094	164.3439	–64.2762	10.039
5239789148260273792	92467	159.7139	–64.4980	7.195	5241109867885123328		164.3560	–64.2497	10.790
5239740804110817664	92478	159.7602	–64.9749	7.585	5238698467088998400	95786	165.4778	–66.0123	7.529
5239895629092870144	92536	159.8450	–64.1117	6.354	5240861412615531136	95911	165.6875	–63.4946	9.107
5239926827735288960	92535	159.8539	–63.7781	8.222	5240380376282066816	96287	166.2079	–64.6157	7.252
5239736199905884416	92570	159.8777	–65.0833	9.189	5337081393150208768	308215	166.9832	–62.0480	10.787
5239304538510338432	310113	159.9163	–65.3489	11.160	5237676539747932032	98616	169.9780	–63.7503	8.657
5253452057710889216		160.0000	–63.2530	10.509	5237036555261723648	99149	170.9130	–65.8344	8.127

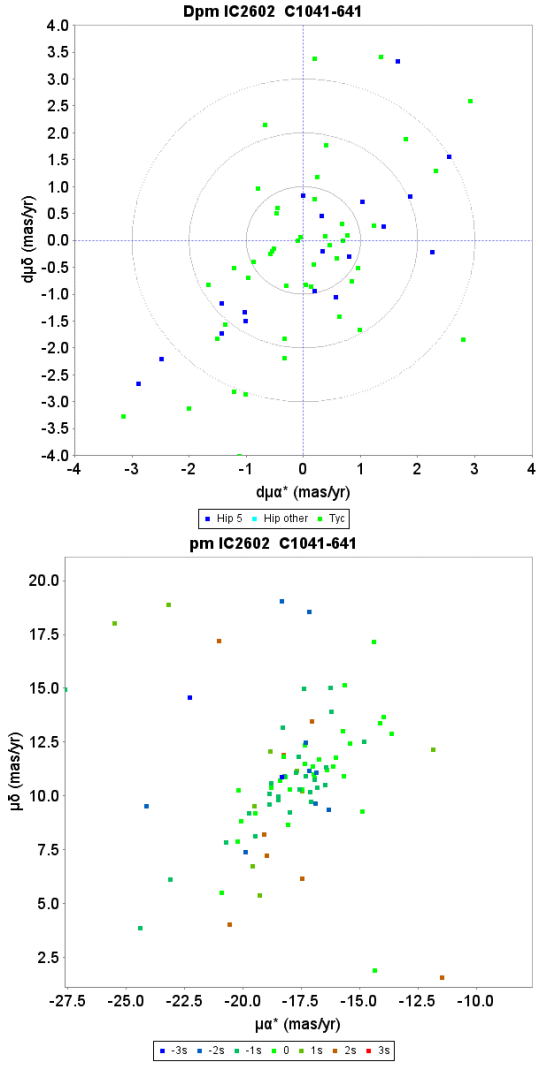

Fig. D.13. Proper motion charts for the cluster IC 2602. *Top*: unit weight residual proper motions. Green dots have first epoch *Tycho-2* data, the dark blue dots have HIPPARCOS first epoch 5-parameter solutions. The concentric circles represent 1–3σ *su* levels. *Bottom*: actual proper motion distribution, where the colour indicate the difference from the cluster parallax in *su* units.

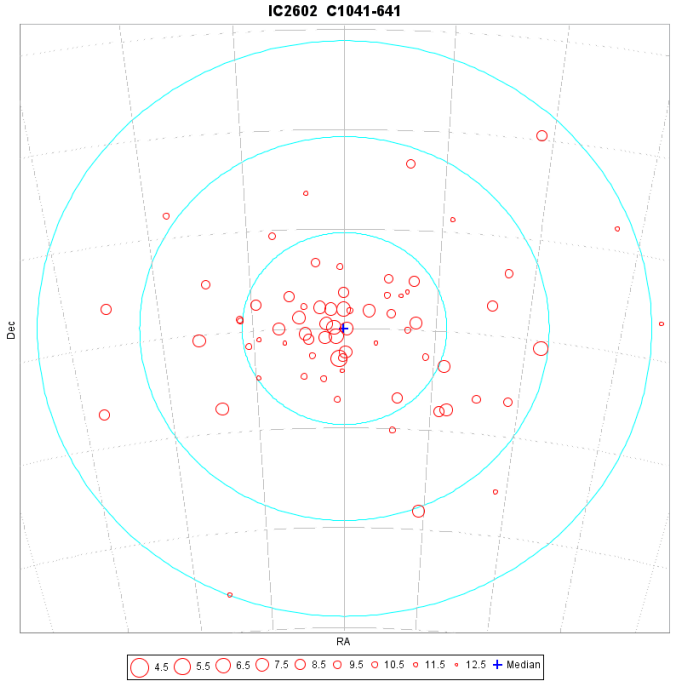

Fig. D.14. A map of members of the cluster IC 2602 as identified from the TGAS catalogue. The coordinate grid is at 2 degrees intervals, the three concentric circles are at 5, 10 and 15 pc from the cluster centre at the cluster distance.

D.8. The cluster Blanco 1

Table D.8. Identifiers and positions for members of the cluster Blanco 1.

SourceId	HD	α (degr)	δ (degr)	G	SourceId	HD	α (degr)	δ (degr)	G
2328281430196519680		357.3891	–27.8397	10.443	2320877215816767360	225111	0.8830	–29.7180	10.024
2327952401341889664		357.9863	–29.0023	12.040	2320770185232173312		0.8901	–30.4783	10.458
2334037751525146624		359.2535	–27.9233	10.312	2320816227281177088		0.9591	–30.0655	10.906
2326921471751885440		359.4123	–29.8351	10.144	2320826432123463040		1.0782	–29.8257	10.378
2326866942847101824		359.4679	–30.0883	11.908	2320979848354547840	225206	1.0955	–29.3816	7.797
2326849247581847296		359.5839	–30.2810	9.943	2320798635095540736		1.1320	–30.2449	11.508
2313104527601463296		359.7039	–33.5562	10.689	2320926178443221888	225264	1.2119	–29.6330	8.330
2326850415812950656		359.7597	–30.2214	10.718	2320610721685102336	225282	1.2223	–30.2566	8.335
2333096432132693632		0.2852	–28.6157	11.436	2320617524913298304		1.2453	–30.1616	11.288
2314771146710725504		0.3521	–30.6495	10.367	2320933153470108032		1.3267	–29.5016	11.129
2320833441510104960		0.3696	–30.2058	10.690	2320612748909666560	50	1.3616	–30.2901	9.646
2320834747180161408	224948	0.4907	–30.1580	9.866	2320903844613139072		1.3790	–29.8856	11.088
2320886218068219264		0.5488	–29.6943	11.651	2320902057906744704	91	1.4291	–29.9606	9.823
2320793893451241344		0.5902	–30.1393	10.570	2321022626228808064		1.4851	–28.9363	11.292
2314555230115494528		0.6372	–30.9921	10.994	2320916763874909568		1.4961	–29.6513	11.450
2333013075407421824		0.6636	–29.0752	10.097	2321010325442474752	141	1.5379	–29.1514	7.941
2320994588682307072		0.7772	–29.3622	11.464	2320709643372054656		1.5682	–30.0992	11.512
2320790285678713984		0.7952	–30.1803	11.147	2313393493000760064		1.6470	–32.8017	11.330
2320869897192498432		0.8360	–29.8230	11.117	2320645734258792064		1.8926	–30.2872	10.421
2320869725393806336		0.8517	–29.8137	10.498	2320702187308925184	343	2.0080	–30.0317	9.687
2320771216024323840		0.8544	–30.4351	11.741	2319380333814252544	704	2.8317	–32.4039	8.436
2320776644862584960		0.8708	–30.3242	10.468	2319554915645229312		3.7501	–31.2733	10.251

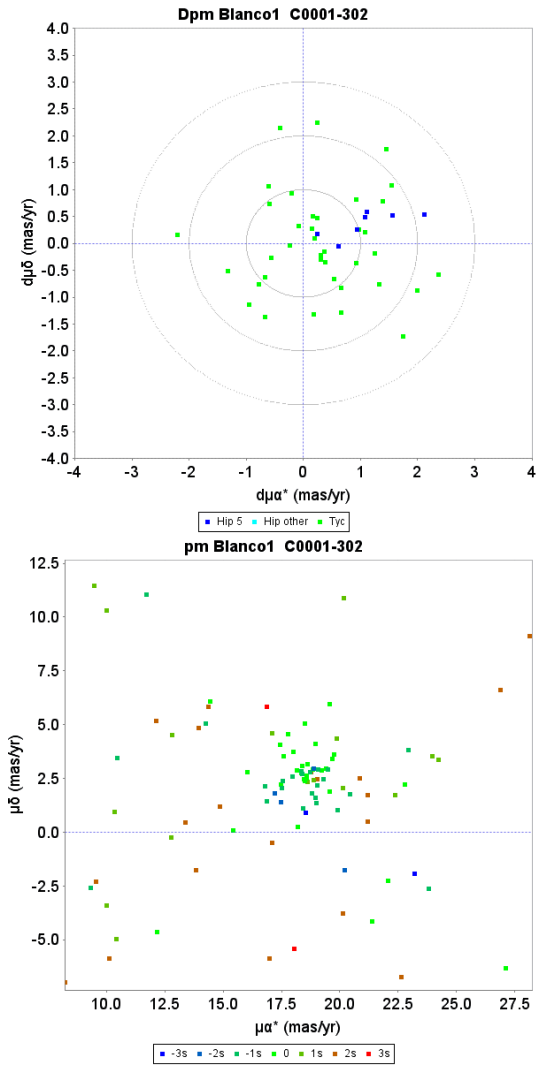

Fig. D.15. Proper motion charts for the cluster Blanco 1. *Top*: unit weight residual proper motions. Green dots have first epoch *Tycho-2* data, the dark blue dots have HIPPARCOS first epoch 5-parameter solutions. The concentric circles represent 1–3σ *su* levels. *Bottom*: actual proper motion distribution, where the colour indicate the difference from the cluster parallax in *su* units.

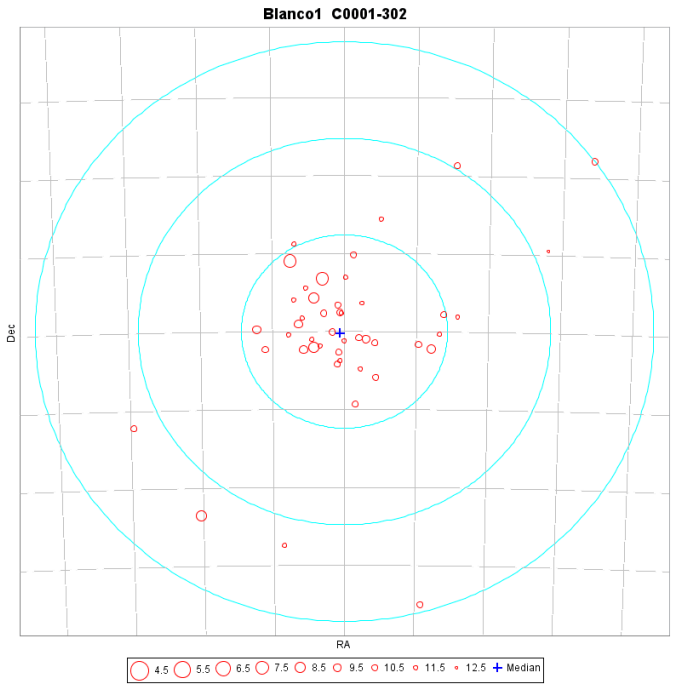

Fig. D.16. A map of members of the cluster Blanco 1 as identified from the TGAS catalogue. The coordinate grid is at 2 degrees intervals, the three concentric circles are at 5, 10 and 15 pc from the cluster centre at the cluster distance.

D.9. The cluster NGC 2451

Table D.9. Identifiers and positions for members of the cluster NGC 2451.

SourceId	HD	α (degr)	δ (degr)	G	SourceId	HD	α (degr)	δ (degr)	G
5585438770393517312	60330	113.0701	–38.1741	8.578	5586861641519108352	62642	115.8727	–37.7505	7.612
5585369844760452224		113.5430	–38.6319	11.380	5538642456004614784		116.1002	–38.5997	10.781
5585190555647523840	61375	114.3182	–39.0545	9.129	5538816247560408448	62876	116.1170	–37.9877	8.624
5588006714160268928		114.4807	–35.9994	10.942	5538637336406254720		116.1170	–38.7782	9.155
5587015401348292736		114.4933	–37.6214	11.132	5538816831675959168	62893	116.1423	–37.9429	5.925
5585278928890699264		114.5179	–38.4535	9.641	5538612253797251456		116.1545	–38.9079	9.369
5587001657452951680		114.5298	–37.7534	11.810	5538598819139552768	62961	116.1828	–39.0207	8.126
5537126538706711936		114.8141	–39.4657	11.702	5538812227471020672	62938	116.1869	–38.0537	7.616
5587037563379531008		114.8219	–37.3751	10.477	5538386166717422080	63198	116.4983	–39.4444	8.867
5536231123926763264		114.8398	–41.9947	9.718	5538855555103296512		116.5371	–37.3991	10.487
5586793471798169600		114.9047	–38.0427	9.854	5538805183726897024	63215	116.5438	–37.9336	5.906
5536717142426664704		115.0181	–40.6927	9.693	5538853596598218112		116.5476	–37.5307	11.055
5588530665810298880		115.1928	–34.6106	9.445	5532490207410038528		116.7050	–43.2293	11.497
5536727106748162816		115.3105	–40.6270	10.983	5538534016672382464	63511	116.9133	–38.6766	8.748
5586820925229156480		115.3260	–37.8968	9.842	5538777695934246656		116.9339	–37.9841	11.602
5586745643042408704		115.3918	–38.0832	10.843	5537606750413835136		118.2994	–40.0162	9.677
5586755676086015232	62479	115.6242	–38.1079	9.057	5534089447072632320		118.7978	–42.3349	11.899
5538660357428319360		115.6419	–38.8488	11.085	5544009309698790400		120.5397	–38.0250	11.414
5587582508831567488	62578	115.7998	–36.0500	5.672					

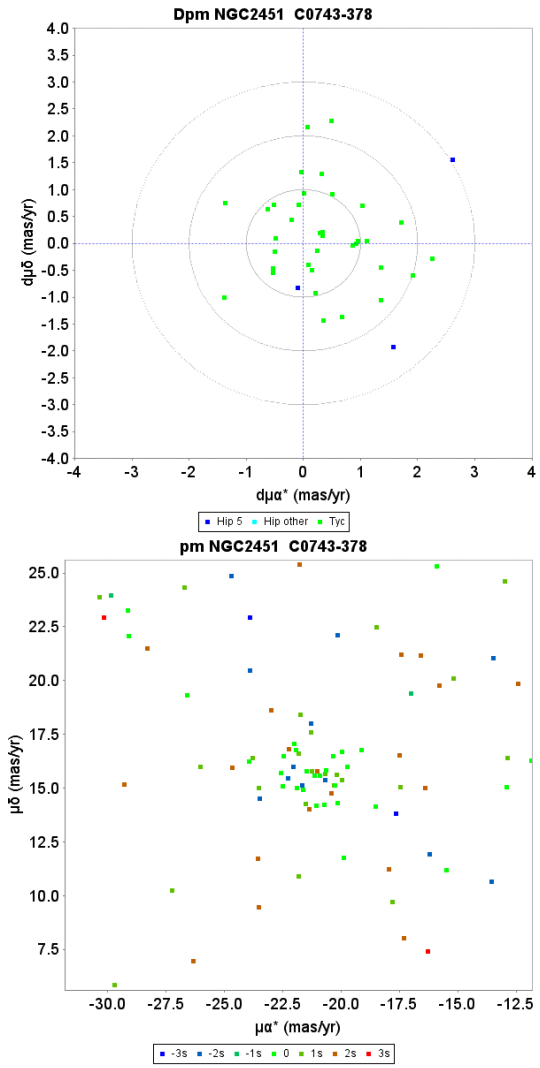

Fig. D.17. Proper motion charts for the cluster NGC 2451. *Top*: unit weight residual proper motions. Green dots have first epoch *Tycho-2* data, the dark blue dots have HIPPARCOS first epoch 5-parameter solutions. The concentric circles represent 1–3σ *su* levels. *Bottom*: actual proper motion distribution, where the colour indicate the difference from the cluster parallax in *su* units.

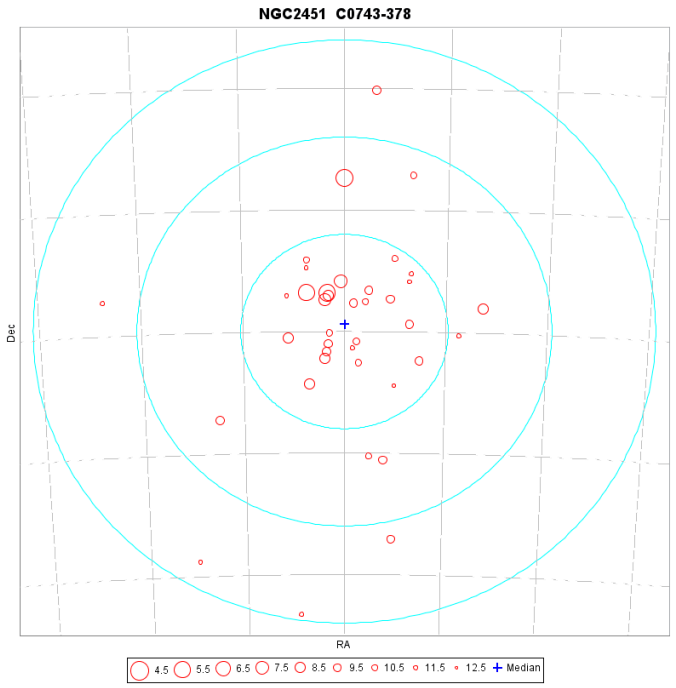

Fig. D.18. A map of members of the cluster NGC 2451 as identified from the TGAS catalogue. The coordinate grid is at 2 degrees intervals, the three concentric circles are at 5, 10 and 15 pc from the cluster centre at the cluster distance.

D.10. The cluster NGC 6475

Table D.10. Identifiers and positions for members of the cluster NGC 6475.

SourceId	HD	α (degr)	δ (degr)	G	SourceId	HD	α (degr)	δ (degr)	G
4041052505956833536	320665	266.7198	–35.6233	10.473	4040637715192089472	162612	268.3694	–35.5117	9.489
4040221824918071424		266.8167	–36.7436	11.605	4040372492371770880	162613	268.3750	–36.5086	7.984
4041744648522172288	161575	266.9481	–34.3107	6.947	4040826521954932096	162780	268.5599	–34.7277	6.876
4040279618003552768	161576	266.9784	–36.0220	9.178	4040728596700624896	320885	268.6121	–35.3338	10.014
4041422491620010368	161651	267.0722	–35.5376	9.027	4040847756273228416	162817	268.6130	–34.4667	6.082
4041554158132660096	161685	267.1030	–34.4658	9.148	4040717532863953408	162839	268.6497	–35.4995	8.443
4040291197235375616	161686	267.1345	–35.7515	8.940	4043113952821300352	162874	268.6594	–33.9563	7.821
4041428264056050816	161855	267.3713	–35.3781	7.342	4043120068854728704	162873	268.6732	–33.9055	7.673
4041458397546585600	320649	267.4005	–35.1666	9.876	4040728287462977152		268.7205	–35.2821	10.985
4041484510943000576		267.4681	–34.7804	11.088	4040744436539998720	162891	268.7234	–35.0893	8.022
4040702002264923136		267.5717	–35.3390	10.824	4040346447690086784	162926	268.7835	–36.4757	6.029
4041629852636717312	162016	267.5731	–34.4761	8.147	4040754984979680512	162942	268.7853	–35.1504	8.579
4041466197202462080		267.6191	–35.0089	11.077	4042353503086066816	162980	268.8133	–34.2356	7.494
4041633151171596928	320741	267.6197	–34.3410	9.694	4042365219756839296	163001	268.8413	–34.0165	9.322
4043474970596660224	318439	267.6642	–32.7352	10.025	4042365013598409856		268.8461	–34.0238	10.500
4041584807019715840	320745	267.7199	–34.4255	9.936	4042333986754687104	320841	268.8799	–34.4817	10.057
4041462245832553856	162144	267.7589	–35.0706	7.616	4040561539657230464	163067	268.9467	–35.3191	9.487
4041464101258425088		267.8166	–35.0052	11.982	4042340171507583104	163109	268.9841	–34.2866	7.977
4041579240742120832	162223	267.8571	–34.5600	8.907	4040766529851750656	320952	269.0952	–34.8332	9.523
4040713134816625792	162224	267.8579	–35.0344	9.046	4042287635467629056	163193	269.0967	–34.4978	8.671
4040603218018657280		267.9507	–35.8614	10.781	4040778590119911424	163194	269.1027	–34.7538	9.089
4040709355245406848	162286	267.9562	–35.1022	9.378	4040519380251978624		269.1672	–35.5569	10.844
4041573605745028096	162285	267.9597	–34.5482	8.643	4042283168701645312	320946	269.1879	–34.5919	9.428
4040603218018656640		267.9611	–35.8542	10.657	4043357254123008640	163274	269.2085	–32.6889	6.658
4040692347178449664	162287	267.9650	–35.3654	7.303	4043274034836706560	318671	269.2626	–33.1078	9.785
4041568795381660288	162348	268.0284	–34.6557	8.997	4040760929214406528	320950	269.2863	–34.9638	9.801
4040808964127026432	320764	268.0413	–34.8946	8.897	4043303721650637696		269.4830	–32.7873	11.081
4040803913245489024	162349	268.0435	–35.0018	8.430	4037427587917137152	320999	269.5119	–36.4534	10.696
4040804153763656576	320768	268.0655	–34.9699	9.131	4042479603329702272	318778	269.5494	–33.6397	10.282
4040804085044179968	162393	268.0834	–34.9745	8.074	4042299489577363200	321043	269.6404	–34.4211	10.758
4040805871752189568	162457	268.1704	–34.9294	8.281	4042063678692927232		269.9128	–34.9376	11.188
4040642972232475136	320776	268.1921	–35.3967	9.791	4042197647312832896	321037	270.2051	–34.3946	10.728
4041595699062347136	162513	268.2352	–34.4461	8.654	4042036878101137152		270.2373	–34.9650	9.851
4040786286701335168	162542	268.2629	–35.1648	8.984	4042036878101137280	321058	270.2404	–34.9665	11.110
4040814461686768640	320863	268.2694	–34.7612	8.880	4042198197068643968	321036	270.2432	–34.3489	10.476
4040814564765981824	320862	268.2812	–34.7478	9.166	4041992313522568064	164108	270.2995	–35.3291	8.739
4040737117915740672	320891	268.2887	–35.3490	10.510	4039009785146773376		270.6158	–35.4038	10.787
4040813259095930752	320864	268.2984	–34.8278	9.198	4042169953363702528		271.1769	–34.2802	11.362
4043179167604718336	162610	268.3394	–33.7643	9.129	4042167616901494784	321249	271.3293	–34.3027	10.132

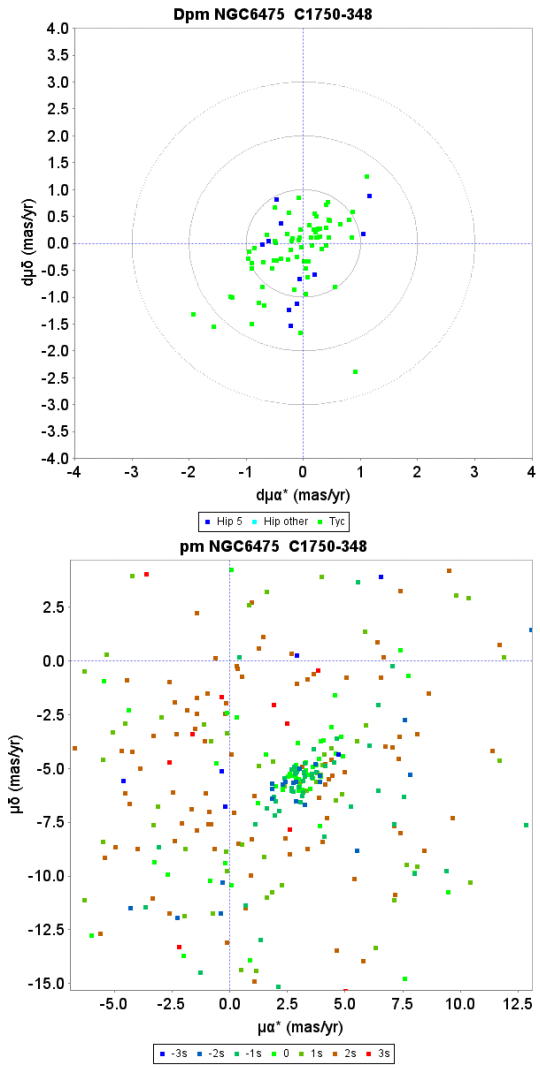

Fig. D.19. Proper motion charts for the cluster NGC 6475. *Top*: unit weight residual proper motions. Green dots have first epoch *Tycho-2* data, the dark blue dots have HIPPARCOS first epoch 5-parameter solutions. The concentric circles represent 1–3σ *su* levels. *Bottom*: actual proper motion distribution, where the colour indicate the difference from the cluster parallax in *su* units.

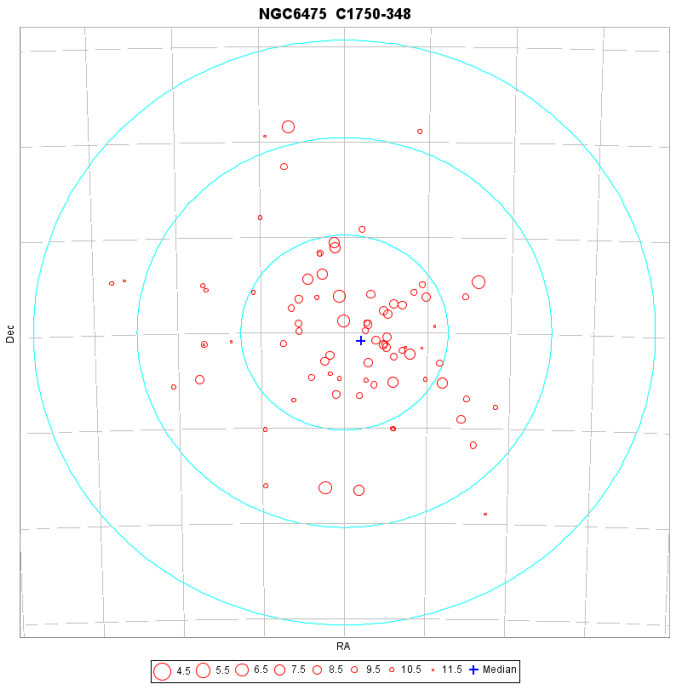

Fig. D.20. A map of members of the cluster NGC 6475 as identified from the TGAS catalogue. The coordinate grid is at 1 degrees intervals, the three concentric circles are at 5, 10 and 15 pc from the cluster centre at the cluster distance.

D.11. The cluster NGC 7092

Table D.11. Identifiers and positions for members of the cluster NGC 7092.

SourceId	HD	α (degr)	δ (degr)	G	SourceId	HD	α (degr)	δ (degr)	G
2170750757152762240		321.6688	48.5799	9.716	1978441947209204736		323.2545	48.2349	9.672
1978555643589899648	204917	322.5789	48.3908	7.385	1978443321598738560	205331	323.2921	48.3033	6.954
1978529633267976704		322.6364	47.9997	11.698	1978742904159340416		323.4489	49.1609	10.317
1978336187938996992		322.7520	47.8002	9.741	1978743350835937536		323.4864	49.1968	9.363
1978533137961284864		322.7939	48.0704	10.097	1978460467108321664		323.8055	48.4372	9.576
1978652744205824384	205116	322.9266	48.5845	6.863	1978484999961562624		323.8920	48.7588	10.381
1978647762043764608	205117	322.9360	48.4843	7.689	1978404495094544128		323.9485	48.1082	9.430
1978648483598270464		322.9565	48.4817	8.874	1977411326859661056		323.9917	46.5545	10.449
1978656214539396352	205198	323.0610	48.6394	8.269	1978464418478228352		324.2888	48.5571	9.685
1978636285891151744	205210	323.0711	48.4437	6.593	1978933291465578240		325.3494	49.3301	10.002
1978740430258165632		323.1142	49.1810	11.285	1977881058837817344		326.6370	48.1986	9.607
1978641852168765184		323.1798	48.4831	9.053					

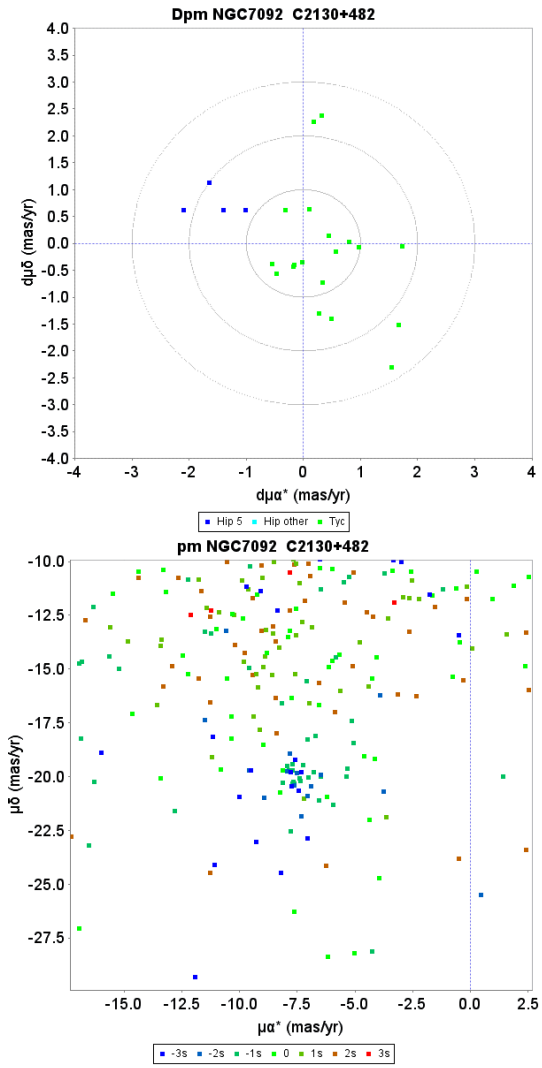

Fig. D.21. Proper motion charts for the cluster NGC 7092. *Top*: unit weight residual proper motions. Green dots have first epoch *Tycho-2* data, the dark blue dots have HIPPARCOS first epoch 5-parameter solutions. The concentric circles represent 1–3σ *su* levels. *Bottom*: actual proper motion distribution, where the colour indicate the difference from the cluster parallax in *su* units.

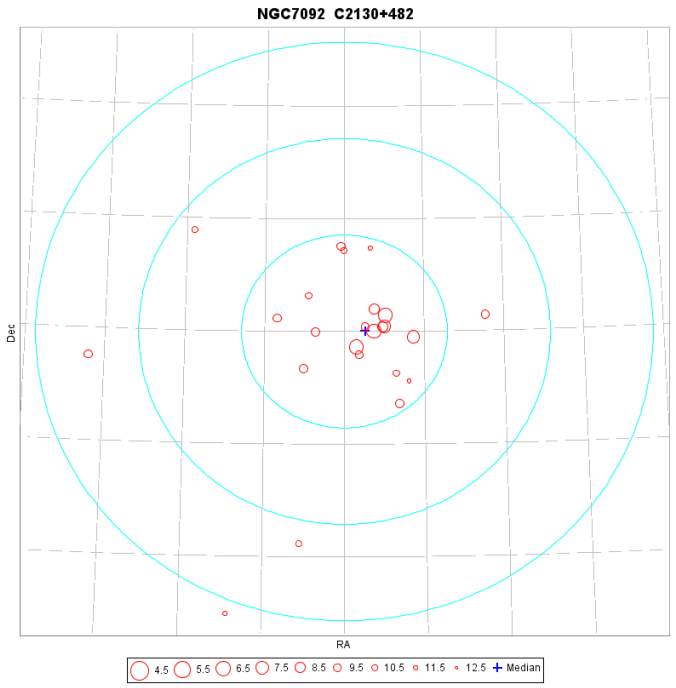

Fig. D.22. A map of members of the cluster NGC 7092 as identified from the TGAS catalogue. The coordinate grid is at 1 degrees intervals, the three concentric circles are at 5, 10 and 15 pc from the cluster centre at the cluster distance.

D.12. The cluster NGC 2516

Table D.12. Identifiers and positions for members of the cluster NGC 2516.

SourceId	HD	α (degr)	δ (degr)	G	SourceId	HD	α (degr)	δ (degr)	G
5292754032119550976	63011	115.8099	–59.8235	9.590	5290642694916327424		119.4840	–61.3655	10.346
5289355166802297984		115.9907	–61.6941	10.333	5290720451004223616		119.4918	–60.8459	8.992
5292478948054155776		116.6608	–60.5114	9.900	5287997854056218880	66081	119.5204	–63.2295	9.413
5294345162885186176	63709	116.7270	–58.9067	8.182	5290673756119783168		119.5542	–60.8741	8.203
5289457318302408960	63872	116.8751	–60.7841	9.648	5291137853105909632	66029	119.5827	–59.4363	9.707
5293999572636389760		116.9295	–60.1684	9.964	5290667949324010240		119.6589	–61.0135	9.435
5294040838682140416	64507	117.7367	–59.6462	7.313	5290767626925303936	66194	119.7106	–60.8244	5.867
5290696124310372352	64644	117.8000	–61.2545	9.075	5291055458454839296		119.7854	–59.8373	10.590
5288322587942769152		117.8623	–62.4960	11.359	5290818582417293696	66259	119.8112	–60.5871	8.382
5290968081639463552		117.8949	–60.4124	10.887	5290767386407134720	66318	119.8644	–60.7964	9.609
5291009519483916160		117.9648	–60.1588	10.286	5290847856916705152	66341	119.9170	–60.2073	6.311
5290968459596583296	64762	117.9885	–60.3843	9.251	5291062467841475456	66388	119.9597	–59.9670	9.574
5294211640940573184	64743	118.0035	–58.9986	9.815	5291542404667473152	66481	120.1364	–58.8667	9.587
5290895513871203712		118.0578	–60.8858	10.239	5290868816357122816		120.2115	–60.1529	11.068
5290918569256484480		118.0700	–60.5472	11.210	5290747079801445248		120.2139	–61.0192	10.270
5291011340551279872		118.2444	–60.0532	10.324	5289989688088614912		120.2572	–61.2432	10.343
5290701931106148096		118.2496	–61.0844	11.283	5289976081632231552	66707	120.3084	–61.3677	9.721
5290682689652668416		118.2528	–61.2178	11.066	5290850468254523904		120.4019	–60.3519	10.772
5294047229593277184		118.2712	–59.4145	9.326	5289811945162807296		120.5536	–61.7774	10.766
5290944098542081280		118.3249	–60.3956	11.355	5289977868338618240		120.5714	–61.2769	11.748
5290901286307238528		118.3321	–60.7136	10.028	5290004668936594560		120.6922	–60.8937	10.771
5290901286307238656		118.3430	–60.7150	10.738	5290863799832998144	67107	120.7604	–60.0696	9.566
5290944132901818880		118.3445	–60.3840	11.546	5290779755912990976		120.8441	–60.7642	10.695
5290943067749932544		118.3564	–60.4320	10.442	5290859401786488704	67197	120.8576	–60.1530	9.357
5290704301928090240		118.5403	–60.9742	11.379	5290030335661147136		121.1402	–60.7379	10.660
5294443294297626368		118.5494	–58.4124	10.888	5289934746866964352		121.1573	–61.2504	11.313
5290940971807119104		118.6115	–60.4304	10.960	5290006146403282432		121.2353	–61.1145	11.219
5290726910635935872		118.6749	–60.9635	10.987	5289697492873552896		121.3343	–61.9716	10.223
5294246962752996736	65387	118.8005	–58.6090	10.263	5290020646214928640		121.4521	–60.7742	11.528
5289781674232532224	65623	118.9673	–62.3468	8.989	5289620664501064832		121.7018	–62.5151	10.946
5290616512796591744		119.1227	–61.5126	11.340	5291290375984527104		121.7257	–59.4200	11.302
5290722924905383808		119.1927	–60.8161	8.783	5290398946935329920	68037	121.8185	–60.5716	10.169
5290724196215701120		119.2482	–60.7838	9.647	5289938285920024960	68058	121.8216	–61.3661	9.257
5291032609228851840		119.3943	–60.2067	10.327	5289748345286306048		121.8795	–61.5315	11.332
5290718733017309824		119.4077	–60.9089	8.770	5290112146196485888		122.8538	–61.4296	10.624
5290725261370377600		119.4561	–60.7212	9.666	5277627432182254208		122.9566	–62.4664	10.367

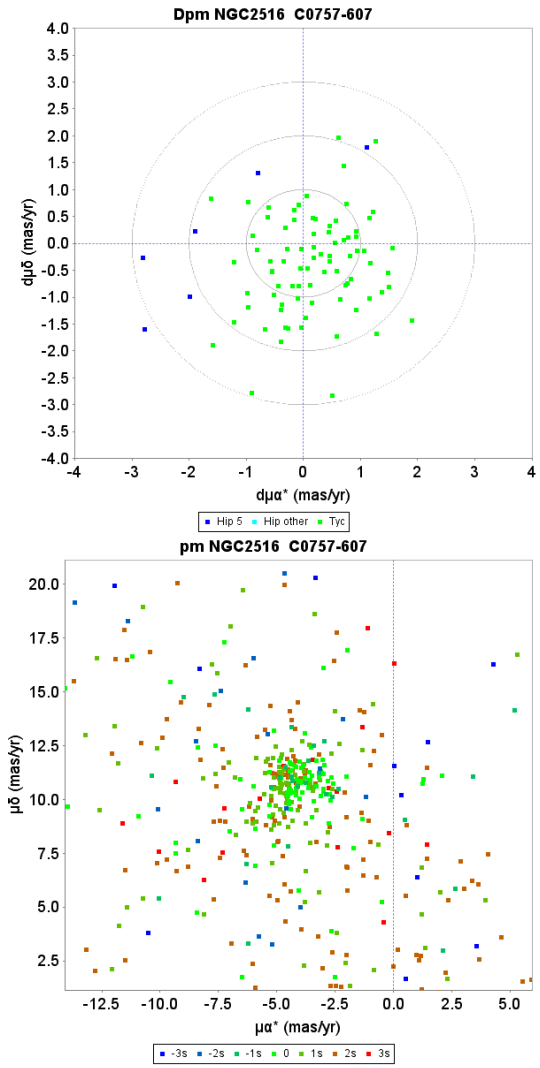

Fig. D.23. Proper motion charts for the cluster NGC 2516. *Top*: unit weight residual proper motions. Green dots have first epoch *Tycho-2* data, the dark blue dots have HIPPARCOS first epoch 5-parameter solutions. The concentric circles represent 1–3σ *su* levels. *Bottom*: actual proper motion distribution, where the colour indicate the difference from the cluster parallax in *su* units.

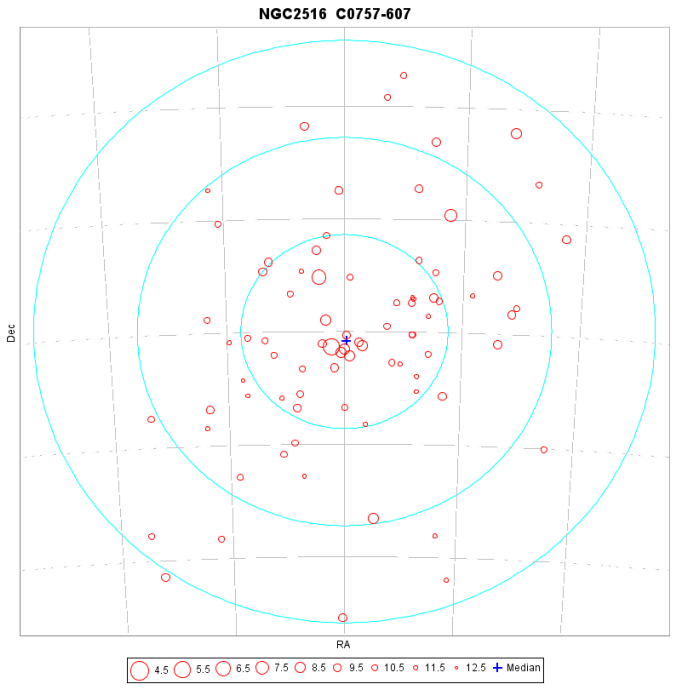

Fig. D.24. A map of members of the cluster NGC 2516 as identified from the TGAS catalogue. The coordinate grid is at 1 degrees intervals, the three concentric circles are at 5, 10 and 15 pc from the cluster centre at the cluster distance.

D.13. The cluster NGC 2232

Table D.13. Identifiers and positions for members of the cluster NGC 2232.

SourceId	HD	α (degr)	δ (degr)	G	SourceId	HD	α (degr)	δ (degr)	G
3116780972691989632	294906	94.9130	–3.9144	10.505	3104529458223283584		96.9888	–4.7122	10.585
3116548975739569664	44702	95.7465	–4.1871	8.688	3117056469074206080	45601	97.0893	–3.4611	8.665
3116554198419796992		95.9913	–4.0883	11.512	3104226817645484672	45627	97.0962	–5.0340	8.915
3008314116254649600		96.0353	–5.3520	10.965	3006948247933933568		97.2972	–7.1706	11.245
3008110637881857664		96.1198	–5.6776	10.219	3104591649350135552		97.4085	–4.0665	11.700
3116951225195812736	295008	96.1369	–3.1461	10.685	3105035336649025408		97.4321	–3.5793	11.306
3104421706081544320	295044	96.2830	–4.8583	9.687	3104155315031782016		97.4766	–5.3775	11.375
3104401502557764224		96.4836	–5.0643	10.847	3104158476127719680	45935	97.5686	–5.2604	9.819
3104454897588787840	45238	96.5333	–4.6282	8.439	3104257500891889280		97.8864	–5.1211	10.543
3007037858130227200	45284	96.5549	–7.3614	7.416	3006897086283522944	46282	98.0469	–7.3063	8.252
3104456031460151296	45321	96.6435	–4.5974	6.275	3103225403071448320		98.7380	–5.7721	11.517
3104452629848438272	45399	96.7436	–4.6251	8.509	3103153694297494400		99.0283	–6.0804	9.830
3104547325287231744	45434	96.7817	–4.5466	9.590	3103128302450862464	47091	99.1701	–6.3635	9.711
3104193316900585856		96.8102	–5.3022	11.211	3100016856344868992		99.1994	–6.7876	11.877
3007264082648616064	45547	96.9668	–6.2919	8.757	3103618581557297536	47340	99.4843	–5.5335	9.142
3117085537415090688	295066	96.9790	–3.1366	10.052					

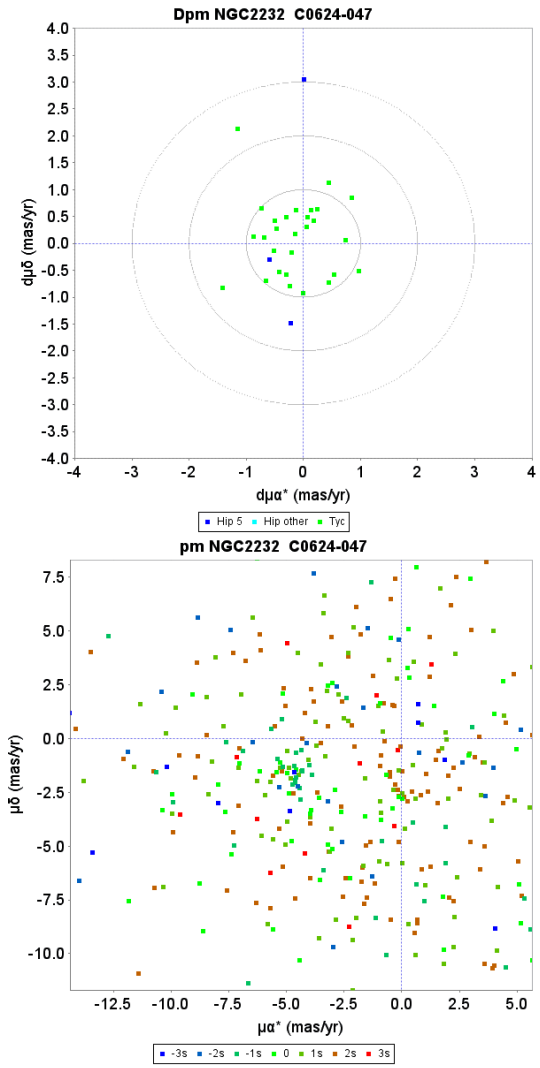

Fig. D.25. Proper motion charts for the cluster NGC 2232. *Top*: unit weight residual proper motions. Green dots have first epoch *Tycho-2* data, the dark blue dots have HIPPARCOS first epoch 5-parameter solutions. The concentric circles represent 1–3σ *su* levels. *Bottom*: actual proper motion distribution, where the colour indicate the difference from the cluster parallax in *su* units.

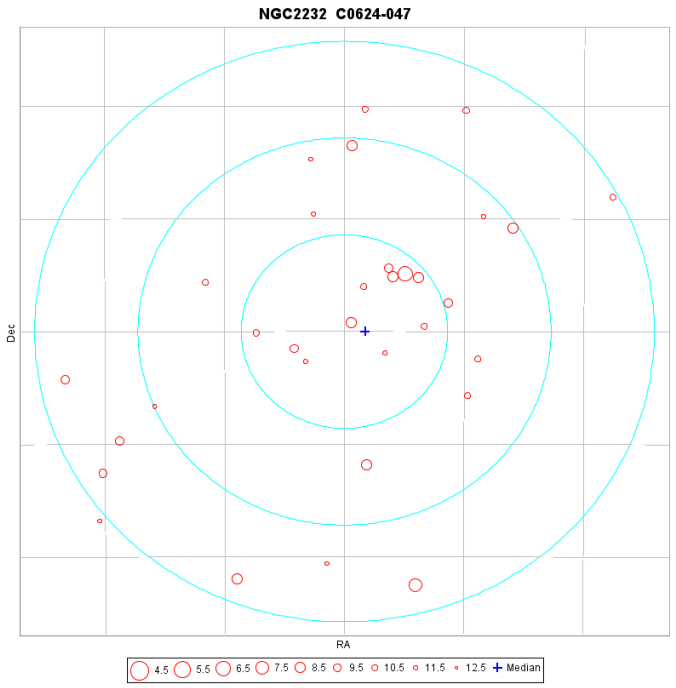

Fig. D.26. A map of members of the cluster NGC 2232 as identified from the TGAS catalogue. The coordinate grid is at 1 degrees intervals, the three concentric circles are at 5, 10 and 15 pc from the cluster centre at the cluster distance.

D.14. The cluster IC 4665

Table D.14. Identifiers and positions for members of the cluster IC 4665.

SourceId	HD	α (degr)	δ (degr)	G	SourceId	HD	α (degr)	δ (degr)	G
4486156425152983680	161055	265.7854	6.2153	9.977	4474071143094987520	161572	266.4878	5.6944	7.602
4473740877289974528	161261	266.0656	5.7143	8.283	4474059082826822144	161603	266.5455	5.6582	7.348
4473363126327469184		266.2138	4.4274	11.181	4474061831605886080	161677	266.6710	5.7742	7.129
4473687173019891328	161370	266.2537	5.5229	9.299	4474057433559379072	161733	266.7590	5.6918	7.998
4486313139920906496	161425	266.3149	6.8997	8.272	4473838905626668800		266.7859	5.2253	10.627
4474064442946007040	161426	266.3220	5.6676	9.042	4473768811760404864		267.0638	4.9130	11.832
4474066504530306688	161480	266.3902	5.7157	7.688	4473992974693569280		267.4240	5.9250	10.610
4473670783424690816	161481	266.3952	5.4265	9.014	4472970772475428224	162954	268.3992	4.8589	7.710

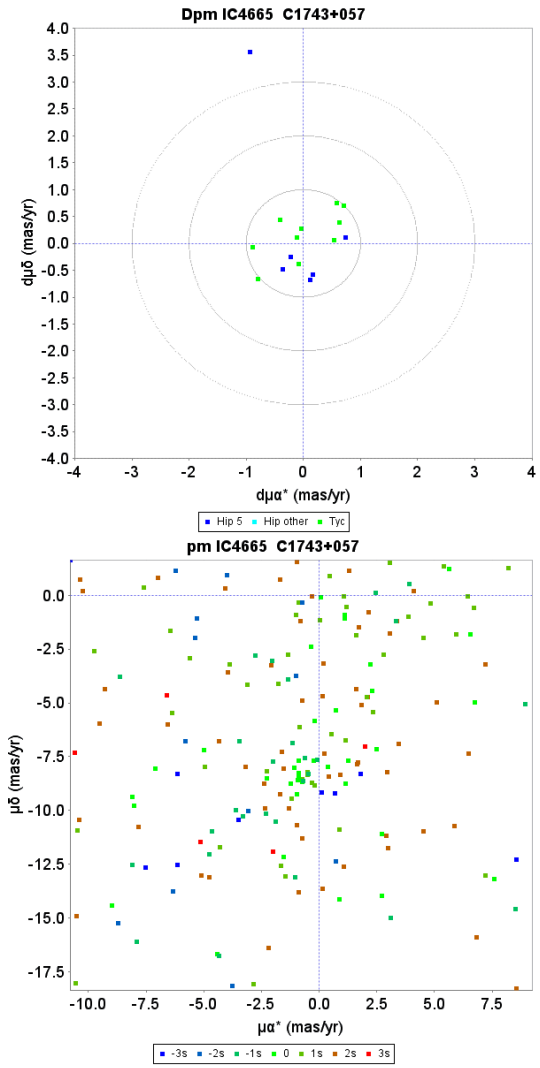

Fig. D.27. Proper motion charts for the cluster IC 4665. *Top*: unit weight residual proper motions. Green dots have first epoch *Tycho-2* data, the dark blue dots have HIPPARCOS first epoch 5-parameter solutions. The concentric circles represent 1–3σ *su* levels. *Bottom*: actual proper motion distribution, where the colour indicate the difference from the cluster parallax in *su* units.

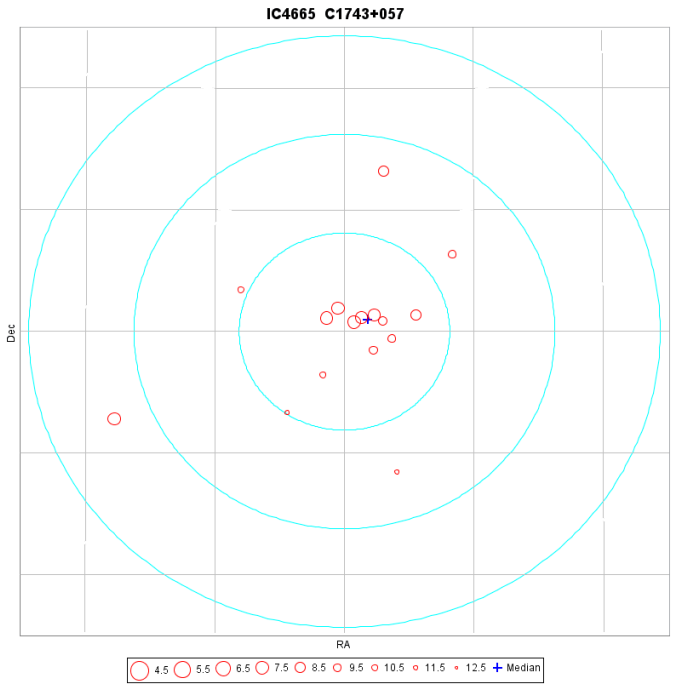

Fig. D.28. A map of members of the cluster IC 4665 as identified from the TGAS catalogue. The coordinate grid is at 1 degrees intervals, the three concentric circles are at 5, 10 and 15 pc from the cluster centre at the cluster distance.

D.15. The cluster NGC 6633

Table D.15. Identifiers and positions for members of the cluster NGC 6633.

SourceId	HD	α (degr)	δ (degr)	G	SourceId	HD	α (degr)	δ (degr)	G
4476902900932589056	168699	275.2333	5.9268	8.350	4477222618306462848	170135	276.9130	6.5321	8.370
4478329620357361792		275.9270	7.8384	10.600	4477173518240339968	170158	276.9487	6.4559	8.992
4478439262280847744	169596	276.2681	8.2389	9.651	4477266461332603776		276.9652	6.8313	10.045
4477430769601777024		276.3198	6.8252	11.738	4477223374220701696	170174	276.9781	6.6001	7.896
4477243234149473664		276.5428	6.6982	9.875	4284608247206265856		276.9947	5.8031	11.737
4477216261754871680		276.5974	6.4182	9.750	4477172521807928448		276.9952	6.4303	11.265
4477231276960532224		276.6133	6.5270	10.670	4477273264560797696	170231	277.0008	6.9143	8.232
4477213444256326528		276.6871	6.4050	10.042	4477569926535247488	170271	277.0490	7.3553	8.859
4477212172946010368		276.6954	6.3490	10.255	4477249109664733568	170292	277.0957	6.7081	8.369
4477212413464176640		276.7201	6.3875	8.719	4477170803821011328	170293	277.0958	6.4139	8.520
4477465198053904768	169984	276.7218	7.1184	9.172	4477374591421100800		277.1231	7.1732	10.493
4477212001147318400		276.7293	6.3490	9.933	4477259761183622400		277.1373	6.8211	11.776
4477214784286122112		276.7518	6.4172	9.406	4477256531368216960	170346	277.1625	6.7896	8.650
4477214028371878528	170011	276.7585	6.4111	8.937	4477256668798782080		277.1792	6.8132	11.278
4477214818645859328		276.7649	6.4315	9.441	4477577073360825856		277.1802	7.4677	12.130
4477268694715597440		276.7975	6.8371	11.258	4477373079596895360		277.2584	7.1701	9.981
4477460387696238336	170053	276.8095	7.0091	6.728	4477373801151400064	170426	277.2733	7.2052	8.954
4477221656230795136	170054	276.8112	6.5186	8.193	4477258077548054528	170472	277.3325	6.8514	9.074
4477266152094957440		276.8323	6.8583	11.273	4477385930139039744		277.4129	7.4038	10.047
4477221381355884672		276.8353	6.4942	9.597	4477305665786045312		277.4593	6.9237	11.578
4477158571754162432	170079	276.8502	6.1430	8.943	4477412009180490624	170676	277.6046	7.5330	9.349
4477160427180032000	170095	276.8599	6.2408	9.442	4284914976584397440		277.6049	5.7124	11.818
4477223820897301248	170094	276.8713	6.5890	9.242	4285146251985356160		278.3180	6.7648	11.769
4477267629563706240		276.9017	6.8809	11.335	4286682269726287872		278.8917	7.3294	11.105

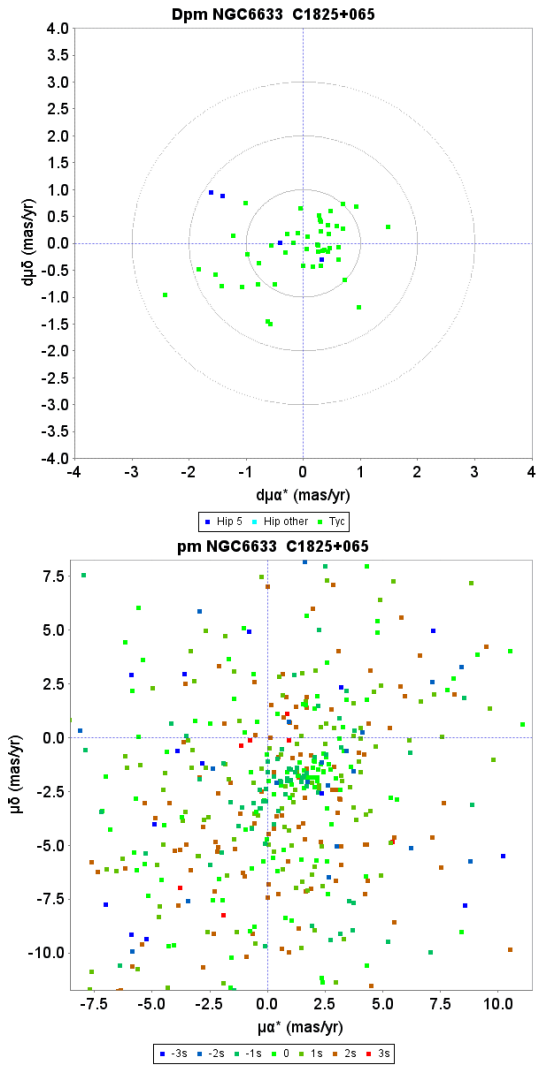

Fig. D.29. Proper motion charts for the cluster NGC 6633. *Top*: unit weight residual proper motions. Green dots have first epoch *Tycho-2* data, the dark blue dots have HIPPARCOS first epoch 5-parameter solutions. The concentric circles represent 1–3σ *su* levels. *Bottom*: actual proper motion distribution, where the colour indicate the difference from the cluster parallax in *su* units.

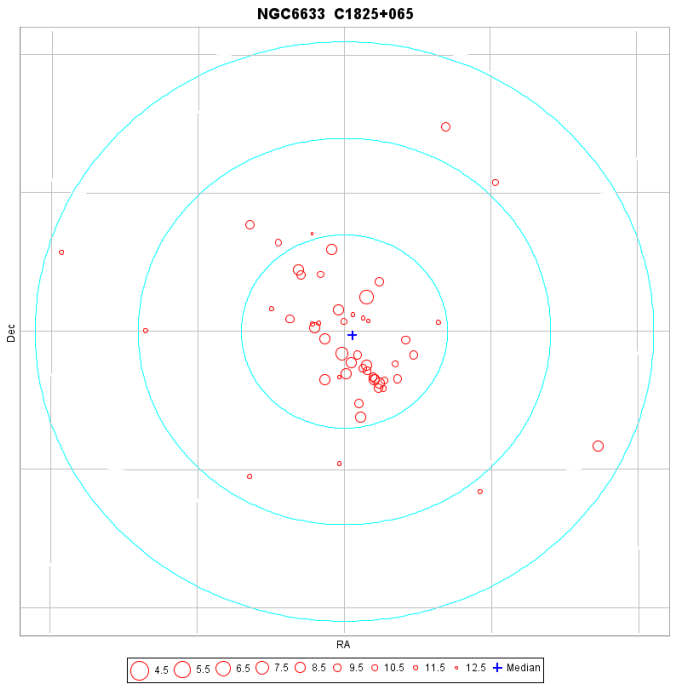

Fig. D.30. A map of members of the cluster NGC 6633 as identified from the TGAS catalogue. The coordinate grid is at 1 degrees intervals, the three concentric circles are at 5, 10 and 15 pc from the cluster centre at the cluster distance.

D.16. The cluster Coll 140

Table D.16. Identifiers and positions for members of the cluster Coll 140.

SourceId	HD	α (degr)	δ (degr)	G	SourceId	HD	α (degr)	δ (degr)	G
5603486910168526464		108.0499	–32.4072	11.380	5592362360756536192		111.2594	–33.7024	11.425
5603528622888474240		108.7214	–31.8839	10.403	5592828107009120896		111.2769	–31.9735	11.187
5604862674090330624		109.7420	–31.6362	11.657	5592585939571471104		111.4850	–32.6238	10.636
5604778011699119232	57759	110.3159	–32.0267	9.425	5591637370276050432		111.7394	–33.7077	11.301
5604898545660357888		110.4101	–31.6288	11.274	5591558445957080576		111.9184	–34.2274	10.947
5592762548628967680	57912	110.4892	–32.1911	8.959	5592608067242958208		111.9360	–32.3345	10.330
5592858343578910976		110.6150	–32.1157	9.854	5593234823235985920	59550	112.2704	–31.4562	5.913
5592859168212619264	58063	110.6485	–32.0460	10.098	5593461838022243072	59572	112.3336	–30.1935	10.141
5592893905908057728		110.9707	–31.7265	10.236	5593416723685787904		112.3633	–30.5931	10.374
5605735961203862144		110.9890	–29.6577	10.213	5591658089201524096		112.6466	–33.7526	9.796
5592878650184244352	58395	111.0086	–31.9106	9.104	5591682759491151744		112.7328	–33.6325	11.236
5592886106247453440	58534	111.1732	–31.7827	7.753	5592948194293169920		112.7961	–32.2772	11.694
5605346734084513536		111.2547	–30.7787	10.970	5591883317281598720		113.4522	–33.3901	10.481

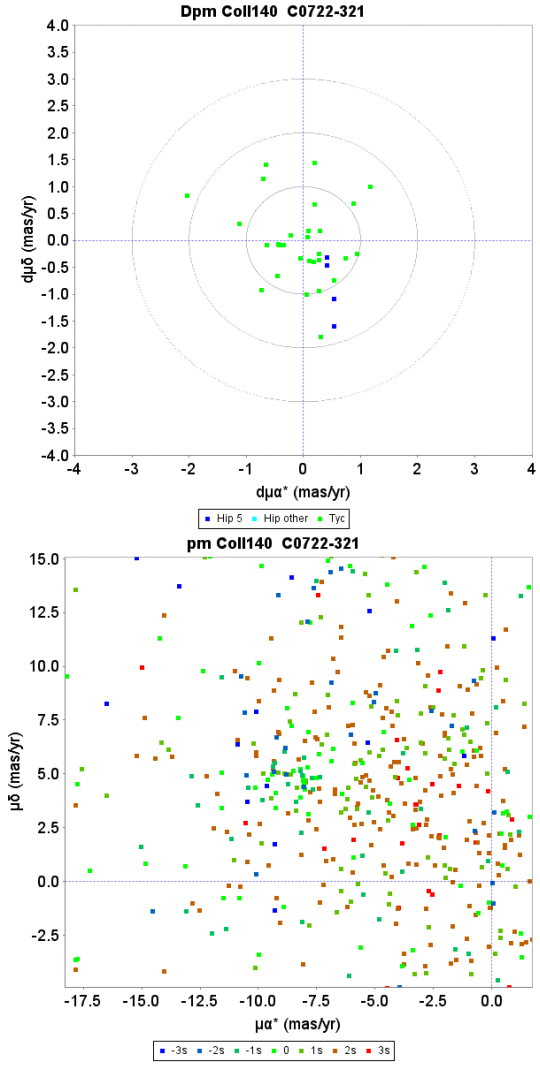

Fig. D.31. Proper motion charts for the cluster Coll 140. *Top*: unit weight residual proper motions. Green dots have first epoch *Tycho-2* data, the dark blue dots have HIPPARCOS first epoch 5-parameter solutions. The concentric circles represent 1–3σ *su* levels. *Bottom*: actual proper motion distribution, where the colour indicate the difference from the cluster parallax in *su* units.

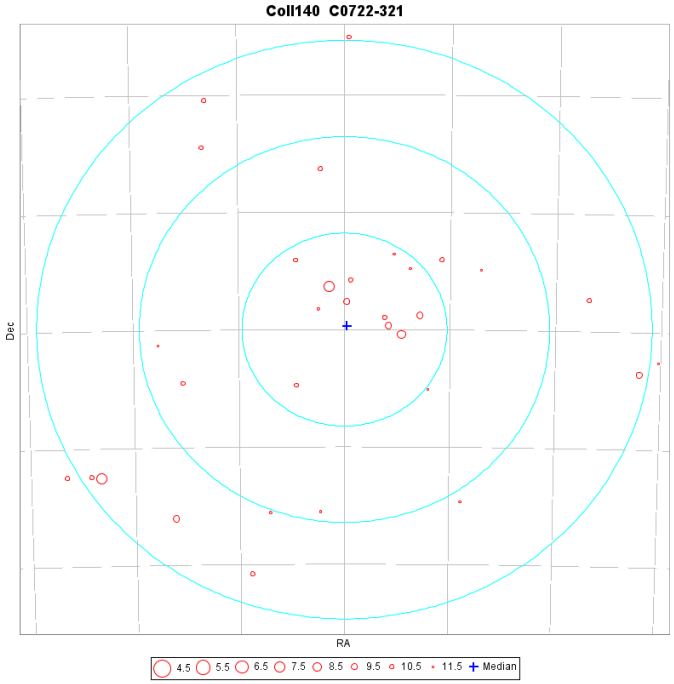

Fig. D.32. A map of members of the cluster Coll 140 as identified from the TGAS catalogue. The coordinate grid is at 1 degrees intervals, the three concentric circles are at 5, 10 and 15 pc from the cluster centre at the cluster distance.

D.17. The cluster NGC 2422

Table D.17. Identifiers and positions for members of the cluster NGC 2422.

SourceId	HD	α (degr)	δ (degr)	G	SourceId	HD	α (degr)	δ (degr)	G
3028626597142894464		111.9480	–14.9703	12.089	3030729172615280128		114.1056	–13.3717	11.339
3033676757130794368	59436	112.3577	–12.6960	9.630	3030228688664529408		114.1149	–14.2268	9.951
3028273619552906368	60050	113.0432	–15.9423	9.878	3030013253105462528	60999	114.1282	–14.6655	8.796
3033318763016101120		113.2187	–13.6996	10.558	3030259956026959616		114.1306	–14.0059	11.110
3030085752152201600		113.2347	–14.8403	10.584	3033778805551456512		114.1490	–12.7578	10.580
3030085442914556800	60278	113.2811	–14.8684	10.154	3030028886786394752		114.1512	–14.4612	7.793
3028387796967333632	60279	113.2828	–15.1784	9.288	3030231781041515520		114.1520	–14.1438	9.830
3033383634202689536	60476	113.5347	–13.0395	7.901	3029807678792327808		114.1908	–15.4626	11.343
3034062685712605824		113.5358	–12.0417	10.209	3030024282581449088		114.4046	–14.4237	8.915
3033837904304239232		113.6452	–12.4722	10.327	3030069259478942336		114.4132	–14.0341	10.507
3030298370214451072	60597	113.6975	–13.9760	10.263	3030004525731877632		114.8204	–14.3367	9.804
3030243051035701632	60624	113.7271	–14.1628	7.590	3030681000261287552		114.8374	–13.4457	9.730
3033756746599448832		113.7453	–12.9845	10.861	3029184393140868480		114.8589	–15.0898	10.704
3030250747617082752	60659	113.7721	–14.0448	9.891	3029983909887619328	61865	115.1938	–14.5134	9.912
3029910448767038592		113.9117	–14.8534	11.993	3029232702927668096		115.2640	–14.5687	10.140
3030247311643245696		113.9129	–14.0425	11.371	3029096878882496384	62051	115.3829	–15.5418	10.175
3029905191727079168		114.0572	–14.9320	10.546	3030376641697207424		115.4815	–14.0834	9.807
3030730306486641280		114.0748	–13.3205	9.775	3030529679972172032		116.1616	–13.4064	12.190
3030025656971005696	60941	114.0797	–14.5923	9.138					

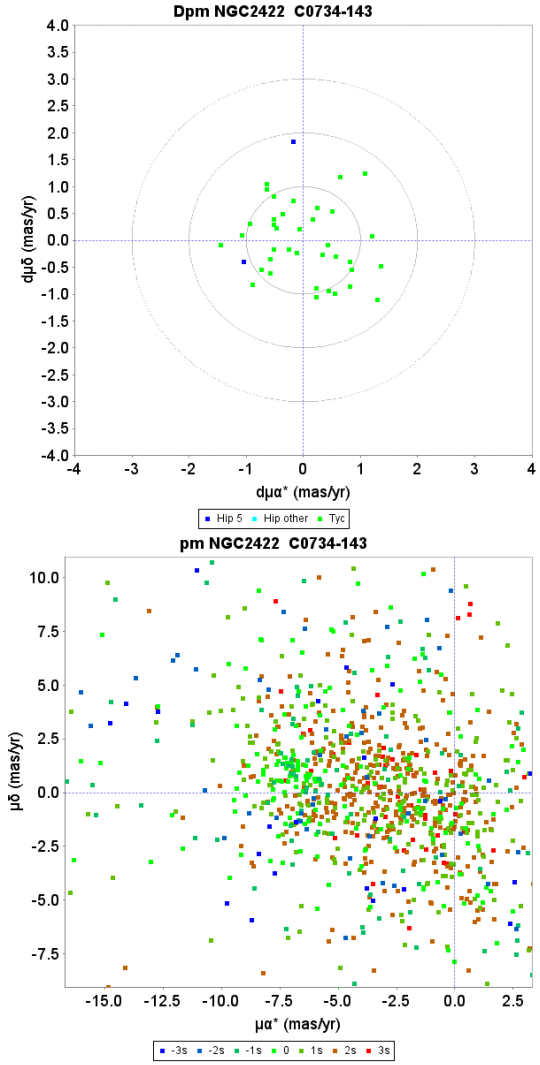

Fig. D.33. Proper motion charts for the cluster NGC 2422. *Top*: unit weight residual proper motions. Green dots have first epoch *Tycho-2* data, the dark blue dots have HIPPARCOS first epoch 5-parameter solutions. The concentric circles represent 1–3σ *su* levels. *Bottom*: actual proper motion distribution, where the colour indicate the difference from the cluster parallax in *su* units.

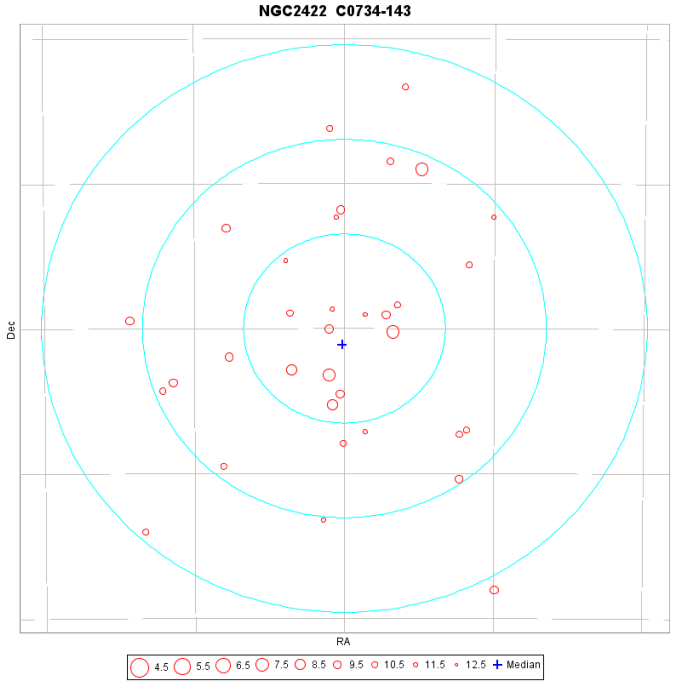

Fig. D.34. A map of members of the cluster NGC 2422 as identified from the TGAS catalogue. The coordinate grid is at 1 degrees intervals, the three concentric circles are at 5, 10 and 15 pc from the cluster centre at the cluster distance.

D.18. The cluster NGC 3532

Table D.18. Identifiers and positions for members of the cluster NGC 3532.

SourceId	HD	α (degr)	δ (degr)	G	SourceId	HD	α (degr)	δ (degr)	G
5350433450039970176	303392	162.3573	–59.1874	10.466	5338661425719301888	96305	166.3195	–58.7836	8.580
5338425339955648384	303505	163.1798	–59.4636	10.152	5340224862533206912	96324	166.3268	–58.1997	9.093
5350988978295475200		163.3526	–57.9345	11.464	5338663693462017408	96304	166.3288	–58.6767	9.561
5338429497484007168	94558	163.4453	–59.3828	8.852	5338661803676414336		166.3869	–58.7305	8.924
5338803606315364096		164.1178	–58.6939	10.323	5338661666237468032		166.3996	–58.7694	8.982
5340558461233008768	301224	164.2416	–56.8914	10.706	5338658745659705344		166.4079	–58.7636	9.652
5338742136743476864		164.3027	–59.4441	11.273	5338658092824688512	96388	166.4268	–58.8362	8.823
5338910671260868352	303540	164.4137	–58.2177	10.062	5338663865260709888		166.4400	–58.6776	7.860
5338776427762345728	95163	164.5684	–59.1025	9.848	5338660841603735680		166.4858	–58.6925	9.269
5338787457238337664		164.7054	–58.8049	11.291	5338660223128448896	96445	166.4947	–58.7248	7.405
5338772132795055104	95290	164.7736	–59.1684	7.708	5338660669805043200		166.5159	–58.6877	7.121
5338559205501201024	95291	164.7977	–59.3981	8.295	5340162052934957440	96472	166.5311	–58.6384	8.593
5338782578155498240		164.8872	–58.9297	11.361	5338651117797806976	96473	166.5326	–58.8922	8.463
5338925514667835904	95412	164.9703	–58.1667	8.883	5338657165111753728	96489	166.5547	–58.8440	8.036
5338594733470670208	95495	165.0972	–58.9831	7.972	5338657680507824256		166.5555	–58.8103	8.846
5338912011289889280	303643	165.1418	–58.4935	10.659	5340176346582639232	96488	166.5562	–58.3198	9.789
5338912389247010816	303641	165.1947	–58.4758	10.480	5340171226981629312	96509	166.5725	–58.4252	9.977
5340428684503196544	95599	165.2757	–57.9364	9.668	5338659157976566144		166.6139	–58.7630	8.958
5338590232345552640		165.2995	–59.0860	11.266	5338659501573946112	96564	166.6493	–58.7441	7.819
5338923590525853184	303627	165.3136	–58.1572	10.187	5338636411829832576	96585	166.6672	–59.0839	9.387
5338693380275987456	303659	165.3185	–58.8121	10.621	5340392812935875328	96583	166.6784	–57.1706	9.879
5338567383119554176		165.4894	–59.4011	11.434	5337712409748364800	96587	166.6921	–60.2453	9.630
5338720112152408320		165.5253	–58.5794	11.357	5338647887982435968	96610	166.7060	–58.7423	8.701
5338729251842805376	95751	165.5284	–58.3540	10.151	5340149236752553216	96609	166.7134	–58.7068	8.641
5338692590002009344	303662	165.5420	–58.8341	10.174	5340306844870519552	96607	166.7228	–57.7840	10.015
5338694204909705472	95765	165.5453	–58.7911	9.299	5340170264908977408	96619	166.7378	–58.4686	10.134
5338721589621157888	303649	165.5556	–58.5785	10.645	5338646960269502080		166.7558	–58.8314	9.783
5338695098262889728	303650	165.5561	–58.7064	10.528	5340170299268715648	96636	166.7572	–58.4637	9.012
5338674207541996032		165.5822	–58.9441	11.076	5338605281905483776	303837	166.7581	–59.3781	10.709
5338720936786128768	95825	165.6228	–58.5752	10.000	5340148996234385280	96653	166.7842	–58.7163	8.368
5338730420073910144	95824	165.6291	–58.3731	9.630	5340172085975106688	96651	166.7855	–58.3902	8.954
5338721108584820352		165.6501	–58.5692	10.789	5340157929762905216	96652	166.7893	–58.5270	9.211
5338706814933672576	95879	165.7108	–58.7019	7.585	5338646651031856256	96667	166.7950	–58.8158	9.625
5338679670740391808	303741	165.7314	–58.9080	10.840	5338644486368342144	96668	166.7976	–58.9074	8.308
5338709220115347968		165.7422	–58.6047	11.521	5338634041007885952	96703	166.8515	–59.1028	9.612
5338669122300733440	95931	165.7701	–59.1115	8.314	5340159819548513792	96714	166.8755	–58.4736	9.434
5338680942050709760	95948	165.8019	–58.8920	9.295	5338630845550826880	96732	166.9026	–59.2184	10.210
5338709117036131712	95947	165.8086	–58.5965	9.939	5340160506743277184		166.9128	–58.3978	10.668
5338085075467999744	95991	165.8253	–60.5955	9.422	5340159029274531712	96772	166.9472	–58.4852	9.555
5338717191574643200	95968	165.8386	–58.4757	9.242	5340159544670605824		166.9510	–58.4488	10.327
5340219571133507072	95967	165.8436	–58.3311	10.227	5340186207827570048	96771	166.9611	–58.2864	9.838
5340240564937995136	303723	165.8814	–58.0948	10.346	5338639469846546688	96791	166.9806	–59.0646	10.235
5338714717673483520	96011	165.8883	–58.5595	9.050	5340159613390081536		166.9997	–58.4378	11.139
5338717019775948416		165.8939	–58.4253	10.602	5340158788756363648	96808	167.0134	–58.5003	8.850
5338703997435135360	96059	165.9719	–58.7653	8.074	5338640088321834496	96826	167.0215	–59.0025	9.599
5340218231107182720	96058	165.9729	–58.3953	8.384	5340290008597838208	96823	167.0266	–57.9414	9.379
5338716641818829696		165.9794	–58.4815	10.345	5338641771949012096	96849	167.0621	–58.9419	8.953
5338713858680020224		166.0231	–58.4518	10.082	5337851944644789632	96881	167.0902	–59.5563	9.609
5338703104081939200	96137	166.0802	–58.7694	8.237	5340155902538341632	96896	167.1518	–58.5332	9.713
5338654347613209216	96157	166.1259	–58.8630	9.858	5340152122970576000	96931	167.1798	–58.7108	9.964
5338709632432217728	96174	166.1409	–58.6943	7.480	5339394765619269760	96944	167.2231	–58.8310	9.075
5340214107938580096		166.1489	–58.4715	11.123	5337886476185146624	303824	167.3680	–59.0708	10.123
5338656649715663232	96175	166.1498	–58.7558	7.334	5339402599637990528	97081	167.4173	–58.6724	9.915
5338656684075397376		166.1549	–58.7306	9.751	5339402256040608512	97093	167.4369	–58.7017	8.714
5338709666791955072	96191	166.1634	–58.6854	9.165	5339438780442473216	97124	167.4662	–58.2624	8.859
5338626756743327488	303755	166.1715	–59.1271	10.514	5337861805889698688	97173	167.5687	–59.5130	8.377
5340226752318802304	303722	166.1771	–58.0930	10.770	5337872594847528960	97272	167.7078	–59.1918	9.443
5338662731389346048	96212	166.1850	–58.6958	8.652	5339422700084933248	97296	167.7704	–58.6294	9.748
5338662284712754048	96227	166.2298	–58.7496	8.226	5337872319969622784		167.7943	–59.2249	11.298
5338663212425678848	96245	166.2351	–58.6659	8.367	5337865963418035200	97396	167.9236	–59.3914	8.059
5338655034807973248		166.2499	–58.8314	9.882	5337757180483341184	306155	168.3274	–60.1784	9.928
5338662971907513344		166.2633	–58.6856	9.542	5339368617855163520	97656	168.3502	–58.6031	8.402
5338628852687359360	96285	166.2787	–59.0167	9.022	5339356935542014848	97669	168.3784	–58.9111	8.518
5338661460079038976	96284	166.2831	–58.7793	9.339	5339472418622698112	97747	168.4811	–58.2820	9.909
5340169027958372864	96283	166.2970	–58.4169	9.452	5339495405287654656	303970	168.9172	–58.1581	10.434
5338655344045619328	96306	166.3047	–58.8424	9.261	5339650676950667520	98833	170.4533	–58.5297	9.874

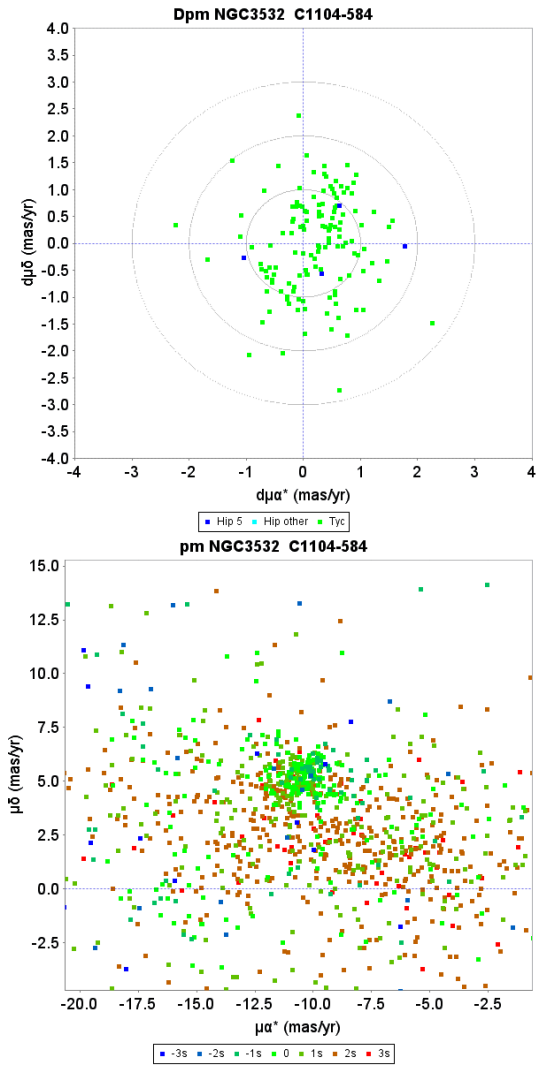

Fig. D.35. Proper motion charts for the cluster NGC 3532. *Top*: unit weight residual proper motions. Green dots have first epoch *Tycho-2* data, the dark blue dots have HIPPARCOS first epoch 5-parameter solutions. The concentric circles represent 1–3σ *su* levels. *Bottom*: actual proper motion distribution, where the colour indicate the difference from the cluster parallax in *su* units.

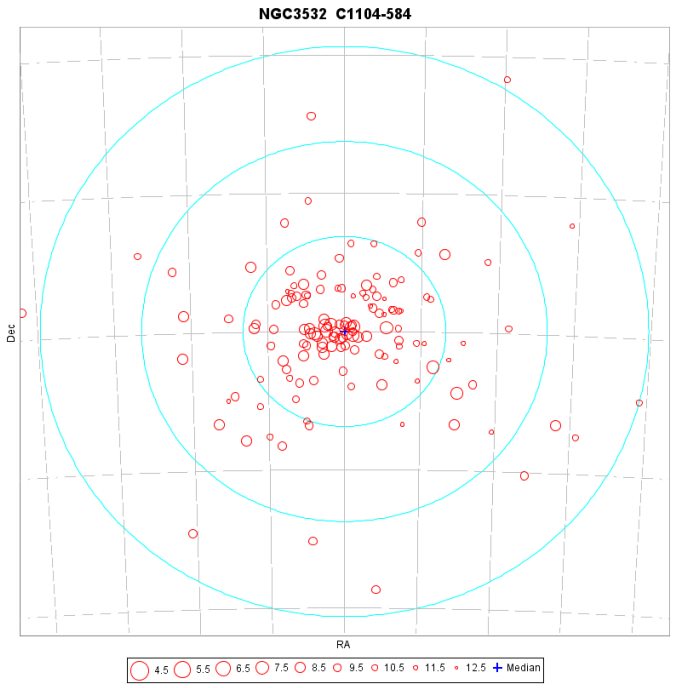

Fig. D.36. A map of members of the cluster NGC 3532 as identified from the TGAS catalogue. The coordinate grid is at 1.0 degrees intervals, the three concentric circles are at 5, 10 and 15 pc from the cluster centre at the cluster distance.

D.19. The cluster NGC 2547

Table D.19. Identifiers and positions for members of the cluster NGC 2547.

SourceId	HD	α (degr)	δ (degr)	G	SourceId	HD	α (degr)	δ (degr)	G
5514542123196527744	67612	121.6349	–49.2020	8.229	5514369465511703936	68496	122.6135	–49.1641	7.947
5514203507976717952		121.6431	–50.2674	10.978	5514372832766057216	68495	122.6310	–49.1084	9.414
5517729435606473728	67610	121.6506	–47.8057	9.876	5514343695707976064	68516	122.6408	–49.5439	9.747
5517679991942975232		121.7884	–47.9315	8.686	5514563735473921280	68558	122.6763	–48.9570	9.745
5514629534372854272	67867	121.9613	–48.6601	10.028	5514356065213760768	68608	122.7481	–49.2844	7.910
5514340568971771008		122.1904	–49.3965	10.633	5514374859990613888	68631	122.7858	–49.0045	9.904
5514334762176002944		122.2064	–49.5606	11.383	5513434433952494592	69260	123.4664	–50.5528	9.895
5514553427552434176	68114	122.2075	–49.2288	9.385	5515810719098074112	69282	123.5370	–49.2344	8.227
5514552705997928576	68115	122.2212	–49.2303	9.697	5513454362600737280	69347	123.5841	–50.3661	8.839
5514638570981291776		122.2895	–48.4566	10.458	5515896206125579392	69360	123.6207	–48.6597	10.381
5514366957250806784		122.4639	–49.1876	9.328	5515011236705810816	69428	123.6768	–49.9832	8.885
5514367060333996032		122.4675	–49.1840	9.641	5515823363481821952	69514	123.8152	–49.1801	8.072
5514362112527719168	68398	122.4833	–49.3250	8.624	5515039720928933376	69595	123.8727	–49.4750	10.470
5514373038924490752	68396	122.4897	–49.1389	8.919	5515049341655679104		124.1441	–49.5485	10.487
5514362799722478464	68397	122.4967	–49.2697	8.156	5514996702536508800	69911	124.2445	–49.7457	9.712
5514362627923788032	68432	122.5327	–49.2766	8.416	5516004920337181824	69909	124.2511	–48.2482	9.520
5514373932277680512	68452	122.5867	–49.0602	9.282	5515955785911323136		124.4473	–48.3585	10.863

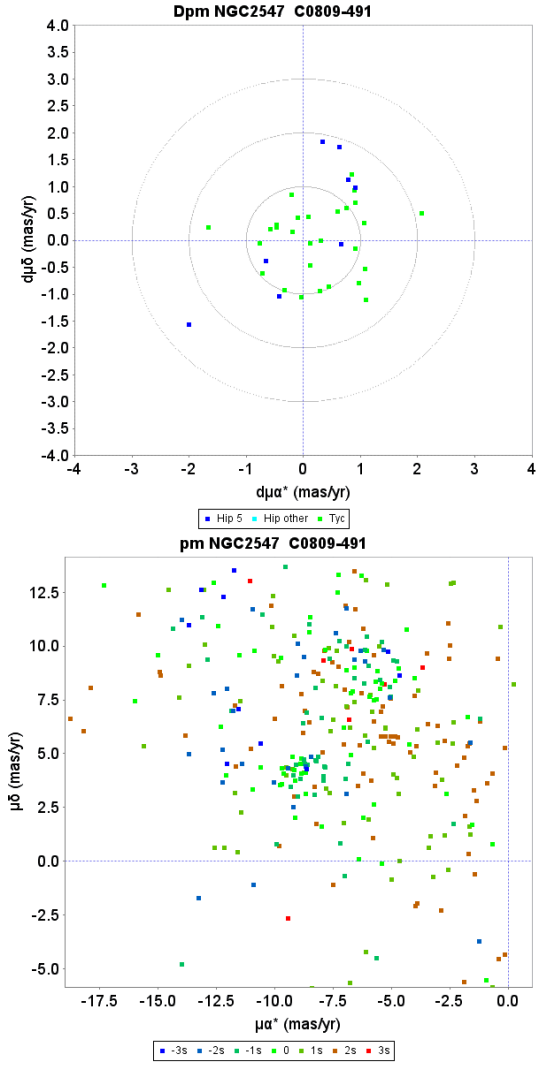

Fig. D.37. Proper motion charts for the cluster NGC 2547. *Top*: unit weight residual proper motions. Green dots have first epoch *Tycho-2* data, the dark blue dots have HIPPARCOS first epoch 5-parameter solutions. The concentric circles represent 1–3σ *su* levels. *Bottom*: actual proper motion distribution, where the colour indicate the difference from the cluster parallax in *su* units.

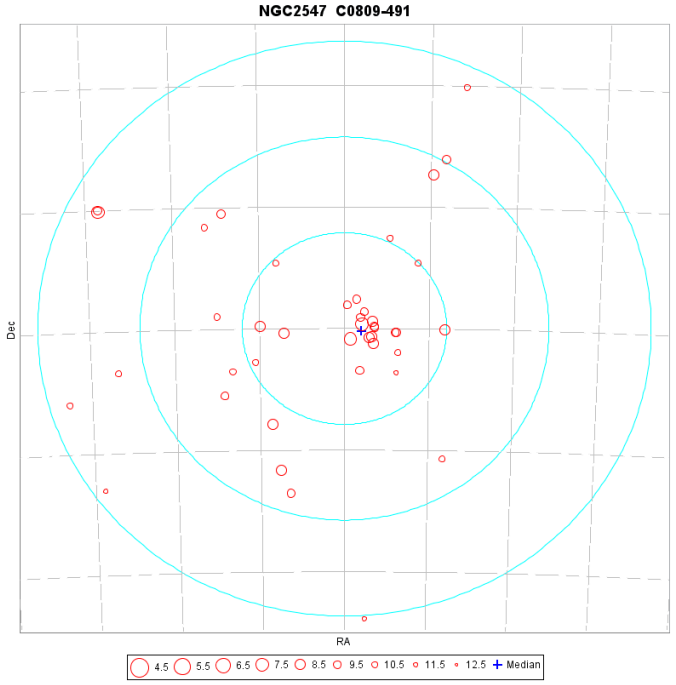

Fig. D.38. A map of members of the cluster NGC 2547 as identified from the TGAS catalogue. The coordinate grid is at 0.5 degrees intervals, the three concentric circles are at 5, 10 and 15 pc from the cluster centre at the cluster distance.